UNIVERSITY OF TRENTO

Department of Physics

FABRICATION OF N-TYPE POROUS SILICON MEMBRANES FOR SENSING APPLICATIONS

PhD Thesis

Candidate:	Supervisor:
Neeraj Kumar	**Dr. Paolo Bettotti**

December 2013

Declaration

I, **Neeraj Kumar**, student of Ph.D. hereby declare that the thesis titled **“Fabrication of n-type Porous silicon Membranes For Sensing Applications”** which is submitted by me to the Faculty of Natural Science, Department of Physics, University of Trento, ITALY in partial fulfilment of the requirement for the award of the degree of Doctor of Philosophy has not previously formed the basis for the award of any Degree, Diploma Associate ship, Fellowship or other similar title or recognition.

Date: December 2013

Place**:** Trento (ITALY) **(NEERAJ KUMAR)**

Certificate

On the basis of declaration submitted by **NEERAJ KUMAR**, student of Ph.D., we hereby certify that the thesis titled **"Fabrication Of n-type Porous silicon Membranes For Sensing Applications"** which is submitted by him to the Faculty of Natural Science, Department of Physics, University of Trento, ITALY in partial fulfilment of the requirement for the award of the degree of Doctor of Philosophy, is an original contribution with existing knowledge and faithful record of research carried out by him under my guidance and supervision.

To the best of our knowledge this work has not been submitted in part or full for any Degree or Diploma to this University or elsewhere.

Date:
Place**:** Trento (ITALY)

Dr. P.Bettotti
(Supervisor)
Nanoscience Lab.
Department of Physics
University of Trento (ITALY)

Acknowledgements

The fortunate and successful culmination of my efforts reminds me indebtedness towards many persons for helping me to complete this Ph.D. research work. I am willing to put on record my gratitude towards all of them who helped me directly and indirectly to complete this course.

There are several people who deserve recognition for the assistance they provided in the successful completion of my Doctor of Philosophy (Ph.D.) work. First and foremost, I would like to thank my supervisor" Dr. Paolo Bettotti" for their help and guidance in not only this effort, but in all of the works I have attempted in three year of my association. Their friendly demeanor, keen insight, and amazingly upbeat attitude in the face of adversity continue to inspire their students and colleagues alike. Special thanks to Prof. L.Pavesi, Prof. M.Scarpa and Dr. Elena (Bio-Physics Lab.), who were more than willing to help out on short notice and for their support in helping me to understand the basics of optics and surface chemistry of porous silicon structure.

This page would not be completed without thanking for all nano-lab members and a special thank to Dr. Romain Guider and Dr. Andrea Tengattini for their time to time supports provided in successful completion of my work.

Finally, I feel plentiful gratitude towards my parents and family members for their constant support and encouragement during this endeavor. Very special thanks to my lovable wife Rashmi Rathi for her emotional support during Ph.D. course.

(*NEERAJ KUMAR*)

TO MY TWIN BABY

Table of contents

Chapter one: Introduction

Chapter two: Fabrication and Experimental Techniques

Chapter three: Fabrication and physical properties of freestanding membranes

Chapter Four: Investigation of surface stabilization of porous layers

Chapter Five: Sensing with porous silicon micro-cavity (MC) structure

Chapter Six: Polarimetry sensing with porous silicon/alumina membranes

Chapter 1

Introduction

1.1 Introduction

Bio-sensors are devices capable to capture the presence of a biological signal and transform it into a recordable signal exploiting several available transduction mechanisms, such as electrochemical [1], piezoelectric [2], gravimetric [3] or optical transducers [4]. Figure 1.1 below explains the general principle of a bio-sensor.

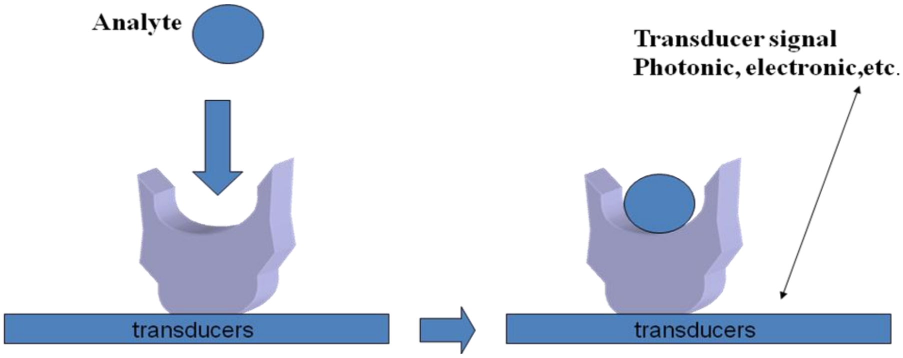

Figure 1.1-Working principal of a biosensor. When an analyte binds to the host matrix, its presence produces a signal that is transformed into a measurable signal and detected

Nowadays bio-sensor is a global industrial market that covers nearly all fields e.g. medical diagnostics [5], drug delivery, fermentation [6], food and beverage industry [7], environmental industry [8] etc..

According to market analysis, the global market of bio-sensor was evaluated 9.9 billion USD in 2011 and expected to cover 18.9 billion USD with a growth rate by 9.6% to year 2018 [9]. Furthermore, in recent years, bio-sensing devices using bio-compatible, bio-degradable membranes and most importantly porous membranes compatible with flow through approach, where the liquid is forced to pass across the material rather than flow over it, make possible to assemble lab on a chip devices [10]. Porous materials have great potential in sensing applications because their high specific surface permits a fine tuning of the interaction between the analyte and the host matrix [11]. Devices with state of the art sensitivity require a great control over their porous structure to tune the sensor properties and maximize their sensitivity. In these regards porous silicon (PSi) has many properties that make it an ideal candidate for the fabrication of highly sensible devices [12, 13]. The electrochemical etching mechanism used to render silicon a porous material permits to tune the PSi properties over a wide range both in terms of structural (pore size can be tuned from few nm to micron scale and surface specific area can achieve up to $500m^2/cm^3$ and optical properties (transparency and fabrication of high quality filters and resonant structures) [14]. Furthermore silicon chemistry is well known and PSi surface properties can be tailored to exhibit highly chemical specificity and reduced nonspecific interactions [15-17]. Finally, PSi is fully compatible with CMOS technology, thus it could be used to fabricate cheap microarrays which exploit multiplexing capabilities.

1.2 Porous Silicon

As mentioned above PSi is an ideal material for label free bio-sensing with many advantages over other porous materials. PSi was accidently discovered in 1956 at the U.S. Bell Laboratories by Arthur Uhlir Jr. and Ingeborg Uhlir during electro-polishing of crystalline silicon wafer [18]. However appearance of visible luminescence in PSi under UV illumination [19] attracts a large research interest because of the possibility to fabricate Si-based active optoelectronic devices. The great technological efforts and the flexibility given by the electrochemical etching have permitted a rapid development of the PSi fabrication process and samples with a number of different morphologies (i.e. pore size and pore morphology) were created [20]. The most popular and less expensive PSi fabrication technique is the electrochemical etching [21]. In this method anodization of c-silicon (both p- and n-type silicon) is done by means of a solution of hydrofluoric acid (HF) diluted in water or alcohols, with or without illuminating the sample. Either current or voltage controlled conditions can be used to induce the oxidation of the surface atoms of c-silicon that, in turn, generates a highly anisotropic etching and the formation of the pores [21-23]. The modulation of the various etching parameters (i.e. reaction time, HF concentration, applied current density/voltage and doping concentration of the silicon wafer), permit to control the morphology of PSi structures (more detail of fabrication setup and effect of various parameters are discussed in *Chapter 2* and in *Chapter 3*). The main point is that, once HF concentration and substrate type are fixed, the pores size is determined mainly by the etching current and the porous layer thickness growth roughly linear with the etching time. Furthermore depending on pore morphology of PSi structure, these structures are divided into three classes: micro$\leq$50nm, 50<meso$\geq$100nm and 100nm<macro-porous structure, as shown in Figure 1.2 and can be used to infiltrate specific for sensing or filtering applications [24]. Mechanism of dissolution of c-Si to fabricate PSi is insulating in Figure 1.3 [25].

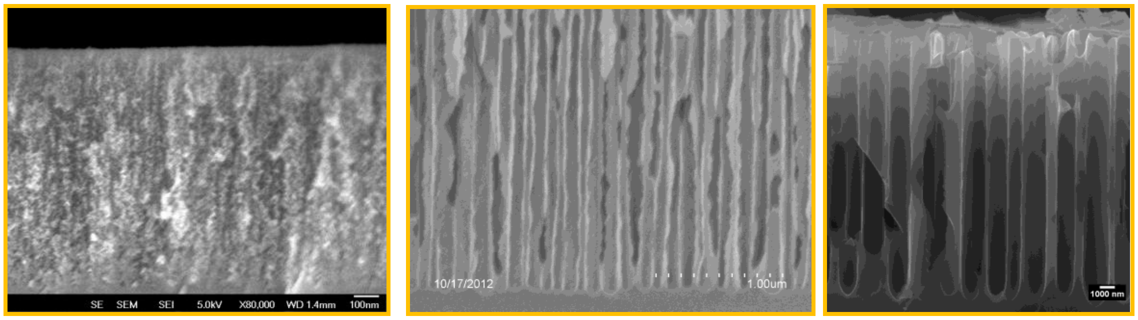

Figure 1.2-SEM images of different types of PSi structure depending on their pore size.(a) micro- PSi, (b) macro-PSi and (c) macro-PSi

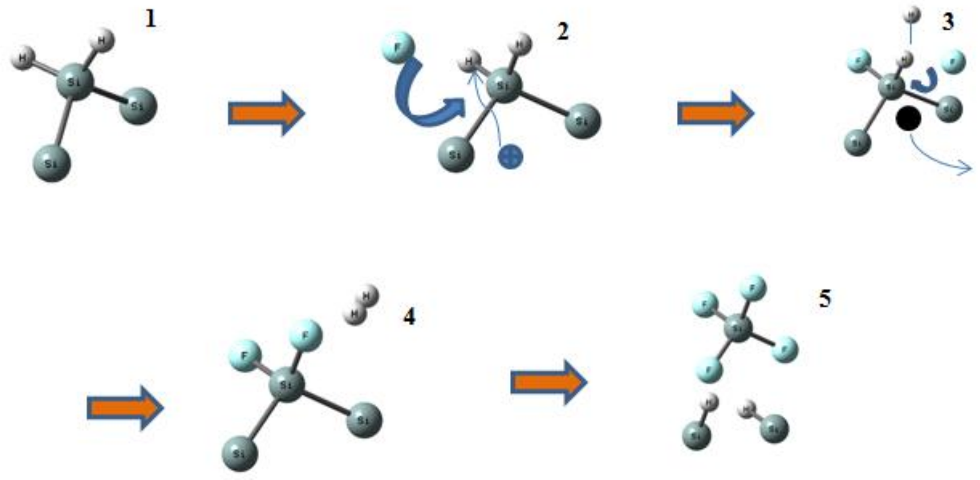

6

$$\boxed{Si + O_2 \rightarrow SiO_2},\ SiO_2 + 6\ HF \rightarrow SiF_6^{2-} + 2\ H^+ + 2\ H_2O$$

Figure 1.3 Mechanism of dissolution of c-Si-In the absence of electron hole, hydrogen saturated surface is protected from fluoride ions present in HF acid (1). When a hole reaches to the surface (2), HF attacks the Si-H bond and a Si-F bond is formed (3), other Si-H bond can be weakened by other holes (4). This further reduces the electron density of remaining Si-Si backbone atoms making them susceptible to be attacked by the HF acid (5). Secondary product silicon tetra-fluoride further reacts with HF acid to form highly stable SiF_6 ion [25]. Furthermore at the same time formation of SiO_2 is achieved that readily dissolved by HF acid (6).

Even though the exact dissolution mechanism is still questionable, the requirement of holes at silicon surface to initiate the reaction of pore formation is widely accepted. As p-type silicon have majority carrier as holes, there is no need of an additional illumination to generate electron/hole pair. On the other hand on n-type silicon substrate electrons are majority carriers and band bending at the interface blocks hole current [26]. As a result p-type silicon is frequently used to fabricate PSi samples because it does not require illumination. Anyway, the main limit of this type of substrate relies on the conical shape of the pores that limit the maximum aspect ratio achievable. On the other hand in case of n-type silicon pore formation and their quality strongly depend on illumination [25, 26]. However recent studies observed that pore formation on substrate with majority carrier concentration is above 10^{18} cm^{-1} can also be done in dark by applying high voltage (>5V) [27].

Nowadays many alternative approaches to the electrochemical etching are available to fabricate PSi from a crystalline silicon wafer such as the chemical vapor etching [28], the metal-assisted etching [29], and the ‘stain etching’ procedure [30]. But all these technique are either quite expensive or suffers of in-homogeneous etching compared to the classic method described in this thesis.

1.3 Sensing with PSi

Bio-sensors can be fabricated using a very large number of materials and structures [31]. Here below I list the most important examples of sensors realized in PSi. As mentioned above among all various available transduction techniques for a biosensor, PSi bio-sensor, electrochemical method and optical method, along with conductivity method are the most frequently used mechanisms of detection. Figure 1.4 resumes the most common type of PSi sensors.

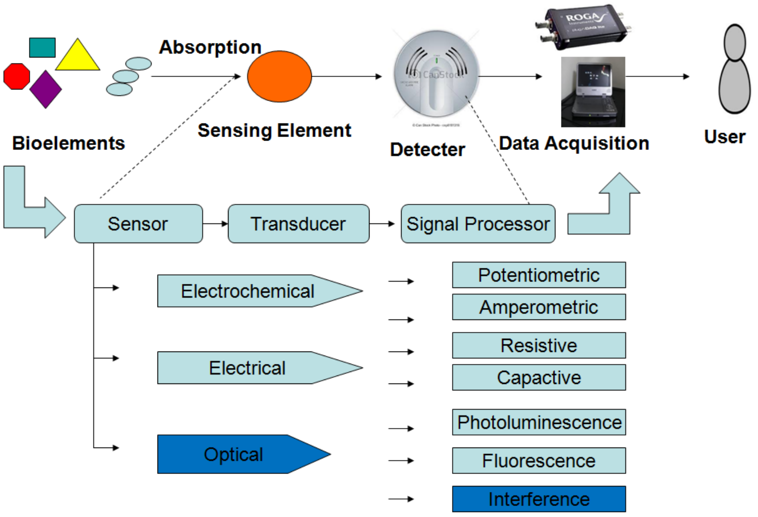

Figure 1.4-Different type of optical PSi bio-sensor according to their transduction mechanism

(1.3.1) PSi electrical and electrochemical-Biosensor

The very large specific surface together with the possibility to measure its electrical properties makes PSi an ideal material to fabricate electrical and/or electrochemical biosensors [32]. In a PSi electrical sensor, when an analyte/target species bind the PSi structure, it induces changes in its electrical resistance/capacitance that is read by appropriately contact the porous sponge. Various gas sensors are the example of electrical PSi sensor [33, 34].

Furthermore electrochemical biosensors are divided in two classes: Potentiometeric and Amperometric/Voltammetric biosensor [35]. In Potentiometric biosensors, the main parameter is the potential difference between the cathode and the anode in an electrochemical cell [36]. In this type of sensor, analyte concentration is related to the measured potential applied between the working and reference electrode [36, 37]. On the other hand, Amperometric and Voltammetric biosensors consider the redox reaction that takes place in the anodization cell, when an analyte of interest is added in the pores of PSi. The reaction causes a current to flow between the working and counter electrode and the amount of current is proportional to the concentration of analyte [38]. Urea sensors and gas sensors are the common examples of PSi based Potentiometeric and Amperometric/Voltammetric sensors [39, 40]. A systematic representation of electrochemical measurement setup is shown in Figure 1.5 [41].

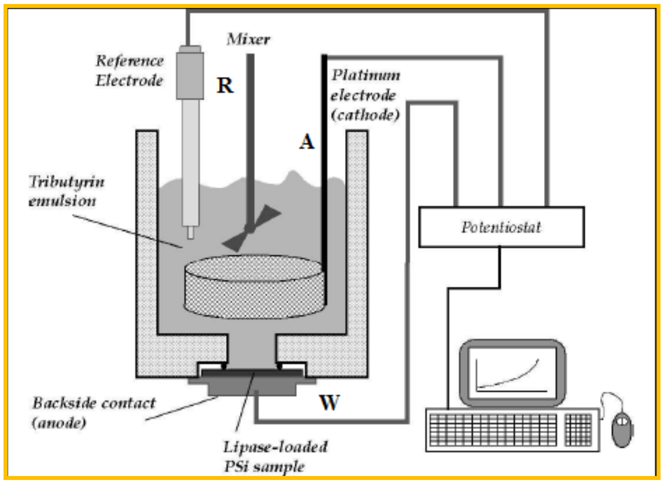

Figure 1.5-Typical measurement system for a PSi based electrochemical sensor, R is the reference electrode, A is other electrode (cathode) and w is working electrode using PSi membrane, Reaction of aqueous tributlyrin and lipase, butyric acid forms, that changes the pH of solution and measured by the variation of open circuit potential between reference electrode and cathode [41]

(1.3.2) PSi optical-Biosensor

The need to detect chemical and biological species very quickly and at very low concentration has stimulated a lot of research to develop highly sensitive PSi-optical biosensor device. The simplest class of PSi sensors determines the analyte concentration by measuring fluorescence signal intensity by a fluorescent marker molecule [42]. During the past years, these types of biosensors were well established in sensor technology, however they need the analyte of interest to be labeled and this fact makes the assay more complex. Hence nowadays label-free techniques attract more attention in sensor technology [43]. Taking the advantage of high sensitivity towards refractive index, in label-free PSi optical-biosensor, analyte detection is done by observing the changes in the optical properties of the sample either of the spectral interference pattern [44] or of the polarization/phase shift of the light [45]. The simplest type of optical-PSi sensor is made of a single layer. The interference pattern changes accordingly to the changes in refractive index due to the binding of the molecules. Despite its great simplicity, a single layer may show very high sensitivity [45]. Nevertheless the scattering of the light due to the porous structure heavily decreases the LoD achievable in PSi samples [45, 46]. Thus more complicated multi-layer and resonant structures can be etched by applying alternating current density during the electrochemical etching. This generates a periodic combination of refractive indexes that induces the formation of narrow resonances in predefined spectral positions [47]. The resonant wavelength is extremely sensitive to changes in the refractive index of the pores and is a well known mechanism of detection as shown in Figure 1.6 and Figure 1.7. This kind of structure offers a far better detection limit compare to PSi single layer based optical-Interferometric biosensor and detection limit can be pushed down to 0.3ng/mm^2 [48].

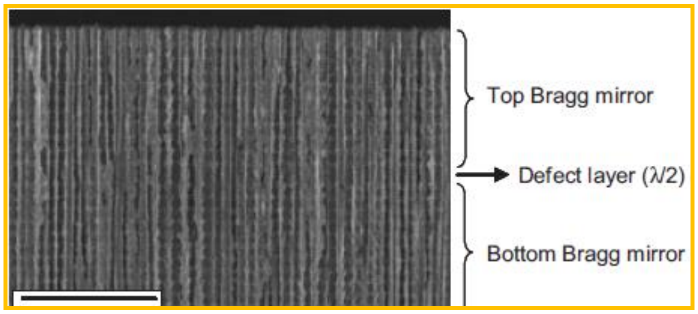

Figure 1.6- Cross-sectional SEM image of multi-layer structure (Scale bar 2µm) [48]

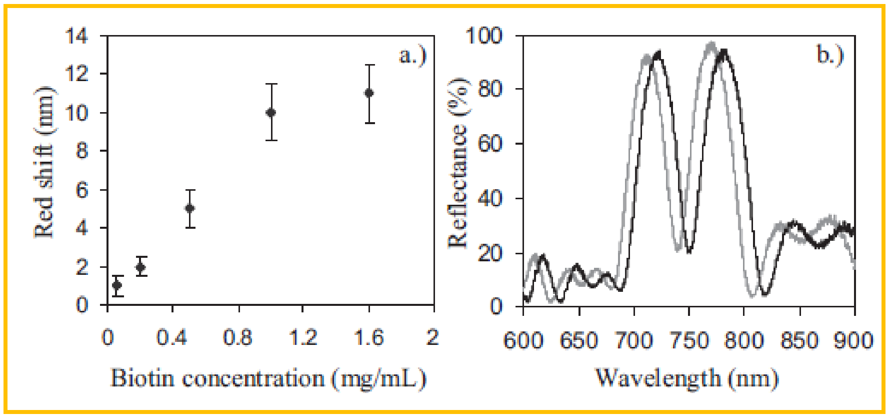

Figure 1.7- (a) Relation between resonance shift and analyte concentration and (b) 10nm resonance shift corresponding to addition of analyte~1mg/mL for multi-layer PSi structure due to change in refractive index within pore [48]

Another label-free approach based on waveguide for better accuracy, high sensitivity and less response time is proposed [49]. In this case PSi waveguide sensor consist two porous layers: a low-index, high porosity layer and a high-index, low porosity layer. The high index layer is the waveguide core (the light is confined here by total internal reflection.), while the low-index PSi layer (above the silicon substrate) works as a cladding and avoids the guided mode to couple with the underlying high index substrate. An incident light is coupled using a prism to the PSi waveguide. Incident light gives rise to an evanescent wave at the interface between the prism and the optical waveguide. At a certain specific incident angles (resonant angles) the propagation constant of the wave within the prism matches that of a waveguide mode. This matching produces a dip in the angular spectrum of the reflected light, so that each change in the refractive index of waveguide layer or any change in thickness at the surface produces a corresponding shift in the position of the dip. Figure 1.8 shows the porous silicon based waveguide sensor structure [50]. As these structures are quite thin and the optical signal is confined within a thin structure where analyte of interest is added, a high sensitivity is achieved [49, 50]. Theoretical studies suggest that this waveguide structure is ~ 60 times more sensitive than surface Plasmon resonance structure where a metal layer acts a resonant layer [51].

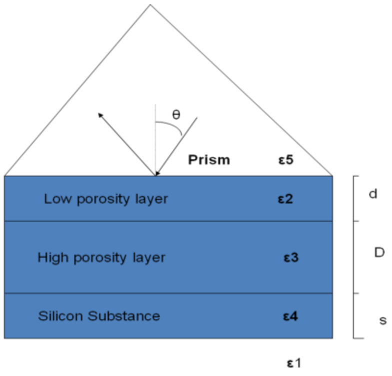

Figure 1.8- PSi based waveguide structure, low porosity layer of thickness d acts as a coupling layer while high porosity layer of thickness D acts as resonant layer [50].

1.4 Motivation of this thesis

Food allergy is one of the most common chronic diseases in all age group over world-wide [52]. In Europe about 6-8% (17 million people with 3.5 million younger than 25 years) of total population is affected by food allergies and occurrence is increasing. Furthermore many of youngsters and children having food allergy are suffering with life-threatening reaction as anaphylaxis [53]. Till now most of allergies are undiagnosed and are subject of self-help. Even though conventional methods for quantitative analysis of allergy are widely available which can identify reaction easily, they either required a few ml of blood and their analysis require a laboratory facility [54] or they are tested directly on the patient and may induce strong allergic reactions. Thus more research is needed to develop analytical strategies compatible with Point of Care (PoC) detection.

To develop an efficient bio-sensor for PoC a number of aspects needed to be considered, from the optical transduction signal to the fluidics design (a direct and effective sample injection method as in flow-through approach, reduces the sample consumption, increases the sampling rate and reduces the detection time) and the optimization of material (tunable pore size and specific area maximize the interaction between analyte and host matrix and increase the sensor sensitivity).

Motivated from above facts this study is a part of an European research project (called POSITIVE) that aims is to realize an ideal platform for fast photonic label-free smart disposable polarimetric biosensor that are able to exhibit a surface concentration detection limit (LoD) below 1 pg/mm^2 with fluidic structure able to incorporate multiple biosensors capable, through scalability, of determining 100s of different analyte with parallel references for each on-a-chip.

Currently most sensors are still attached to the substrate [55]. Because of this sensor require a complex microfluidic circuit to bring the analyte in contact with the active area and furthermore they cannot be washed effectively. This fact can reduce significantly the sensor response. The above mention problems can be solved using freestanding porous structure based bio-sensors, which can be easily fabricated from silicon substrates [56]. In addition PSi high surface area is further advantage to achieve such low LoD as 1pg/mm^2. However many random structural factors in the fabrication of PSi have great influence on sensing performance of a sensor. In particular, pore shape i.e. cone shaped or branched and surface roughness that induces light scattering/depolarization effects results in lower sensitivity of the device and poor fluidic properties [57]. Therefore, much careful effort is required to elucidate the interesting physics of PSi structure and its morphological effect.

As mentioned above p-type silicon substrate requires an easier etching setup because they do not need back illumination; on the other hand they have well known limitations for the maximum pore aspect ratio achievable [26, 27]. Even though these nanoporous samples have good optical transparency, their pores are too small to allow any efficient fluidics and cannot be used to fabricate LoC devices. However n-type Si substrate constitutes a reliable alternative because it allows the fabrication of with pore size in the range 100-200nm [47]. Their typical length scale and their high aspect ratio permit to maximize the interaction between the matrix and the bio-molecules while keeping a good optical transparency. Thus n-type Si can be used to fabricate high sensitivity and compact device compatible with flow through and microarray technology. On these substrates, we can etch straight and smooth pores having dimension lager as analyte size, by adjusting and controlling the different etching parameters [47, 58].

However such ideal porous structures are still limited due to the in-availability of freestanding membranes. Several articles were published on the fabrication of p-type PSi thin free-standing membranes (FSM) [26, 27, 56, 59]. But only very recently the fabrication of free standing porous layer on heavily doped n-type (0.001-0.003 Ωcm) silicon, has been reported for the first time. Their small pore size (<10nm) render them not compatible with flow-through devices [60].

During the thesis I optimized an etching protocol to fabricate free standing PSi membranes with straight and smooth pores of about 100nm diameter able to sustain liquid flow of about 1µl/minute. In collaboration with the University of Valencia we demonstrated that such n-type PSi membranes reach a sensitivity of around 1250nm/RIU and have long term stability [61]. We further improved the process to increases the pore size and at the same time to reduce the pore surface roughness and increases both the optical and the fluidic properties.

1.5 Structure of thesis

The thesis is organized as follows:

Chapter1 describes the perspective work and various issues of existing PSi based micro-fluidic technology and flow-through bio-sensor technology. Issues like sensitivity, sample volume, reproducibility and response time have been identified as crucial points of the sensor technologies. Factors affecting the possible use of PSi in sensor technology and their solutions are also discussed.

Chapter 2 describes the basic working principles of various characterization techniques and fabrication setup used for studied PSi structures. Different methods have been used for studying the morphology of the PSi samples such as scanning electron microscopy

(SEM) and atomic force microscopy (AFM). Moreover the optical properties of all fabricated samples (i.e. refractive index of the layers and spectral response) were analyzed using UV-VIS spectroscopy. Sensing measurements were performed using both a VIS-NIR spectrometer and a polarimeter. Chemical analysis of samples fabricated were performed using UV-VIS and FITR spectrometer and with Micro-Raman.

Chapter 3 reports the optimization for PSi fabrication and its morphological characterization. We found that the stable growth of smooth and straight pores in n-PSi is restricted to a narrow range of etching conditions; the lift off of the membrane is a self-limited process that does not require as large burst of current is required to detach the porous layer from the substrate, as generally done in case of p-type substrate. We describe an improved etching method that exploits two electrolytic solutions to fabricate PSi FSM with the desired thickness and able to fabricate micro, meso and macro-pores in moderately doped n-type silicon substrates (0.01-0.02 Ωcm). The method we propose opens new possibilities for the fabrication of flow-through sensors and membrane filters.

Chapter 4 describes the results obtained in the surface stabilization of PSi by thermal oxidation and chemical modification for both samples supported by a Si substrate and free standing membranes. As mentioned above that PSi internal surface provides a sensible interface that has to be stabilized against the environment. Otherwise modifications induced by the ageing of the samples can heavily affect the sensing properties and performance. The surface of freshly prepared PSi is strongly reactive with air and water, due to presence of unstable silicon hydride “Si-H” species that should be stabilized for future use. Different sets of samples were prepared and oxidized at different conditions in a dry environment. The oxide grown on the sample surface was thin enough to maintain the sample optical quality and, at the same time, avoid drift in the spectral response either after immersion in water for long time or storage in air for several weeks. A step towards the fabrication of bio-sensor, functionalization procedures performed showed that PSi surfaces can be effectively functionalized using different organic molecules, and with simple methods. Here we demonstrates that both polar and non-polar molecules can be used to this aim, their main difference of their use being that fresh etched samples have to be used in the case non-polar molecules, while aged or thermally oxidized PSi is required for the polar molecules. The reaction procedures considered here constitute efficient and versatile methods for modifying the surface of the PSi to provide an intermediate layer for the attachment of other functional groups. Bio-sensing efficiency is evaluated in next sequential chapters.

In *chapter 5*, we present a comparative study for MC sensor attached to silicon substrate versus free-standing MC. We investigate how the mass transport across the nano-porous structure influences the response due to non-specific signal by comparing flow-through versus flow-over geometries. Experimental results suggest that sensor on silicon/flow-over shows higher sensitivity (~0.9nm/mg) to "BSA" dose than free-standing sensor/flow-through (~0.4nm/mg) due to residue of protein/impurity that persists in pore. This result was verified by measuring similar samples in both flow through and flow over configuration, as well as their residual response after blockage of all their active sites. We also notice that sensors based on free standing membranes show similar results independently from the fact that mass transport is induced by either an external pressure source or simply by brownian motions. The present comparative analysis may serve as a set of design criteria to help engineers fabricate an efficient biosensor.

In *chapter 6,* an effort is directed towards more sensitive flow-capable polarimetric bio-sensor. This has been achieved through PSi free-standing membranes as discussed in *chapter 3* and results were compared with porous alumina membrane. Aim of this work is to explore these membranes potentially for efficient and high sensitive real time bio-sensor. PSi membranes of ~15µm thick with ~100nm pores and porous alumina membrane of ~60µm with ~200nm pores were used for real time bio-sensing. For anisotropic nature of these PSi and porous alumina membranes, they were characterized for both in-plane and out-plane birefringence. Both membranes show anisotropy with in-plane, originated due to their exposed surfaces that have irregular pores shape than perfectly circular one and out-plane birefringence increase with rotational angle with respect to incident light direction. Furthermore real time sensing is demonstrated for both porous alumina and PSi membranes. Both membranes show easy filtration of liquid through them. With polarimetric setup, sensitivity of about 0.32degree/NaCl% and 0.23degree/NaCl% for porous alumina and PSi membranes was observed. Even though both membranes have equal porosity ~50%, considering sensitivity per unit thickness (as porous alumina membrane is four time thicker than PSi membrane), PSi membrane shows higher sensitivity (0.0053degree/Nacl%-µm and 0.0148degree/NaCl%-µm) and preferable for bio-sensing than porous alumina membranes. The LOD/ µm ~$6.0*10^{-3}$ and $1.7*10^{-2}$ are observed for PSi and porous alumina FSMs respectively. Furthermore with these FSMs BSA sensing are demonstrated as model system for future LOC devices. The work presented in this thesis is summarized in *Conclusions*. Also the future scope of the present work for further study of materials is being discussed.

1.6 Summary of study

In this work we have proposed a PSi based flow through bio-sensor able to perform fast and sensitive real time analysis. The present work is summarized as:

1. We have presented a simple fabrication method for n-type PSi free-standing membranes with straight and smooth pores of up to ~100nm of diameter.

2. A two solution method is presented to fabricate free-standing porous membranes.

3. Our process maintains a very good planarity of the interface as demonstrated by the fabrication of very thin and large area free standing membranes. No HF concentration gradient effect is noticed.

4. We found that membranes detachment does not require a high current burst but it is a self-limited process that involves a thin transitional layer at the bottom of the porous region.

5. Covalent functionalization of silicon surface is found to be suitable used to stabilize the porous surface and to act as intermediate layer for binding of other bio-molecules.

6. Role of non-specific binding in sensing efficiency is analyzed by comparing flow over and flow-through sensing for sensor fabricated on silicon substrate and sensor in free-standing nature.

7. Real time sensitivity per unit length of 0.0053degree/NaCl% and 0.0148degree/NaCl% was observed respectively for porous alumina and PSi membranes and PSi was found more suitable and sensitive for bio-sensing applications.

References

[1]Yuqian Ren , Huimin Deng , Wei Shen and Zhiqiang Gao "A Highly Sensitive and Selective Electrochemical Biosensor for Direct Detection of MicroRNAs in Serum" Anal.Chem., *85* (9), pp 4784–4789 (2013)

[2]Sara Tombelli, Maria Minunni, Marco Mascini "Piezoelectric biosensors: Strategies for coupling nucleic acids to piezoelectric devices" Methods, 37, pp 48-56 (2005)

[3]R. Gabl, H.-D. Feucht, H. Zeininger, G. Eckstein, M. Schreiter, R. Primig, D. Pitzer, W. Wersing "First results on label-free detection of DNA and protein molecules using a novel integrated sensor technology based on gravimetric detection principles" Biosensors and Bioelectronics, 19(6) pp 615–620 (2004)

[4]Matthew A. Cooper "Optical biosensors in drug discovery" Nature Reviews Drug Discovery, 1, pp 515-528 (2002)

[5]T. Vo-Dinh, B. Cullum "Biosensors and biochips: advances in biological and medical diagnostics" Fresenius' Journal of Analytical Chemistry, 366 (6-7), pp 540-551 (2000)

[6]Ashok Mulchandani and Amarjeet S. Bassi "Principles and Applications of Biosensors for Bioprocess Monitoring and Control" Critical Reviews in Biotechnology, 15(2) pp 105-124 (1995)

[7]Lucilene Dornelles Mello, Lauro Tatsuo Kubota "Review of the use of biosensors as analytical tools in the food and drink industries" Food Chemistry, 77(2) pp 237-256 (2002)

[8]S. Rodriguez-Mozaz, M.-P. Marco, M. J. Lopez de Alda and D. Barceló "Biosensors for environmental applications: Future development trends" Pure Appl. Chem., 76(4), pp 723-752 (2004)

[9]Global Biosensors Market Is Expected to Reach USD 18.9 Billion in 2018 - Transparency Market Research, Albany, New York (PRWEB) July 12, (2013)

[10] Álvarez, J., Serrano, C., Hill, D., & Martínez-Pastor, J.," Real-time polarimetric optical sensor using macroporous alumina membranes" Optics letters, *38*(7), pp 1058-1060 (2013)

[11]Shashishekar P. Adiga, Chunmin Jin, Larry A. Curtiss, Nancy A. Monteiro-Riviere, Roger J. Narayan;" Nanoporous membranes for medical and biological applications" Nanomedicine and Nanobiotechnology, 1(5), pp 568–581 (2009)

[12]Ji-Ho Park, Luo Gu, Geoffrey von Maltzahn, Erkki Ruoslahti, Sangeeta N. Bhatia & Michael J. Sailor "Biodegradable luminescent porous silicon nanoparticles for in vivo applications" Nature Materials 8, pp 331 - 336 (2009)

[13]Victor S.-Y. Lin "Nanomedicine: Veni, vidi, vici and then... vanished" Nature Materials 8, pp 252 - 253 (2009)

[14]C. Pacholski, "Photonic Crystal Sensors Based on Porous Silicon," Sensors 13(4), pp 4694-4713 (2013).

[15]John A. Howarter and Jeffery P. Youngblood, "Optimization of Silica Silanization by 3-Aminopropyltriethoxysilane," Langmuir 22(26), pp 11142-11147 (2006).

[16]M. Hiraoui, M. Guendouz, N. Lorrain, A. Moadhen, L. Haji, M. Oueslati, "Spectroscopy studies of functionalized oxidized porous silicon surface for biosensing applications," Materials Chemistry and Physics 128(1-2), pp 151-156 (2011).

[17]L. Velleman, C. J. Shearer, A. V. Ellis, D. Losic, N. H. Voelcker, J. G. Shapter, "Fabrication of self-supporting porous silicon membranes and tuning transport properties by surface functionalization," Nanoscale 2(9), pp 1756-1761 (2010).

[18]Uhlir A. "Electrolytic shaping of germanium and silicon" Bell Syst.Tech. J., 35, pp 333–347 (1956)

[19]L. Canham "Silicon quantum wire array fabrication by electrochemical and chemical dissolution of wafers" Appl. Phys. Lett. 57, pp 1046 (1990)

[20]P. C. Searson, J. M. Macaulay, F. M. Ross, "Pore morphology and the mechanism of pore formation in n-type silicon," Journal Applied Physics 72(1), pp 253-258 (1992).

[21]V. Lehmann and U. Gösele "Porous silicon formation: A quantum wire effect" Appl. Phys. Lett. 58, pp 856 (1991)

[22]V. Lehmann and H. Foll "Formation Mechanism and Properties of Electrochemically Etched Trenches in n-Type Silicon" J. Electrochem. Soc., 137(2), pp 653-659 (1990)

[23]H. Ohji, P.J. French, K. Tsutsumi, "Fabrication of mechanical structures in p-type silicon using electrochemical etching" Sensors and Actuators A: Physical**,** 82(3), pp 254–258 (2000)

[24]Christopher C. Striemer, Thomas R. Gaborski, James L. McGrath and Philippe M. Fauche, "Charge- and size-based separation of macromolecules using ultrathin silicon membranes" *Nature* 445, pp 749-753 (2007)

[25]O. Bisi, Stefano Ossicini, L. Pavesi, "Porous silicon: a quantum sponge structure for silicon based optoelectronic" Surface Science Reports 38(1-3), pp 1–126 (2000)

[26]R. L. Smith and S. D. Collins, "Porous silicon formation mechanisms" J. Appl. Phys. 71, R1 (1992)

[27]H. Foll, M. Christophersen, J. Carstensen, G. Hasse, “Formation and application of porous silicon” Materials Science and Engineering: R: Reports, 39 (4), pp 93–141 (2002)

[28]Takao Yonehara, Kiyofumi Sakaguchi and Nobuhiko Sato, “Epitaxial layer transfer by bond and etch back of porous Si” Appl. Phys. Lett. 64, pp 2108 (1994)

[29]Ming-Liang Zhang, Kui-Qing Peng, Xia Fan, Jian-Sheng Jie, Rui-Qin Zhang, Shuit-Tong Lee and Ning-Bew Wong, “Preparation of Large-Area Uniform Silicon Nanowires Arrays through Metal-Assisted Chemical Etching” J. Phys. Chem. *C,112* (12), pp 4444–4450 (2008)

[30]Coffer J. L., "Porous silicon formation by stain etching", in Properties of Porous Silicon, Canham, L. T., Institution of Engineering and Technology, London, pp 23–28 (1997)

[31]Turner, Anthony; Wilson, George and Kaube, Isao (eds.) (1987). Biosensors:Fundamentals and Applications. Oxford, UK: Oxford University Press. pp 770

[32]Bakker, E. and M. Telting-Diaz, Electrochemical Sensors. Analytical Chemistry, 74, pp. 2781-2800 (2000)

[33]C Baratto, E Comini, G Faglia, G Sberveglier, G Di Francia, F De Filippo, V La Ferrara, L Quercia, L Lancellotti, “Gas detection with a porous silicon based sensor” Sensors and Actuators B: Chemical, 65 (1-3), pp 257–259 (2000)

[34]Mingda Li, Ming Hu, Peng Zeng, Shuangyun Ma, Wenjun Yan, Yuxiang Qin, “Effect of etching current density on microstructure and NH_3-sensing properties of porous silicon with intermediate-sized pores” Electrochimica Acta, 108 (1), pp 167–174 (2013)

[35]D. R. Thevenot, K. Tóth, R. A. Durst and G. S. Wilson, “Electrochemical Biosensors: Recommended Definitions and Classification” Pure Appl. Chem., 71 (12), pp 2333-2348 (1999)

[36]Mahir S. Ozdemir, Marcin Marczak, Hugo Bohets, Kristien Bonroy, Dirk Roymans, Lieven Stuyver, Koen Vanhoutte, Marcin Pawlak and Eric Bakker, “A Label-Free Potentiometric Sensor Principle for the Detection of Antibody–Antigen Interactions” Anal. Chem., 85 (9), pp 4770–4776 (2013)

[37]R.Ravi Kumar Reddy, Anju Chadha, Enakshi Bhattacharya,” Porous silicon based potentiometric triglyceride biosensor”, Biosensors and Bioelectronics, 16 (4-5), pp 313–317 (2001)

[38]Cosimino Malitesta , Francesco Palmisano , Luisa Torsi , Pier Giorgio Zambonin,” Glucose fast-response amperometric sensor based on glucose oxidase immobilized in an electropolymerized poly(o-phenylenediamine) film” Anal. Chem., 62 (24), pp 2735–2740 (1990)

[39]YUN Dong-Hwa, SONG Min-Jung, HONG Suk-In, KANG Moon-Sik, MIN Nam-Ki,” Highly sensitive and renewable amperometric urea sensor based on self-assembled monolayer using porous silicon substrate” Journal of the Korean Physical Society, 47, pp. S445-S449 (2005)

[40]Joseph R. Stetter, Jing Li,” Amperometric Gas Sensors－A Review”Chem. Rev., 108 (2), pp 352–366 (2008)

[41]Salis, A., Setzu, S., Monduzzi, M., & Mula, G.,” Porous silicon-based electrochemical biosensors. Biosensors-Emerging Materials and Applications”, pp 333-352 (2011)

[42]Frédérique Cunin, Thomas A. Schmedake, Jamie R. Link, Yang Yang Li, Jennifer Koh, Sangeeta N. Bhatia and Michael J. Sailor,” Biomolecular screening with encoded porous-silicon photonic crystal” Nature Materials 1, pp 39 - 41 (2002)

[43]Andrew Jane, Roman Dronov, Alastair Hodges, Nicolas H. Voelcker,” Porous silicon biosensors on the advance” Trends in biotechnology, 27 (4), pp 230–239 (2009)

[44]Victor S. Y. Lin, Kianoush Motesharei, Keiki Pua S. Dancil, Michael J. Sailor, M. Reza Ghadiri,” A Porous Silicon-Based Optical Interferometric Biosensor” Science, 278(5339), pp 840-843 (1997)

[45]Özkumur, E., Yalçın, A., Cretich, M., Lopez, C. A., Bergstein, D. A., Goldberg, B. B., & Ünlü, M. S.,”Quantification of DNA and protein adsorption by optical phase shift’, Biosensors and Bioelectronics, 25(1), pp 167-172 (2009)

[46]M. E. Kompan, J. Salonen, and I. Yu. Shabanov,” Anomalous Birefringence of Light in Free-Standing Samples of Porous Silicon” Journal of Experimental and Theoretical Physics, 90(2), pp 324–329 (2000)

[47]Nee, S. M. F.,”Depolarization and retardation of a birefringent slab”, .JOSA A, 17(11), pp 2067-2073 (2000)

[48]H. Ouyang, M. Christophersen, R. Viard, B. L. Miller and P. M. Faucher, Adv. Funct. Mater,. 15, pp 1851 (2005)

[49]Optical DNA sensing based on resonant porous silicon structures", Proc. SPIE 6477, Silicon Photonics II, 647717 (February 09, 2007)

[50]Porous waveguide in the Kretschmann configuration for small molecule detection", Proc. SPIE 7322, Photonic Microdevices/Microstructures for Sensing, 732205 (April 29, 2009)

[51]Jarkko J. Saarinen, Sharon M. Weiss, Philippe M. Fauchet, and J. E. Sipe,” Optical sensor based on resonant porous silicon structures” OPTICS EXPRESS, 13(10) pp 3754 (2005)

[52]Hugh A Sampson, MD,” Update on food allergy” Journal of Allergy and Clinical Immunology, 113(5), pp 805–819 (2004)

[53]Thisanayagam Umasunthar, Jo Leonardi-Bee, Matthew Hodes, Paul J. Turner, Claudia Gore, Parviz Habibi, John O. Warner, Robert J. Boyle,” Incidence of fatal food anaphylaxis in people with food allergy: a systematic review and meta-analysis” Experimental Allergy, 2013 DOI: 10.1111/cea.12211

[54]R. E. Poms, C. L. Klein and E. Anklam,” Methods for allergen analysis in food: a review” Food Additives & Contaminants,21 (1),pp 1-31 (2004)

[55]H. Zhang, Z. Jia, X. Lv, J. Zhou, L. Chen, R. Liu, J. Ma, “Porous silicon optical microcavity biosensor on silicon-on-insulator wafer for sensitive DNA detection,” Biosensors and Bioelectronics 44(1), pp 89-94 (2013)

[56]C. S. Solanki, R. R. Bilalov, J. Poortmans, J. -P. Celis, J. Nijs and R. Mertens,” Self-Standing Porous Silicon Films by One-Step Anodizing” J. Eletrohem. Soc. 151 (2004) C307

[57]Soe-Mie F. Nee,” Depolarization and retardation of a birefringent slab” JOSA A, 17(11), pp 2067-2073 (2000)

[58]S. Matthias, F. Müller, J. Schilling, U. Gösele,” Pushing the limits of macroporous silicon etching” Applied Physics A, 80(7), pp 1391-1396 (2005)

[59]M. Ghulinyan, C. J. Oton, G. Bonetti, Z. Gaburro, L. Pavesi, “Free-standing porous silicon single and multiple optical cavities,” Journal of Applied Physics 93(12), pp 9724-9729 (2003).

[60]Yanjun Xiao, Xiaopeng Li, Han-Don Um, Xuejiao Gao, Zhongyi Guo and Jung-Ho-Lee,” Controlled exfoliation of a heavily *n*-doped porous silicon double layer electrochemically etched for layer-transfer photovoltaics” Electrochimica Acta 74, pp 93 (2012)

[61]J. Alvarez, N.Kumar, P. Bettotti, D. Hill, J. Martinez-Pastor, "Phase-Sensitive Detection for Optical Sensing With Porous Silicon,” IEEE Photonics Journal 4(3), pp 986-995 (2012)

Chapter 2

Fabrication and Experimental Techniques

2.1 Introduction

In this chapter, we will discuss the basics working principle of the fabrication and characterization techniques used during the present work.

2.2 Sample fabrication

In this section we describe in detail all the elements that compose the fabrication system and how they affect the quality of PSi samples.

2.2.1 Electrochemical cell

The electrochemical cell is an important part of the fabrication because the homogeneity and quality of the PSi samples depends on its structure. Based on literature survey the most common type of cell that has been used for the fabrication process is a cylindrical cell with the sample placed at its bottom [1]. The cell body is made of Teflon and shaped in a cylindrical-section to avoid electric field in-homogeneities due to edge effects. Teflon is chosen because it is a highly acid-resistant polymer [2].

In this type of cell silicon wafer is located at the bottom of the cell, as can be observed in the diagram of Figure 2.1. The silicon wafer acts as the anode and its back-side is modified by ion implantation and aluminum deposition to improve the *Ohmic* contact. The front side of the wafer is sealed with an O-ring, so that only this part of the wafer surface is exposed to the electrolyte solution. Platinum grid acts as cathode. The electrolyte solution contains hydrofluoric acid in 48% aqueous solution diluted in water or ethanol at different concentrations [3]. To get homogeneous porous structure magnetic stirrer was used to mix the electrolyte solution during the etching. For aqueous hydrofluoric solution the stirrer was used at slow speed because the surfactant (Triton) tends to form bubbles that stick at the cathode and enhance the in-homogeneity in PSi samples.

The sample homogeneity of PSi layers obtained with this electrochemical cell is pretty good as demonstrated by the homogeneous color of the etched area and by the straight and smooth interface viewed in cross section SEM images shown in Figure 1.2 of *Chapter 1*.

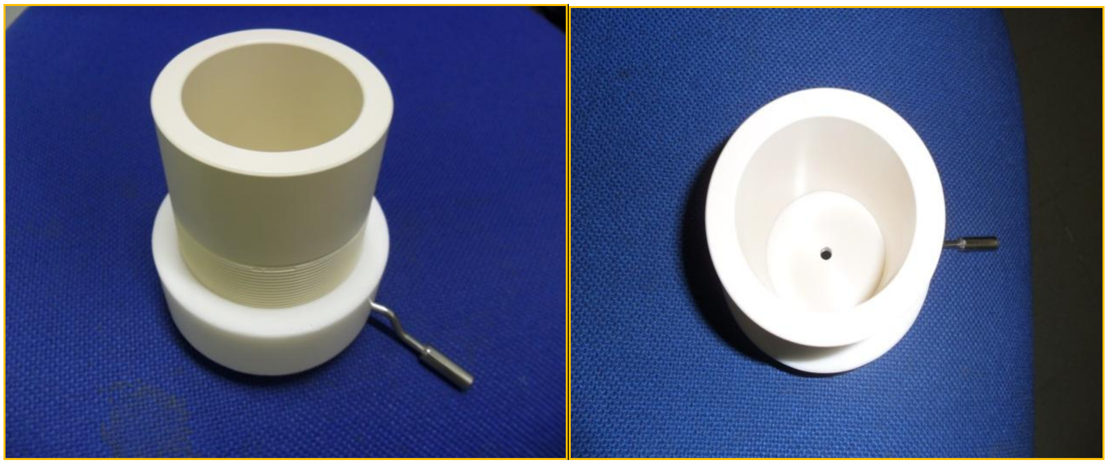
(a) (b)

Figure 2.1-Optical photograph of electrochemical Teflon cell used to fabricate PSi structures (a) side view of the cell (b) top view of the electrochemical cell. In the center, the hole represents the Si area exposed electrolytic solution. In the bottom metallic connector is used to connect with metallic plate attached with Si wafer

2.2.2 Programmable constant current source

Figure 2.2 shows the scheme of the etching setup employed for the fabrication of PSi samples. A programmable current/voltage source (Keithley, 2400-Meter, SourceMeter) is used. The whole system is controlled by software that continuously monitors and registers both current and voltage. These data are used to control the reproducibility of the etching.

The software is controlled by an input file. This is a text delimited file defined by the user that lists and the duration time of each step and applied current. The output file registers the time duration, the applied current and the measured voltage.

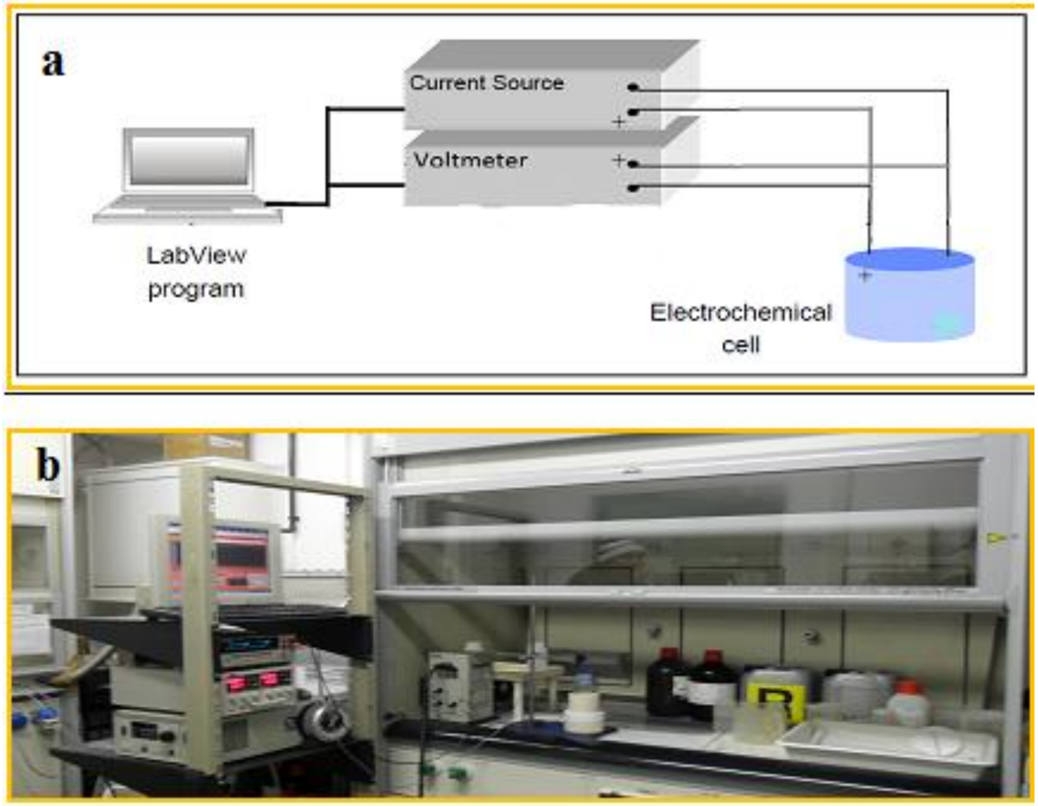

Figure 2.2 (a) Sketch diagram of all elements involved in chemical etching of Si. Specific voltage or current is forced to flow between two electrodes and visualize on computer screen (b) Optical photograph of electrochemical setup used to fabricate PSi structures

2.3 Characterization techniques

2.3.1 UV-VIS spectroscopy

The optical properties of the fabricated sample are closely related to the porous structure [4]. UV-VIS Spectroscopy is a versatile and a non-destructive technique that reveals detailed information about the porous structure [5]. In fact the spectral information collected is related to the values of the optical path (i.e. the product between the physical layer thickness and its refractive index) of the layers that compose the PSi sample and are used to optimize the etching process and to check the quality of the sample [6].

General principle

UV-VIS spectroscopy on PSi thin film is typically used to analyze the interference phenomena which the thin film creates [7]. PSi sample consist of single or multi porous thin layers that creates interface effects. When a light wave is transmitted/reflected to the porous thin layers, on the optical boundaries of thin porous layers, a portion of light is transmitted/reflected results two or more light wave interact each other. The light waves that are in phase go to constructive interference, while the light wave that is in out phase goes to destructive interference. Superposition of these light waves generates an interference (fringe) pattern due to their wave nature; the mechanism of interference generation is shown in Figure 2.3. Furthermore the quality of the interference of porous layer depends on the thickness of layers, their refractive index difference, the number of layers and how smooth their interface is. For a single layer sample, depending on layer thickness/phase shift induced by layer, the interference pattern varies from sample to sample and can be used to determine basic sample optical properties [7, 8]. For a single thin layer, the interference pattern directly depends on its refractive index and its thickness. Once one of the two is known, the other can be calculated. These measurements are typically performed to optimize the etching process. The following expression relates the different quantities [8];

$$\boxed{d = \frac{m}{2D_n\sqrt{(n^2 - \sin^2\theta)}}}$$

Where d is the thickness of porous layer, n is its refractive index, θ is the angle of light incidence, m is number of fringes observed and D_n is wave-number region used.

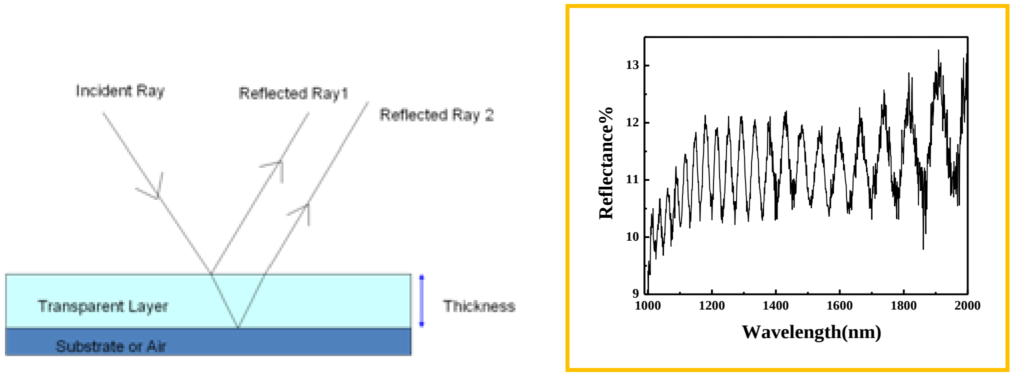

(a) (b)

Figure 2.3 (a)Interference developed by PSi structure; for an air and thin porous layer, two reflected beam, one from top surface and other from the interface of porous layer and silicon substrate interact with each other resulting an interference pattern: in the right is generated (b)

2.3.2 <u>FTIR and micro-Raman Spectroscopy</u>

As discussed in *Chapter1* that sensing properties of PSi strongly depends on its quality of porous structure i.e. refractive index that depends on the molecules attached in pores. In fact if chemical method is used to stabilize PSi against environment or undesired aging effect, one need to confirm about a proper coverage of the porous surface by the molecules attached [9]. In this sense Infra-Red Spectroscopy is an extremely reliable fingerprinting method for the analysis of proper attachment of chemical compounds to PSi wall surface [10]. Both FTIR and micro-Raman technique are used to obtain spectra of various organic molecules used to stabilize PSi surface [11]. In this study micro-Raman is preferred over FTIR technique as many compounds are not IR active. Furthermore there is no need to take a special care for sample preparation and very small sample i.e. micro dimension can be analyzed with greater accuracy [11, 12].

2.3.2.1 General principle of FTIR

FTIR is an absorption measurement of IR frequency by the sample [10]. Absorption by different functional groups in the infrared region results in changes in vibrational and rotational status of the molecules. The absorption frequency depends on the vibrational frequency of the molecules, whereas the absorption intensity depends on many factors including absorption cross-section (larger the absorption area, larger IR signal), phase state of sample and integration time that defines how effectively the infrared photon energy is transferred to the molecule [10, 13]. Furthermore, a molecule will absorb infrared light only if the absorption causes a change in the dipole moment [13].

In PSi case, analysis is carried out in a wavelength interval 200-4000cm^{-1} along both sample cross-section and top surface. The species of interest have typical characteristic absorptions like those listed below [13]

3700-2500 cm^{-1}	X-H Stretching (X=C, N, O and S)
2300-2000 cm^{-1}	C=X Stretching (X=C or N)
1900-1500 cm^{-1}	C=X Stretching (X=C, N and O)
1300-800 cm^{-1}	C-X Stretching (X=C, N and O)

2.3.2.2 General principle of micro-Raman

As discussed above, rather than direct absorption as in FTIR spectroscopy, micro-Raman works on the principle of scattering of monochromatic light [14]. The incident monochromatic photon interacts with electron cloud of molecules and further goes either elastic (Rayleigh scattering) or inelastic scattering (Raman scattering). During this process energy is exchanged between photon and molecule results the scattered photon may have energy lower or higher than the incident photon [15]. The Raman shift in energy is the measurement of the vibration energy of molecule. A complex molecule may have many vibrational modes and Raman intensity versus Raman shift gives Raman spectrum, which is characteristic of each individual material and can be used to identify its structure. For a Raman active material, the net molecular polarizability must be changed. Moreover as most of the photons collide with molecules with no change in their energy than Raman scattering as a result very small signal is observed. However this problem is solved using a monochromator with two or three dispersion stage. Furthermore since the discovery of Raman spectroscopy a large effort have been made to develop this technique.

Raman spectroscopy combined with microscopy named as micro-Raman uses 180 degree sample geometry with an optical microscope [16]. In this technique laser beam is focused on the sample with an optical microscope objective that limit the exposed area to its diffraction limit, hence spectra can be collected from a small ~1µm dimension. Employing backscattering, Raman signal form the sample is collected by the same microscope objective and a detection limit of nano-grams with molecular selectivity can be achieved. Furthermore confocal microscopy enhances its efficiency and now micro-Raman has become one of the most analytical tools to have fingerprint of material in industry and in research applications.

In this study FTIR and micro-Raman technique is used to examine the attachment of bio-molecules in the pores used for surface stabilization of PSi surface against undesired oxidation.

2.3.3 Atomic Force Microscopy

Atomic Force Microscopy (AFM) finds widespread application in surface sample analysis [17]. With this technique surface roughness and topographic image are acquired. In case of Optical properties of PSi layer that strongly depend on its microstructure and its topographical structure, AFM plays an important role. Thus AFM analysis is to be examined to identify surface topography of PSi samples. Surface morphology and roughness of porous samples were investigated using Atomic Force Microscopy (AFM, NTMDT mod. P47H) working in contact mode.

General principle

Binning et al. in 1986 was invented the atomic force microscopy (AFM) [18]. A sharp tip is attached to a cantilever. Due to either attractive or repulsive forces of interaction between tip atom and sample surface atom causes positive or negative bending of cantilever which is monitored by a laser beam deflection. A schematic block diagram of an AFM is shown in Figure 2.4.

AFM works in three main modes [19]:

1**. Contact Mode**: In this mode AFM tip makes a soft physical contact with the surface of the sample and deflection in cantilever is proportional to the surface topography.

2. Non Contact Mode: In this mode the interaction between the tip and the sample is minimized. In this mode the tip does not contact the sample surface.

3. Tapping Mode: In tapping mode the cantilever tip is forced to oscillate at a constant resonance frequency.

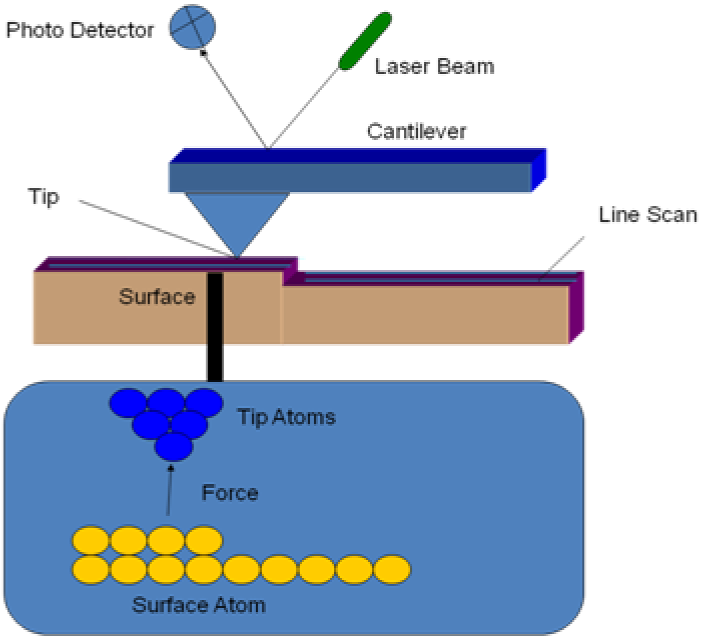

Figure 2.4 Block diagram of AFM set up; Atomic force induces an interaction between sample surface atom and tip atoms, results in scanning the surface, incident beam is reflected as per surface morphology, laser beam from cantilever is mapped to image surface topography

2.3.4 Optical Polarimetry

The rotation of light, when passed through a substance raised a keen interest since long time [20]. Optical polarimetry is a very sensitive and non-destructive technique to measure the light rotation produced by organic and non-organic substances [21]. These types of substances are said optically active and when properly aligned to respect the incident light, can be used to rotate the light polarization [21, 22]. PSi is a highly birefringent material and is of interest in polarimetry based optical detection [22]. Optical polarimetric characterization of the PSi layers was done by in-line, quarter wave plate based polarimeter (PAX5710-T THOR LAB.). The complete setup of optical polarimeter for PSi samples is shown in Figures 2.5 and Figure 2.6.

General principle

As many crystalline materials have complex crystal structure rather than simple cubic structure and this complex arrangement may induce different refractive index corresponding to different crystallographic directions [23]. Such materials that have non-uniform spatial distribution of optical properties are known as birefringent materials i.e. calcite and PSi. These materials are further characterized as uniaxial, biaxial material depending on directions along which optical isotropy is maintained [23, 24]. In simplest case uniaxial birefringent material; optical properties in directions perpendicular to optics axis of sample are different due to difference in refractive index in these directions. If the incoming light wave is along this optical axis of the sample, the two polarization components, ordinary and extra-ordinary mode, do not feel any change in refractive index; hence no phase change is observed. As the angle of incidence of light with respect to sample optic axis is changes, the effective refractive index and optical path length changes for ordinary and extra-ordinary light. As a result when the incident beam cross-over the sample these two light beam superimpose and generate a light beam of different degree of polarization than incident light beam. The observed phase shift between two polarization components of incident light, increases as incident angle increase with respect to its optical axis. The phase shift ($\Delta\phi$) between these two components can be written as:

$$\Delta\phi(\lambda) = \frac{2\pi}{\lambda} \cdot d \cdot \Delta n(\lambda)$$

λ is the incident wavelength of light, d the PSi membrane thickness and $\Delta n(\lambda)$ its birefringence.

The optical polarimetric instrument used for characterization of all samples was composed by an input laser source, a polarizer to have a well defined polarization state, a quarter wave-plate, an analyzer and a photodiode. Quarter wave-plate combined with analyzer is used to analyze the state of incoming laser beam. If quarter wave-plate have fast axis parallel to analyzer axis and incoming light beam is linearly polarized as a result the out-beam will be linear polarized. The light transmitted to photo diode is converted into current that is proportional to the optical power and is further analyzed by software. Furthermore for the same if in-coming beam phase is modified i.e. 45degree by birefringent sample, the transformed output beam will be circularly polarized. As a result of fixed axis of quarter wave plate and the analyzer, photon transferred to photodiode will be different hence current observed will be different. In conclusion for each change in phase of incoming beam, a different current will be observed due to quarter wave plate fixed axis and optical phase state of light is calculated by software.

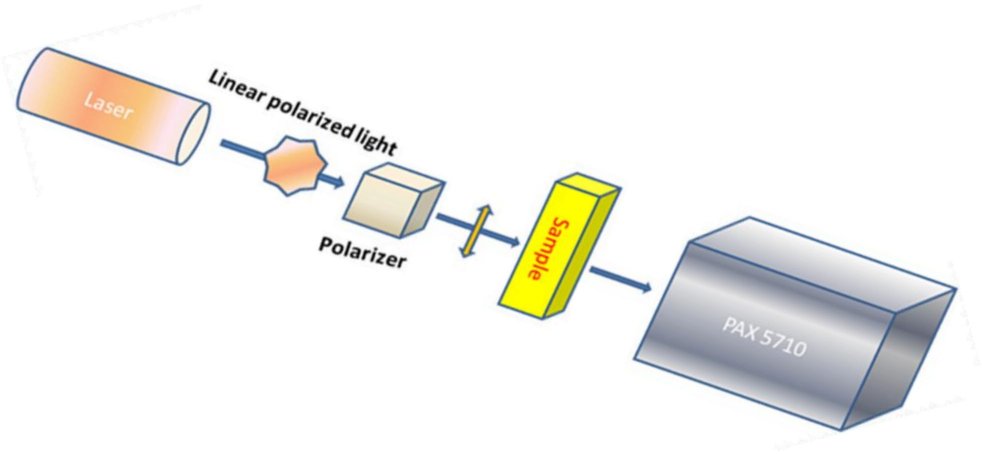

Figure 2.5 Measurement setup for polarimetric experiment

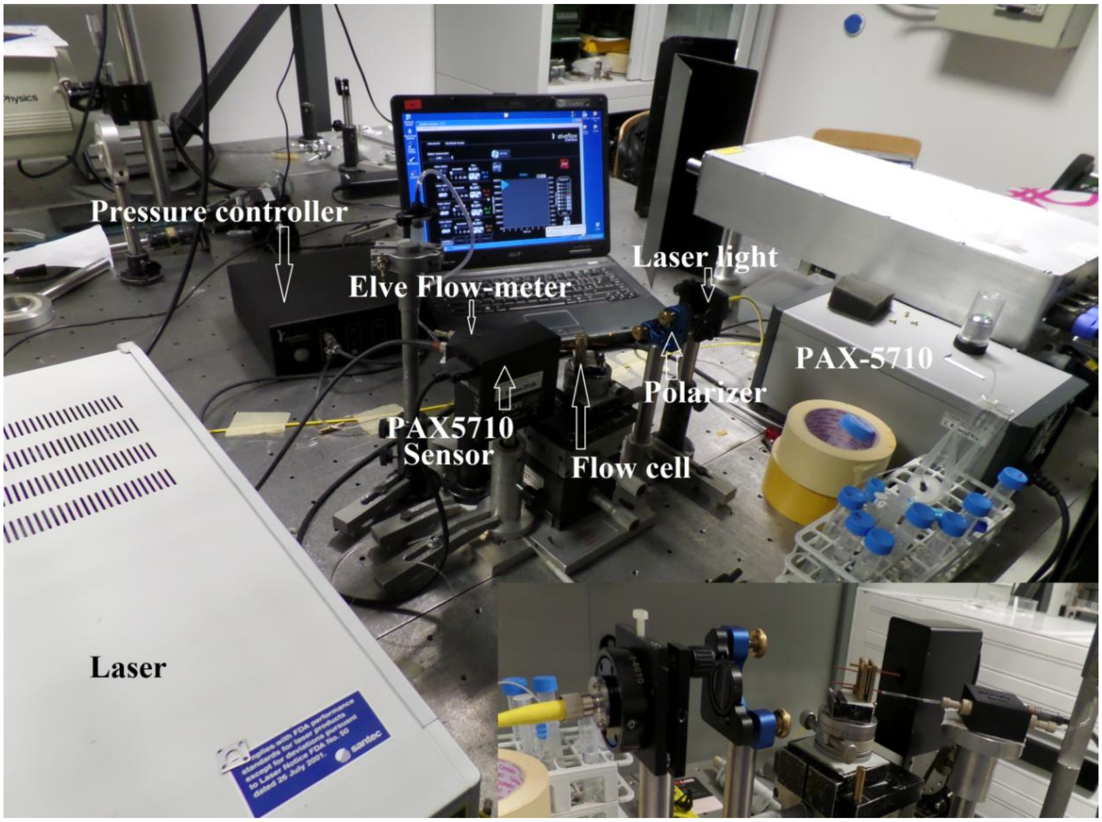

Figure 2.6 Optical photograph of measurement setup for polarimetric experiment with fluidic setup, below in the figure, a zoom of setup is shown.

References

[1]Ying Kang and Jacob Jorné,” Morphological Stability Analysis of Porous Silicon Formation”, J. Electrochem. Soc., 140(8), pp 2258-2265 (1993)

[2] Föll, H., Christophersen, M., Carstensen, J., & Hasse, G.,”Formation and application of porous silicon”, Materials Science and Engineering*: R:* Reports, *39*(4) pp 93-141 (2002)

[3]R. Memming, G. Schwandt,” Anodic dissolution of silicon in hydrofluoric acid solutions”, Surface Science, 4(2), pp 109–124 (1966)

[4]Richard A. Bley, Susan M. Kauzlarich, Jeffrey E. Davis and Howard W. H. Lee,” Characterization of Silicon Nanoparticles Prepared from Porous Silicon”, Chem. Mater.*, 8* (8), pp 1881–1888 (1996)

[5]V. Agarwal and J. A. del Río,” Tailoring the photonic band gap of a porous silicon dielectric mirror”, Appl. Phys. Lett. 82, pp 1512 (2003)

[6]Andreas Janshoff, Keiki-Pua S. Dancil, Claudia Steinem, Douglas P. Greiner, Victor S.-Y. Lin, Christian Gurtner, Kianoush Motesharei, Michael J. Sailor and M. Reza Ghadiri,” Macroporous p-Type Silicon Fabry−Perot Layers. Fabrication, Characterization, and Applications in Biosensing”, J. Am. Chem. Soc., *120* (46), pp 12108–12116 (1998)

[7]J C Manifacier, J Gasiot and J P Fillard,” A simple method for the determination of the optical constants n, k and the thickness of a weakly absorbing thin film”, J. Phys. E: Sci. Instrum., 9, pp 1002 (1976)

[8]B Gauthier-Manuel,” Simultaneous determination of the thickness and optical constants of weakly absorbing thin films”, Meas. Sci. Technol., 9, pp 485 (1998)

[9]Rabah Boukherroub, J. T. C. Wojtyk, Danial D. M. Wayner and David J. Lockwood,” Thermal Hydrosilylation of Undecylenic Acid with Porous Silicon”, J. Electrochem. Soc., 149(2) pp H59-H63 (2002)

[10]Shih Song Cheng, Daniel A. Scherson, Chaim N. Sukenik,” In situ observation of monolayer self-assembly by FTIR/ATR*”,* J. Am. Chem. Soc., 114 (13), pp 5436–5437 (1992)

[11]H. D. Fuchs, M. Stutzmann, M. S. Brandt, M. Rosenbauer, J. Weber, A. Breitschwerdt, P. Deák, and M. Cardona,” Porous silicon and siloxene: Vibrational and structural properties”, Phys. Rev. B, 48, pp 8172–8189 (1993)

[12]Y. H. Seo, H.-J. Lee, H. I. Jeon, D. H. Oh, K. S. Nahm, Y. H. Lee, E.-K. Suh, H. J. Lee and Y. G. Kwang," Photoluminescence, Raman scattering, and infrared absorption studies of porous silicon", Appl. Phys. Lett., 62, pp 1812 (1993)

[13]Johnston, C. T.; Aochi, Y. O.," Fourier transform infrared and Raman spectroscopy", Methods of soil analysis. Part 3 - chemical methods. pp. 269-321 (1996)

[14]Di Peter Larkin," Infrared and Raman Spectroscopy; Principles and Spectral Interpretation", (2011)

[15]George Turrell and Jacques Corse," Raman Microscopy: Developments and Applications", (1996)

[16]Jian Ling, Steven D. Weitman, Michael A. Miller, Rodney V. Moore, and Alan C. Bovik," Direct Raman Imaging Techniques for Study of the Subcellular Distribution of a Drug", Applied Optics, 41(28), pp 6006-6017 (2002)

[17]JC Vickerman and IS Gilmore," Surface analysis: the principal techniques", Wiley Online Library (2009)

[18] Binnig, G., Quate, C. F., & Gerber, C.,"Atomic force microscope",Physical review letters, *56*(9), pp 930 (1986)

[19]Meyer, E. R. N. S. T.," Atomic force microscopy",Progress in surface science, 41(1), pp 3-49 (1992)

[20]John A. Schellman," Symmetry rules for optical rotation", Acc. Chem. Res., 1 (5), pp 144–151 (1968)

[21]D. Hill," Advances in Nanophotonic Sensing Technologies During Three International Label-Free Lab-On-Chip Projects", BioNanoScience, 1(4), pp 162 (2011).

[22]J. Alvarez, N.Kumar, P. Bettotti, D. Hill, J. Martinez-Pastor, "Phase-Sensitive Detection for Optical Sensing With Porous Silicon," IEEE Photonics Journal 4(3), 986-995.

[23]Jesús Álvarez, Paolo Bettotti, Isaac Suárez, Neeraj Kumar, Daniel Hill, Vladimir Chirvony, Lorenzo Pavesi, and Juan Martínez-Pastor," Birefringent porous silicon membranes for optical sensing", Optics Express, 19(27), pp. 26106-26116 (2011)

[24]W. Kaminsky and A. M. Glazer," Measurement of optical rotation in crystals", Ferroelectrics, 183(1), pp 133-141 (1996)

Chapter 3

Fabrication and physical properties of free-standing membranes

3.1 Introduction

PSi has gained remarkable attention due to its easily tunable optical properties and proves it's self as a potential candidate for optical sensor [1, 2, 3, 4]. The simple fabrication method, its bio-compatibility and flexibility in tuning its refractive index/porosity, makes it a suitable and promising platform for bio-sensing applications [5]. Furthermore the fabrication of free standing membranes (FSM) permits to exploit the flow through approach and to achieve multi spot analysis on a microarray configuration. Unfortunately the release of free standing membranes is easily achieved on p-type silicon but this type of substrate allows for the fabrication of layer of limited thickness because of the lateral pore growth [6].

On the other hand n-type PSi structures provide an alternative material in which macro-pores larger than 50nm can be realized, while keeping high pore aspect ratio and smooth inner pores surface [7]. This is the ideal structure to fabricate high sensitivity devices and to achieve an efficient filtration of bio-molecules in flow through devices [8].On n-type substrates; we can etch pores with dimension in the range 50nm to 200nm by adjusting and controlling the different parameters (i.e. silicon wafer resistivity, concentration of HF solution, current density, anodization time [9]). The pore formation on these substrates is partially explained by different models. One of the most used is the so called "space charge region" (SCR) model by which pore size and pore spacing are defined by the space charge layer created at the silicon-electrolyte junction [10, 11]. However SCR model cannot explain several of the pore morphologies which can be etch in PSi (e.g the branched structure, when pore grows in <113> direction). Another model is the "Current burst model" (CBM) that essentially explains the fabricated PSi as a balance between chemical and electrochemical dissolutions of Si [10, 12]. This model is frequently used to explain the fabricated porous structure with electrolytic solution that contains oxidizing agent in addition to increase its pore size. Christophersen et al. and Harraz et al. reported the fabrication of macroporous structure on n-type substrate with electrolytic solution that contains CrO_3 and $KMnO_4$ as an oxidant and explains the fabricated porous structure on the basis of CBM [13, 14]. In same line D.H.Ge et al. demonstrated the fabrication of macro pores with another oxidizer H_2O_2 with a growth speed up to 1800µm/hour [15]. Furthermore by modifying electrolytic solution (HF/H_2O_2/ethanol), authors were able to fabricate smooth macro-pores, branched meso-pores and spongy micro-pores on this silicon substrate [16].

Unfortunately FSM with macroporous structure are difficult to fabricate and no reports were published about their fabrication via electrochemical etching method. Recently Striemer et al. demonstrated the fabrication and filtration of bio-molecules through 10nm thin PSi FSM having pore size ~ 5-25nm [17]. Even more Hassan et al. fabricated ultra thin PSi membrane (1µm, 5µm and 10µm) using xenon difluoride-base isotropic dry etching method [18]. Various available technical approaches as electron-beam lithography combined with side wall transfer process or thermal annealing of ultra-thin amorphous silicon were proposed to produce mesoporous FSM as alternative to the electrochemical etched PSi, but they all involve complex and multistep methods with limited tunability in term of porous structures attainable [19, 20]. Hence a simple technique to fabricate macroporous self-supporting PSi membranes has to be developed.

As, it is well known that in highly doped p-type silicon wafer, it is quite easy to fabricate partial or complete detached FSM using electrochemical etching using and applying a high bust of current at the end of the process [1]. *To the best of our knowledge, there is no report about the fabrication of high quality free standing membranes having structure~100-200nm on n-type silicon substrate using simple electrochemical etching method.* The goal of this chapter is to describe the optimization we have performed to achieve a robust and reliable process to fabricate thin micro/meso/macro-porous silicon membranes with tunable pore size and thickness by optimizing the correct etching parameters and conditions i.e. solution and current density.

3.2 Experimental Details

N-type silicon wafer with resistivity of either 0.1 Ω-cm or 0.01 Ω-cm were used as the initial study material. Wafers were oriented along the [100] direction and one side polished. PSi layers and free standing membranes were prepared by electro chemical etching method. The anodization was performed at room temperature in the absence of light and computer controlled current source was used to have a precise control over applied current density as described in experimental *chapter 2*. After fabrication of porous samples, all samples were rinsed in ethanol and dried in N_2 flow. For structural morphology of PSi structures, high-resolution scanning electron microscopy (SEM, JEOL mod. JSM 7401F) studies were also performed.

3.3 Results and discussions

3.3.1 <u>Effect of Silicon wafer resistivity</u>

It is well known that several parameters such as doping concentration and crystal orientation of the substrate, electrolyte composition, applied current density and etching time play an important role in structural morphology of PSi [8-12, 21]. Silicon wafer resistivity is one of the most influencing parameter, which directly affects the homogeneity, porosity, strength/hardness, pore size, thickness of detached membrane and etch rate of porous layer. As well known partially and completely detached membranes having pore size ~ 40-50nm can be easily achieved on p-type silicon wafer (0.01Ωcm (100) aligned) followed by subsequent high applied burst current [1, 22, 23]. On the other hand, n-type silicon wafer can produce a large variation in pore size depending on wafer resistivity and electrolyte solution.

As we aimed to fabricate, macropores of about 100-200nm diameter we choose two types of n-type silicon wafer with resistivity 0.1Ωcm, 0.01-0.02Ωcm. The electrolytic solution contains 25 ml HF acid (48.99%), 200ml de-ionized water and 1 ml “Triton” as a surfactant. Figure 3.1, shows SEM cross-sectional and top view of porous layers fabricated on 0.1Ωcm and 0.01-0.02Ωcm silicon substrates, respectively.

For 0.01-0.02Ωcm silicon substrate, pore size, pore smoothness and etching rate increases with applied current density as expected because, for a fixed HF concentration, a higher applied current density provides a larger number of holes that enhance the etching of silicon. Low current density (12mA/cm^2) gives etching rate of about 0.01um/sec and produces rough and heavily branched pores of about 20nm of diameter. On the other hand larger current density (70mA/cm^2) increases the etch rate up to 0.023um/sec and produces smooth pores of about 100nm in diameter. It is of interest to note that rough and branched pores persist up to 48mA/cm^2 current density. The porous silicon layers obtained at high current density has a porosity of about 75% (estimate with interference method). At larger current density (80mA/cm^2), we observed the formation of smooth macropores with branched structure rather than straight pores.

The porous structures obtained on 0.1Ωcm silicon substrate are rather different: pores have much larger average diameter. Furthermore pores shape is highly dependent on the applied current density, being roughly of cylindrical shape for low applied current density and become square shaped at the top and star-like at the bottom at higher applied current density. Even in this case the main pore axis grows along the <100> direction but star-like shape with four branched deformation appear as the applied current density is increased (i.e. at 120mA/cm^2 four branched deformation is clearly visible in SEM image of Figure 3.1. The orientation of pore growth on this substrate is shown in Figure 3.1 and can be explained in terms of etching anisotropy in <100>, <010> directions [24, 25].

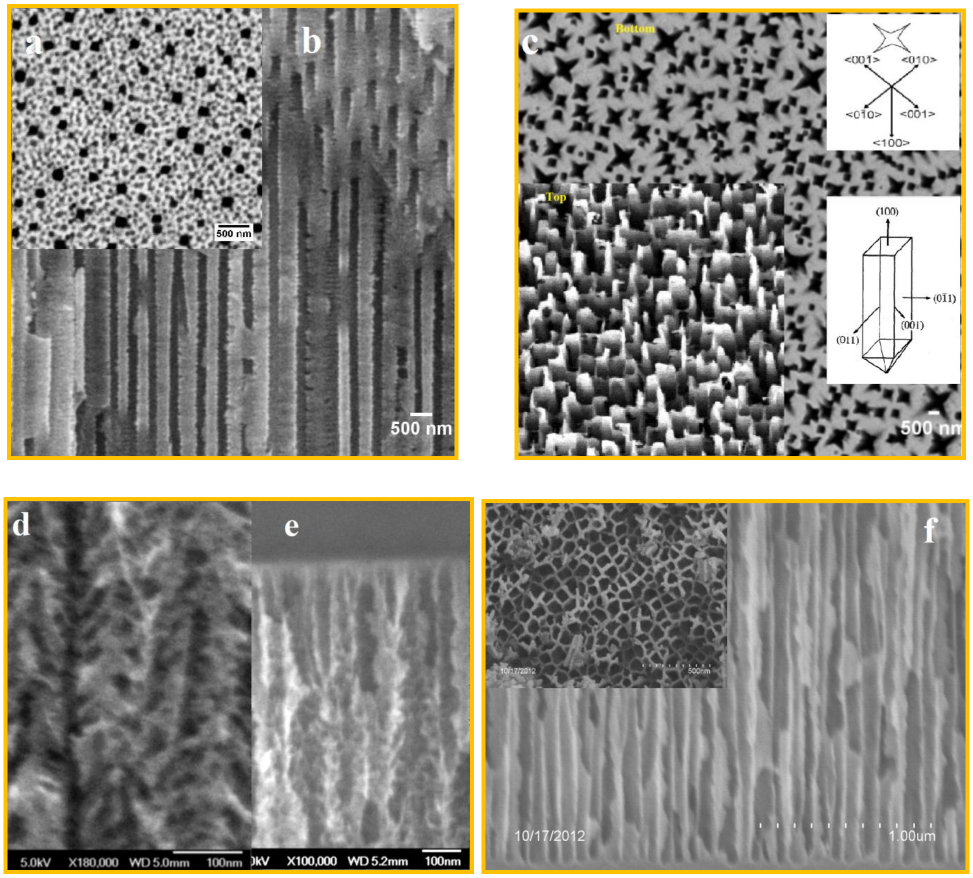

Figure 3.1. SEM images of porous silicon (PSi) monolayer. "a-b shows the top and cross-section of PSi fabricated with 37mA/cm^2 and "c" top and bottom surface morphology fabricated with 120mA/cm^2 on 0.1Ω-cm (in figure inset pore growth direction is shown). "d, e & f" shows the pore structure fabricated with 12, 36 and 70mA/cm^2 on 0.01-0.02Ω-cm

Also in this substrate pore size increases with the applied current density i.e. at 20mA/cm^2 current density pores have roughly 120nm diameter and it increases up to 250nm at 40mA/cm^2 current density. To be sure to have roughly rounded pores the PSi layer obtained on high resistivity wafers was etched using current density of 37mA/cm^2. The main limit of these samples is that their porosity is of only 7% as calculated from SEM image (shown in Figure 3.1). Figure 3.2 shows the transmittance and absorbance characteristic of these FSM (~30µm). From the observed data it can be seen that these FSM behaves as completely opaque in the wavelength region of interest (1000-1500nm) and cannot be used for sensing applications.

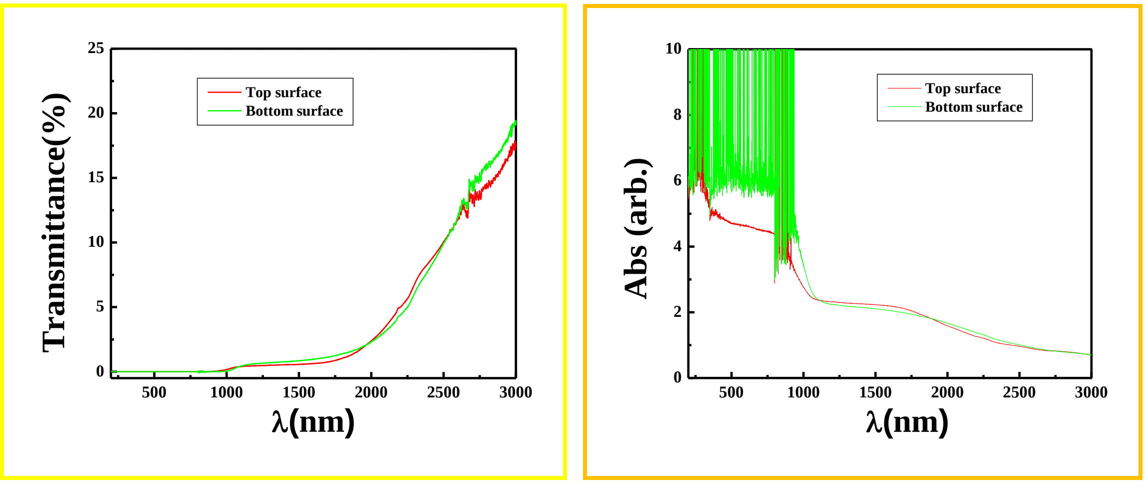

(a) **(b)**

Figure 3.2 (a) Transmittance and (b) absorbance spectra for FSM of ~30µm fabricated on 0.1Ωm-cm silicon substrate

Furthermore as discussed above pore growth on highly doped n-type silicon substrate is explained by either space charge Region (SCR) model or Current Burst Model (CBM) [10-12]. In this study, it is observed that for 0.1Ωcm silicon substrate follows SCR model as pore wall thickness is about twice the pore size (~300 nm), whereas for 0.01Ωcm substrate theoretical SCR width is ~60nm at 3V that implies pore wall thickness should be ~120nm. This value contradicts the experimental observed pore wall thickness that, for the current density used, is of about 10nm [15]. From observed data, it can be concluded that the fabrication of macro-porous structures on 0.01Ωcm substrate are not due to SCR effect and may be explained with the CBM [11-16].

We found that on both substrates pore size increases proportionally to the etching current density. The main difference among the two is that on 0.1Ωcm silicon substrate the larger the etching current the more pronounced is the etching anisotropy along the <001> and the <010> directions that originates a square shaped pores. Based on these morphological characterizations i.e. pore size and pore surface, these two silicon substrates are of great interest for the fabrication of intermediate porous structure that over the micro/meso and macro range and that are suitable to both sensing and filtering applications. Furthermore 0.1Ωcm silicon substrate is difficult to find, so due to their limited availability, we further concentrate more on n-type 0.01Ωcm silicon substrate.

3.3.2 Effect of electrolyte solution

In this section the nature of the solvent and the role of HF acid concentration are studied in detail. During the etching hydrogen evolves. If the etching solution does not wet the pore surface, hydrogen bubble can form and stick within the pore. This fact induces in-homogeneities on the etching (because bubbles stops the etching process and are hardly removed from the pores) [26, 27]. Thus it is important that electrolyte have to easily wet the silicon pore surface and penetrate easily within the pores. Keeping these points in mind, we add “Triton” as a surfactant in the aqueous based solution. The electrolyte that we have used for the fabrication of n-type (100) porous silicon samples is composed of high purity HF 48.99% aqueous solution diluted in ethanol and water varying concentration from 11.11% to 33.33% of HF acid). All samples were prepared with a fixed current density of 80mA/cm^2. Figure 3.3 and Figure 3.4 shows the effect of HF acid concentration both in water and ethanol based solution i.e. pore size, pore roughness and pore morphology.

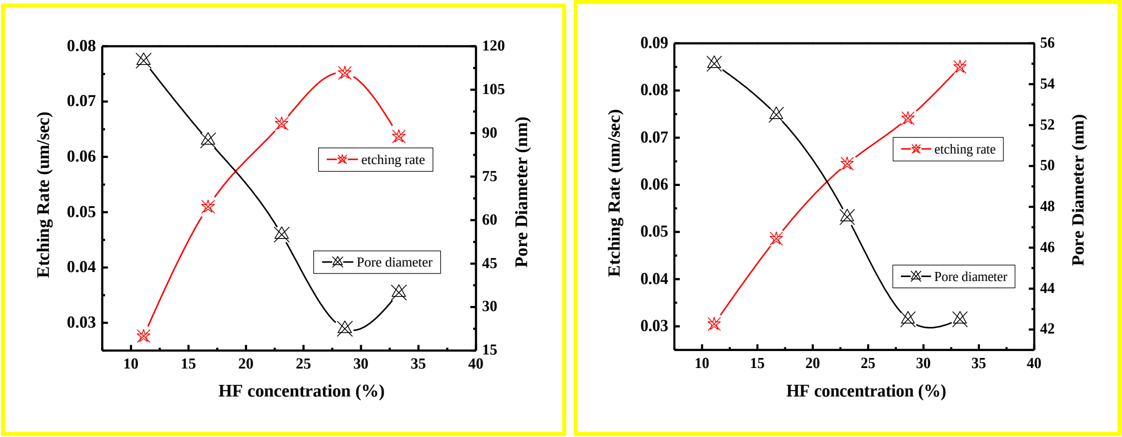

Figure 3.3 (a) Optimized and observed parameters for the fabrication of micro, meso and macro-porous structure on n-type (0.01-0.02Ω-cm) silicon substrate for water based solution. (b) Optimized and observed parameters for the fabrication of meso-porous structure on n-type (0.01-0.02Ω-cm) silicon substrate for ethanol based solution. Note the different y-axis on the two graphs.

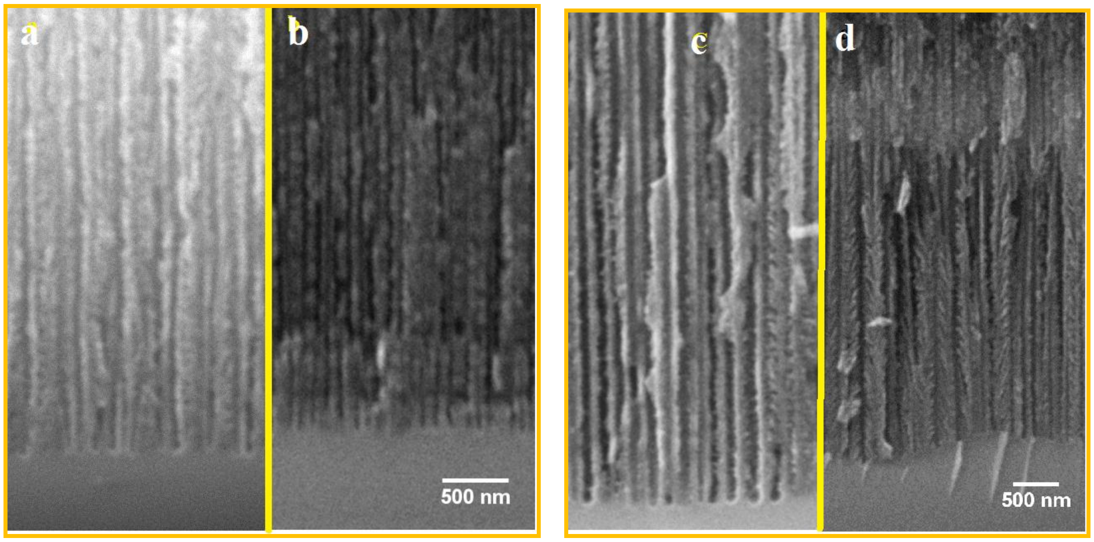

Pore Size~50-60nm *Pore Size~40-45nm* *Pore Size~85-90nm* *Pore Size~30-40nm*

Figure 3.4. SEM images of porous silicon (PSi) monolayer fabricated with different electrolyte (all the samples were fabricated with 80mA/cm^2 and etching lasts for 300s): Image "a" and "b" for Ethanol+HF acid (16.67% and 33.33%), Image "c" and "d" for Water+HF acid (16.67% and 33.33%). Scale bar for all images is 500nm.

It is observed that with decreasing HF concentration in both solvent i.e. pore size and pore wall smoothness increases. With decreasing HF acid concentration a reduction in etching rate is observed for these solutions probably because of the reduction of the direct dissolution via HF acid. Etch rates decrease from 0.085µm/sec to 0.031µm/sec and from 0.064µm/sec to 0.028µm/sec for ethanol and water based solution, respectively. With 11.11% HF acid concentration in aqueous solution, macro-porous (~110nm) structure can be fabricated and furthermore increasing the HF acid concentration up to 33.33% of solvent a branched morphology is achieved with pore size of roughly 25 nm. On the other hand in ethanol based solution pore size of about 50nm-60nm can be fabricated. From the observed data for ethanol and water based solution, relative increase in pore size is ~31% and 229% as HF acid concentration is relatively reduced by a factor of three. It seems that for ethanol based solution HF acid concentration is not a critical parameter whereas it largely determines the porous structure i.e. pore size and pore roughness for water based solution at large current density (80mA/cm^2).

If we compare these two solutions, water based solution provide much smoother pores, faster etching speed and high porosity compared to ethanol based solution. This fact is probably due to the oxidant nature of the water. Thus we believe that for bigger and smoother pore strong oxidant with aqueous solution of low HF concentration is required.

Based on results observed above we have optimized a mixed “water and ethanol” based solution added with a 10% volume concentration of H_2O_2. In this way we try to exploit the wetting capability of the ethanol based solution with an increased oxidant power due to the addition of hydrogen peroxide to an aqueous solution to increase pore size, reduce pore wall roughness and the bottom surface roughness to get thin free standing membrane. Recently a similar study has been performed by D.H. Ge et al. [15, 16] They found that pore formation in such solution are explained by CBM in terms of a balance among the direct dissolution of silicon due to HF acid and indirect dissolution obtained by oxidant as water (and H_2O_2 in our case) that partially oxidize pore walls which are then readily dissolved in HF solution. If there is an imbalance i.e. indirect dissolution is smaller compared to the direct dissolution, then pores will not follow straight path but rather they tend to form a branch structure. Moreover D.H. Ge et al varied the ratio between HF and H_2O_2 (HF:H_2O_2-2:1, 1:1 and 1:2) for a fixed applied current density and they found that a stable growth of smooth macropores happened for HF:H_2O_2=1:2 [16].

To get an idea about absolute effect of HF:H_2O_2, the ratio is changed from 1:0.43 to 1:3.7. During the etching we use the maximum current density that we can apply for 300s without entering into the electro-polishing regime. Addition of H_2O_2 (10.03%) in ethanol+HF based solution, it increases pore size from ~45nm to 60nm. Furthermore pore roughness can be reduced further using water in electrolytic solution. With this new ethanol/water/H_2O_2 based solution and because HF concentration is decreased from 23.07% (2.3:1) to 16.67% (1.5:1), pore wall becomes smooth and pore size increased to ~80nm as shown in Figure 3.5(a)-(d). Also in this case by decreasing the HF concentrations etch rate also decreases from 0.075µm to 0.044µm/sec.

In brief with increasing H_2O_2 concentration and decreasing HF concentration, smooth macroporous can be fabricated. So we further test two other electrolytic solutions with increased H_2O_2 concentration to ~20.6 and 21.8% and with HF a diminished concentration of ~10.7% and ~5.7% respectively. More interestingly as we were expecting, maximum porosity was achieved with 10.71%HF (1.04:2) based solution with ~100nm pore size with refractive index ~1.6 (calculated with interference method).

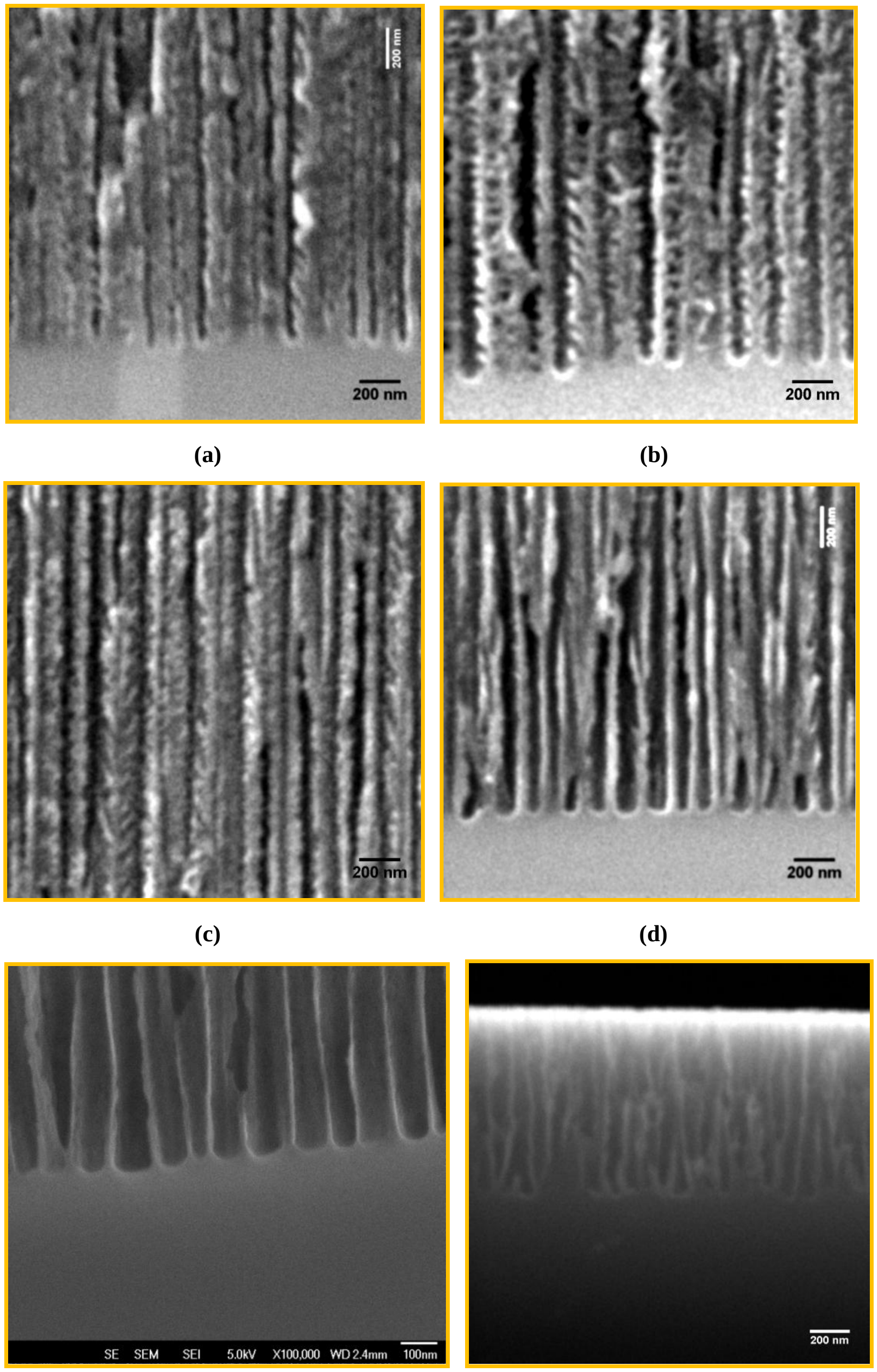

(a) (b)

(c) (d)

(e) (f)

Figure 3.5. SEM images of porous silicon (PSi) monolayer fabricated with different electrolyte (see Table 3.1)

	Solution	**HF:H_2O_2**	**Current density (mA/cm^2)**	**Etching rate (µm/sec)**	**Maximum Pore size**	**Minimum membrane Thickness**
(a)	**23.07%HF+Ethanol**	**23.07:0**	**80**	**0.057**	**40-45nm**	**≥20µm**
(b)	**23.07%HF+Ethanol +10.03%H_2O_2**	**2.30:1**	**80**	**0.050**	**60-70nm**	**≥10µm**
(c)	**23.07%HF+(Ethanol+H_2O) +10.03%H_2O_2**	**2.30:1**	**160**	**0.075**	**60-65nm**	**≥12µm**
(d)	**16.67%HF+(Ethanol+H_2O) +10.87%H_2O_2**	**1.53:1**	**120**	**0.044**	**70-80nm**	**≥10µm**
(e)	**10.71%HF+(Ethanol+ H_2O) +20.60%H_2O_2**	**0.52:1**	**80**	**0.030**	**~90-100nm**	**<2> µm**
(f)	**5.66%HF+(Ethanol+ H_2O) +21.77%H_2O_2**	**0.27:1**	**15**	**0.005**	**~70-80nm**	**<2> µm**

Table 3.1: Optimized and observed parameters for the fabrication of meso and macro-porous structure on n-type (0.01-0.02Ω-cm) silicon substrate for ethanol and water based solutions. For each electrolytic solution cross-section SEM image of observed porous structure is shown in Figure 3.4.

Table 3.1 shows the applied and observed parameters with Water+Ethanol+H_2O_2 based solutions. Further decreasing the ratio of HF:H_2O_2 to 0.27:1, smooth, but branched pores are observed. Figure 3.5(e)-(f) shows cross-sectional SEM images of these porous samples.

Thus our experimental results suggest that depending on the HF:H_2O_2 ratio, different porous structure morphology can be obtained. To fabricate macro-porous structure ~100nm on 0.01-0.02Ωcm silicon substrate using electrolytic solution containing H_2O_2, HF:H_2O_2 window lies in between 1:1 and 1:2. On the other hand for either too high or too low HF/H2O2 ratio branched porous structure is observed.

3.3.3 <u>Free standing membranes (FSM)</u>

FSM are more appealing due to their high selectivity and flow capability are used in many separation techniques i.e. extraction, adsorption and ion-exchange etc., however besides their many advantages only few reports are available on fabrication of thin self supporting membranes[16-19, 28], in this section, FSM were achieved on both n-type silicon wafer (0.1Ωcm and 0.01Ωcm) substrates. For the first time PSi FSM on these substrates were prepared by electro chemical etching method with different types of studied electrolyte solution without back side illumination. We also optimized to get thin (2μm) FSM with smoother pore~100nm using two electrolytic solutions (water+11.11%HF and 10.71%HF + (ethanol+H_2O_2) at room temperature.

3.3.3.1 One step-current density model

Recently C.S. Solanki et al. also have reported fabrication of self-supported thin films for p-type silicon substrate (0.02-0.05Ωcm) and demonstrated that self lift-off may occur [6]. Lift-off time depends on HF acid concentration and applied current density [6, 22]. The anodization lift-off time is predetermined for each combination of applied current density, HF concentration and water content in electrolytic solution. We demonstrated that on n-type silicon wafers (0.1Ωcm and 0.01Ωcm), complete detached FSM with water based solution (11.1%HF+Water+Triton) was achieved successfully with one step current method using 120mA/cm^2 and 80mA/cm^2 for high resistive and low resistive silicon wafer respectively. With this solution, the detachment of porous membrane was completely self-limiting: on both silicon wafers, membrane detachment was achieved after a fixed etching time~1000-1100sec and without applying any high current burst at the end. Also in this case the membrane detachment is clearly indicated in the recorded voltammogram by a sharp and sudden increase in voltage, as shown in Figure.3.6 (in the blue box).

Unfortunately these etching conditions show no tunability in the attainable porous structure: neither pores size nor membrane thickness can be tuned to fabricate FSM with different properties. Furthermore on 0.1Ohmcm substrates the self limiting etching conditions of 120 and 80mA/cm^2 in H_2O +HF (12.5%) creates a thick FSM (>60µm) with deformed (star like pores as shown in Figure 3.1). Such branched pores are not valuable for bio-sensing and filtering. Moreover as discussed above these FSM behave as opaque material due to small porosity ~7%. Furthermore due to the limited availability of 0.1Ωm-cm silicon substrates, we concentrate on 0.01Ωm-cm substrate to have thin transparent FSM.

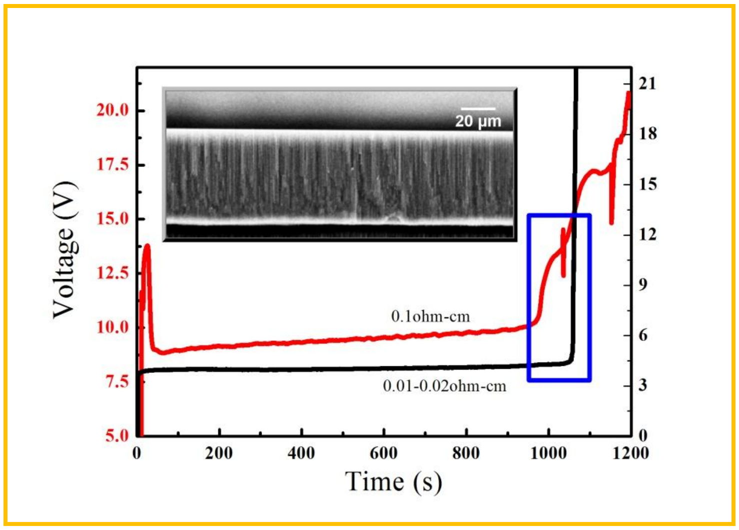

Figure 3.6. Voltage-time domain for one step current model for 0.1Ωcm and 0.01Ωcm silicon substarte. Inset shows the cross-sectional SEM image of partially detached porous layer on 0.1Ωcm substrate

As discussed in previous section 3.3.2 that porosity is inversely proportional to HF acid concentration and it can be further improved with addition of an oxidant i.e. H_2O_2. So we decided to optimize to get thin FSM on 0.01Ωm-cm substrate. We use two electrolytic solutions (5.7%HF+ethanol+H_2O+H_2O_2 and 10.7%HF+ethanol+H_2O+H_2O_2) with different HF concentration. Initially we used 5.7% HF acid solutions. This HF concentration shows etch rate of only 3 nm/s whilst applying the largest current density ($14 mA/cm^2$) that allows the etching of samples several microns thick, without electro-polish them. Moreover pores are highly branched. We found that the 10.7% HF concentration is the concentration that permits to obtain the larger pore size and, at the same time, the etching of very thick samples with stable pore structure while keeping the possibility to detach membranes.

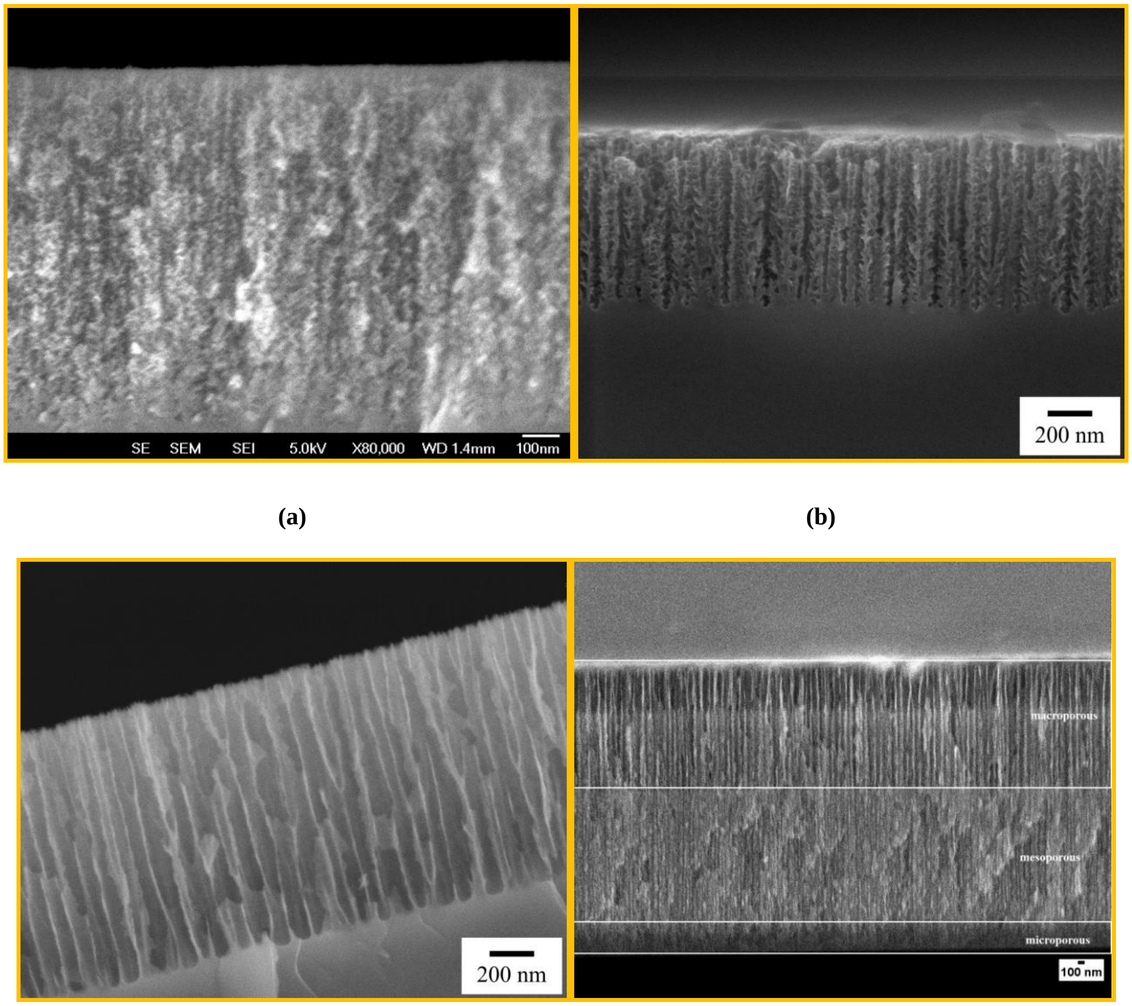

(a) (b)

(c) (d)

Figure 3.7 Panels (a), (b) and (c) show cross-sectional SEM images of n-type PSi etched using ethanoic solution. Current densities are, respectively, $4 mA/cm^2$, $20 mA/cm^2$ and $80 mA/cm^2$. Similar structures are obtained using aqueous solutions. (d) Cross section of a macroporous , mesoporous and microporous multilayer structure. The thin dark layer at the bottom is the low porosity microporous region.

Figure.3.7 (a-c) summarizes the limiting structures that can be obtained using ethanoic solutions at low and large current densities, respectively. As expected, both pores size and etching rate increase with current density. Rough and tree-like (micro-meso) porous structure develops at low current density using both types of solutions, while smooth and straight macro-pores grow if the current is increased. Very similar structures are obtained using aqueous based solution. The most important differences induced by the use of water based solutions are: a shift in the current density required to obtained smooth pores (larger current are required), slightly larger pore size and faster etch rates. Figure 3.8 summarizes these key features as a function of current density for both investigated solvents below.

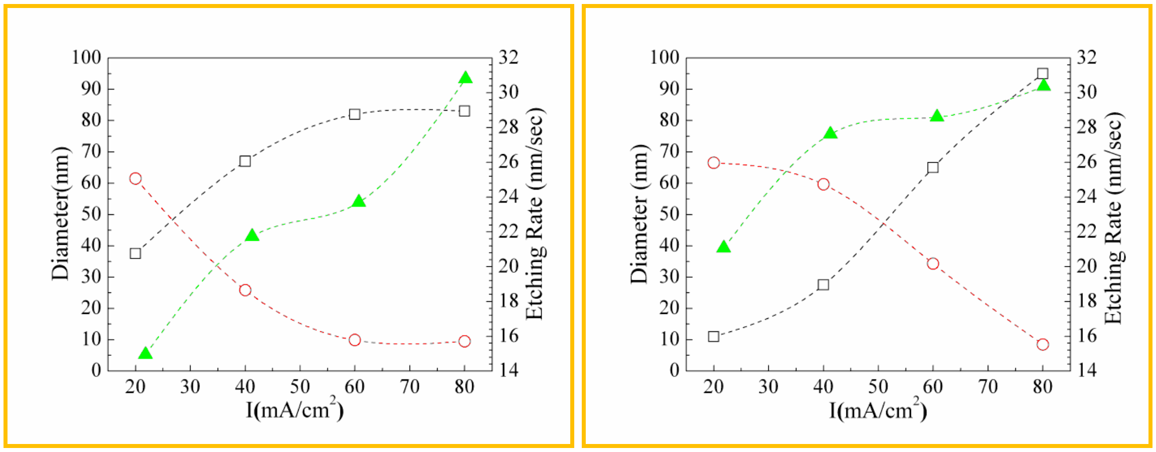

(a) **(b)**

Figure 3.8. Structural key parameters and etching rate of PSi samples. (Left axis) Black open squares indicate pore diameter, while red open circles pore wall thickness. (Right axis) Green filled triangles indicate etch rates. (a) Data for samples etched in ethanol based solution, (b) data for mixed solution.

Etch rates range from 15nm/s to 30nm/s, respectively at 20mA/cm^2 and 80mA/cm^2 and are similar for both solvents. When using the ethanoic based solution the resulting pores have nearly 35nm pore diameter at 20mA/cm^2, which increases to around 80nm using current density of 60mA/cm^2. On the other hand using aqueous solution the pores are slightly larger (up to 100nm). This fact is probably due to the higher polishing current density that is sustained by solutions containing oxidants. In fact the threshold to obtain straight and smooth pores depends on the solution composition: it is smaller with ethanoic solution (60mA/cm^2) and increase with aqueous solution (80mA/cm^2). To note that pores are perfectly open up to the surface of the PSi. Both pore size and etch rate is larger for aqueous based solutions compared to ethanoic one.

The careful optimization of porous structure allows us to obtain homogeneous PSi layers and, thus, the fabrication of large area, free-standing porous layer (micro-meso-macro) on the same substrate. Figure 3.7d shows the fabricated multilayer micro-meso and macro porous structure, 4mA/cm^2 for low porous micro layer, 40mA/cm^2 to etch meso-porous layer following 60 and 80mA/cm^2 for high porosity macro-porous layer and to detach it from silicon substrate. A flat interface between micro-meso and macro can be seen in SEM image 3.7 (d). Current density 80mA/cm^2 and 60mA/cm^2 for respective solutions i.e. water and ethanolic solution was sufficient to fabricate a very thin porous layer (~couple of um) and to detached this layer from the silicon substrate. At these current densities, etching was completely self-limiting. However this recipe can be applied to detach any fabricated porous layer on this “n-type (0.01-0.02Ωcm silicon” substrate. Figure 3.9 (a)-(b) shows the voltage behavior during fabrication and variation of lift-off time with applied current density for respective solutions.

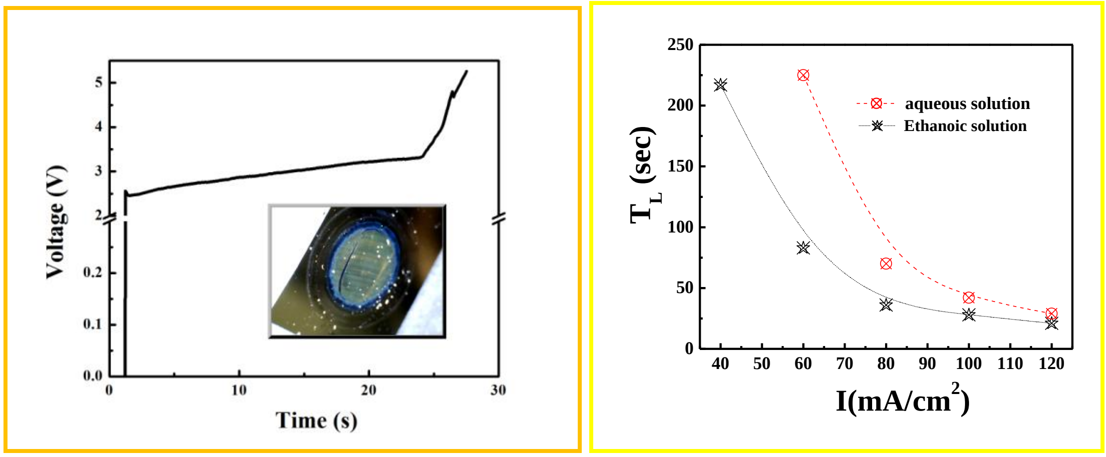

(a) **(b)**

Figure 3.9. (a) Voltage-time domain observed with ethanolic solutions, an increase in voltage is observed as porous layer is separated from silicon substrate. Inset shows the photograph of partially detached layer (b) lift off time of FSM Vs applied current density for studied solution. Lift off time decrease as applied current density is increased.

3.3.3.2 Two step-current density method

We found that the aqueous solution of 11.11%HF was the optimum because it permits to fabricate macro-porous layer with cylindrical pore of about 200nm of diameter in the high-resistivity wafer (at 37mA/cm^2) and pores of about 110nm of diameter on the low-resistivity wafer (at 70mA/cm^2). It is known that, for a fixed HF acid concentration, porosity mainly depends on the applied current density. Thus, on p-type substrates, FSM are usually obtained by applying a very high current density at the end of the etching (the so-called current burst). Such large current density completely dissolves the silicon at the end of the porous layer and produces the detachment of the porous layer itself [1, 6, 22]. The random selection of high burst current density cannot be used for n-type silicon substrates as it generally damages the porous layer without detaching it from substrate. However completely detached free standing macro-porous membrane were achieved with an optimized two step current density method: initially a current density is applied to obtain the chosen pore size, then in a second step a very thin high porosity translational layer is fabricated by applying a larger current density to either partially or completely detach the porous layer from silicon substrate. The main difference to respect the p-type case is that this second step of current density is strongly dependent on the first step applied, and cannot be chosen at will. If we choose a much larger current density to detach the porous layer, we got it damaged. This is because to detach the membrane we don't need to suddenly enter into the electro-polishing regime and completely dissolve the silicon, rather we have to etch a thin and highly porous layer at the bottom of the PSi sample. In summary for each specific first step current density, a second step current density has to be properly optimized. We found that the optimum values of the two current steps for the current densities generally used by use are the following: for the high resistivity wafer if an etching current of 37mA/cm^2 is used the 2nd step have to be of 80mA/cm^2; while for the low resistivity wafer if the 1st step if of 60mA/cm^2 the 2nd have to be of 200mA/cm^2). Detachment of porous layer is traced by the voltammogram with a sharp and sudden increase in the voltage as shown in Figure 3.10. Similar behavior was also observed by Searson et al. during the etching of whole wafer for self-supporting porous layer [18]. Unfortunately with these applied etching conditions, membrane thickness cannot be tuned much in order to get high quality thin transparent macro-porous (~100-200nm) self-supporting membranes and only porous layer thicker than 30um could be detached in a reproducible manner on 0.1Ωm-cm silicon substrate.

Furthermore we tried this two step current method to both ethanolHF+H_2O_2 and water+ethanol+HF+H_2O_2 based solutions (optimized as described in section 3.3.1 and 3.3.2) to detach thin FSM on 0.01Ωm-cm substrate. We found that with applied current density of 80mA/cm^2-200mA/cm^2 for ethanol+HF(23.07%) solution membrane thickness can be tuned from 60 µm down to ~20µm. From cross-sectional SEM image shown in Figure 3.11, it is observed that second step current density produces a thin and highly porous layer with pore size~110 at the bottom. Such fragile interface layer helps the detachment of the first porous layer.

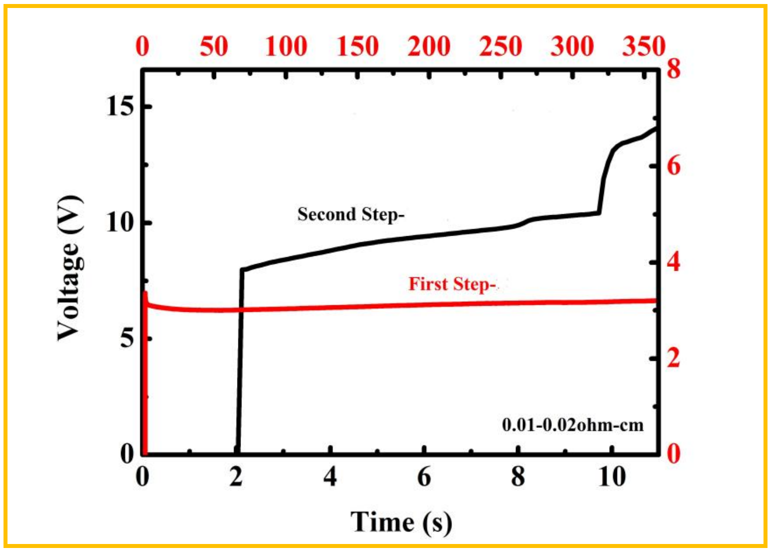

Figure 3.10. Voltage-time domain for two step current model: "in first step porous layer is fabricated with desired structure and then in second step, current density is applied to detach porous layer from silicon substrate"

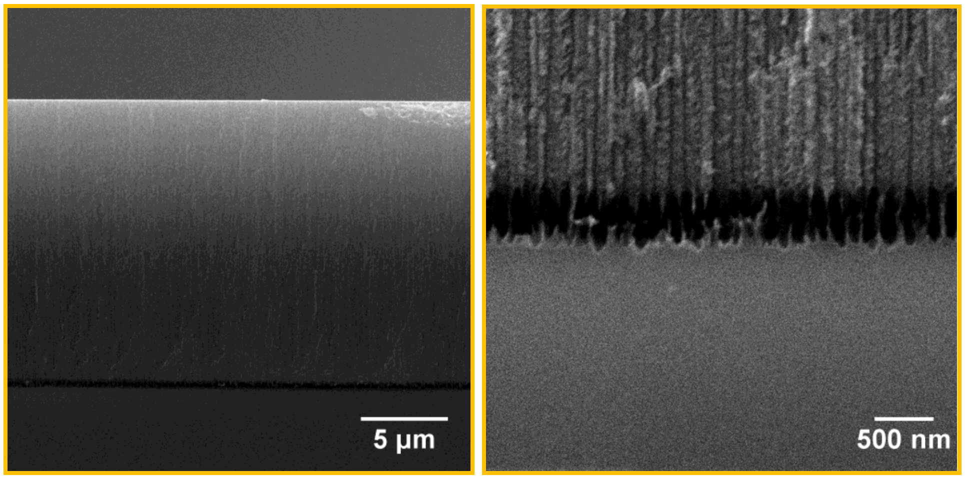

(a) (b)

Figure 3.11. SEM image of n-type PSi macro-structure with ethanol+23.07%HF just before detachment, SEM image of lower high porous layer at higher magnification is shown in the right

On the other hand using the ethanol+ H_2O_2+HF(23.07%) solution and applying 80mA/cm^2-200mA/cm^2, transparent and thinner membrane (10µm) can be fabricated. However pores are quite rough and limited to ~60nm. We found that the best structure is obtained using the Water+Ethanol+H_2O_2+HF(16.67%) solution, with 120mA/cm^2-200mA/cm^2 of applied current densities. In fact smooth pores of about 80nm of diameter can be further etched, as shown in Figure 3.12. With these solutions, we successfully were able to tune membrane thickness and we are able to fabricate membranes as thin as 10µm.

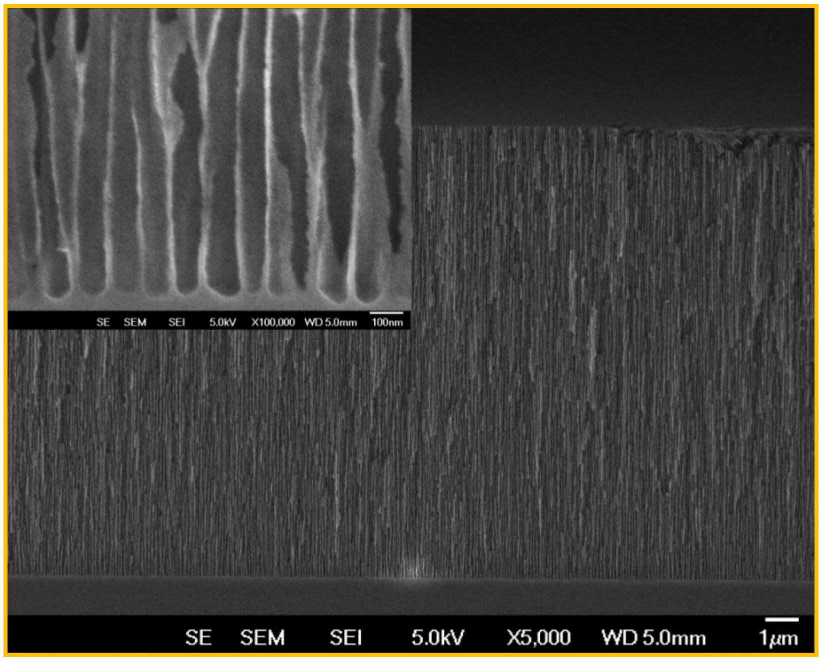

Figure 3.12. SEM image of n-type PSi macro-structure with ethanol+23.07%HF just before detachment. Inset shows the cross-sectional SEM at higher magnification.

During the fabrication of FSM we noticed a reproducible change of the voltage versus time that indicates the separation of the porous layer from the silicon substrate as shown in Figure 3.10. Optimized minimum membrane thicknesses are listed in Table 3.1 for studied electrolytic solutions.

3.3.3.3 Two solution model

Realizing from above optimization, furthermore we optimized to fabricated FSM of variable thickness from couple of µm to tens of µm thickness with previously optimized etching solution (Water+Ethanol+H_2O_2+HF(10.71%) having straight and smooth macropores. With two solution methods, we first etch a high quality macroporous layer with cylindrical and smooth pores (as optimized in Sec. 3.3.1) and then they were detached using the Water+Ethanol+H_2O_2+HF(10.71%) solution. We successfully fabricate high quality transparent FSMs, with thickness tunable from couple of µm up to tens of µm. Figure 3.12(a) shows the observed voltage behavior during the etching and when FSM is detached.SEM image of cross-section of partially detached porous layer fabricated and optical photograph of transparent thin FSM with improvements made with this etching method is shown in Figure 3.13 (b-d). Because of large pore size, we believe that these free-standing membranes could be of great interest and could be more advantageous in sensing application because of their freestanding nature.

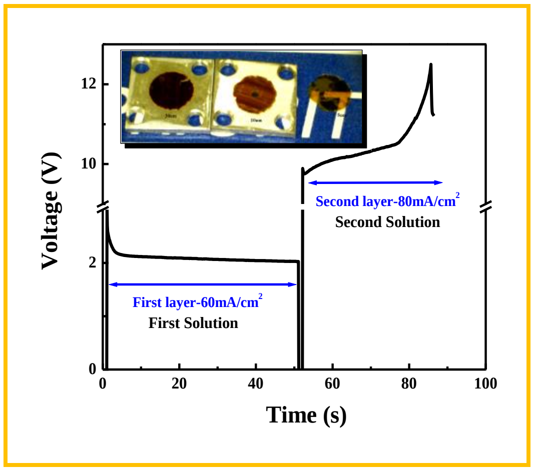

(a)

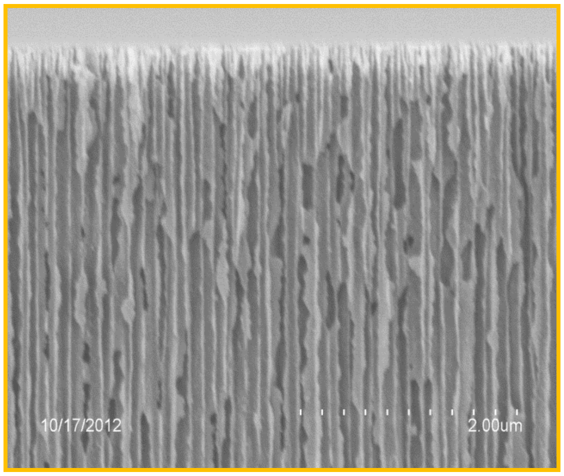

(b)

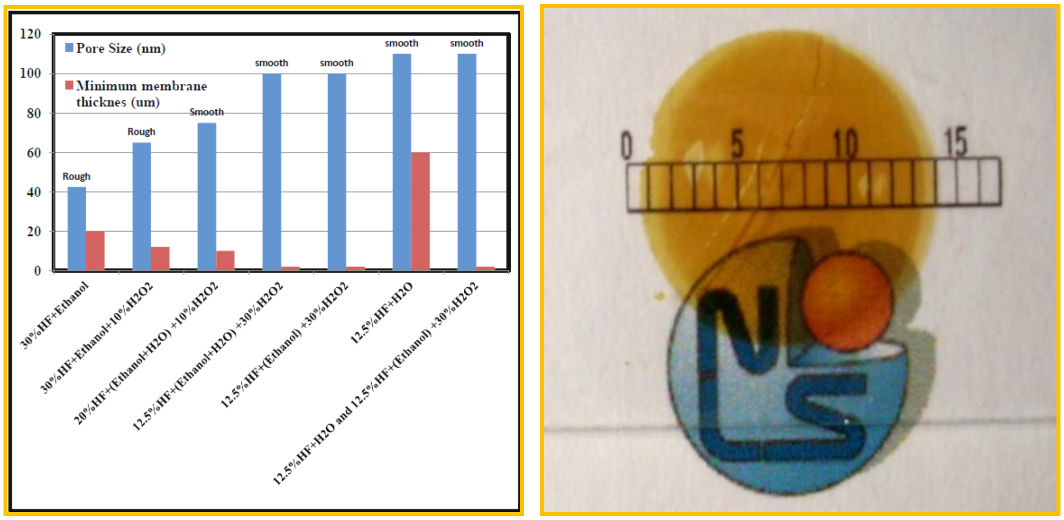

(c) **(d)**

Figure 3.13. (a) Voltage-time domain observed with two solutions (inset shows FSM glued on metallic holder) and (b) cross-section SEM of n-type PSi membrane. (c) Improvement graph made on n-type PSi membrane and (d) photo-graph of thin transparent (~3um) detached n-type membrane

3.3.4 <u>Effect of oxidant in addition to electrolyte solution/POST etching</u>

Considering the upper limit of pore size achievable using a single step etching method (on the order of 70 - 80nm) from a 0.01Ωcm wafer, we also tried a radically different approach and adopted a post etching treatment to increase pore size. After PSi etching, we immersed the porous samples in a dilute solution of either Potassium Hydroxide (KOH) or Tetra Methyl Ammonium Hydroxide (TMAH), both known reagents for anisotropic etching of silicon [29, 30]. Despite being predominantly used for patterning silicon based microstructures, we exploited their anisotropic etching in order to reduce the inner pore roughness and, at the same time, to increase pore diameter.

We noticed a large difference between the behaviors of these two solutions. SEM images of PSi fabricated and treated with different solution are shown in Figure 3.14 and in Figure 3.15. We notice that porous layer fabricated with ethanol HF solution have no effect on its pore morphology, where as PSi fabricated with H_2O_2 is strongly affected with these two oxidants. KOH increased pore size but etched away also a thick amount of the porous layer; on the other hand it seems that TMAH does not affect the porous layer thickness but pore size still increases. In both using KOH and TMAH pores enlarged by about 20-25% from 70-80 nm to more than 100 nm. Experimental data is summarized in Tables. 3.2 and 3.3

Solution	**Oxidant**	**Treatment Time (minute)**	**Etch thickness**	**Pore size**
30%HF+Ethanol	*NO*	-	*21.71um*	*25-30nm*
	KOH	*1*	*16.05um*	*~30nm*
	KOH	*2*	*10.97um*	*~35nm*
	TMAH	*5*	*21.56um*	*~30nm*
	TMAH	*10*	*21.61um*	*`30nm*

Table.3.2 Effect of the post etching treatment on samples etched in ethanolic solution

From Table 3.2 it is clear that the post etching treatments have no effect on the pore size of freshly etched samples. From the aggressive nature of the solutions used, and considering the decrease of PSi thickness when the sample is brought in contact with KOH solution, it is reasonable to assume that both KOH and TMAH solution does not enter inside the pores of freshly etched samples because of the highly hydrophobic nature of the surfaces. The pore size remains constant after the post etching and only a reduction in PSi thickness treated with KOH is noted due to etching of the superficial layer which is directly in contact with the KOH solution (the reason why TMAH seems not to affect the PSi thickness is not yet clear and deserves further investigations).

Reference sample

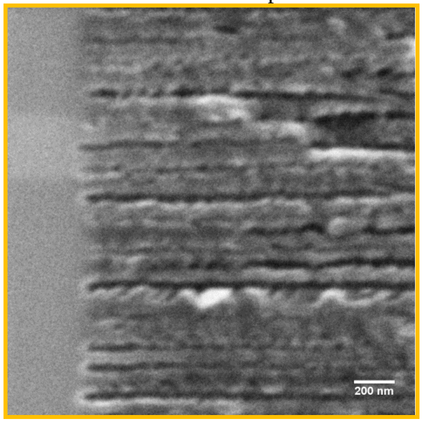

1minute KOH (1.73%) post-treatment

2minute KOH (1.73%) post-treatment

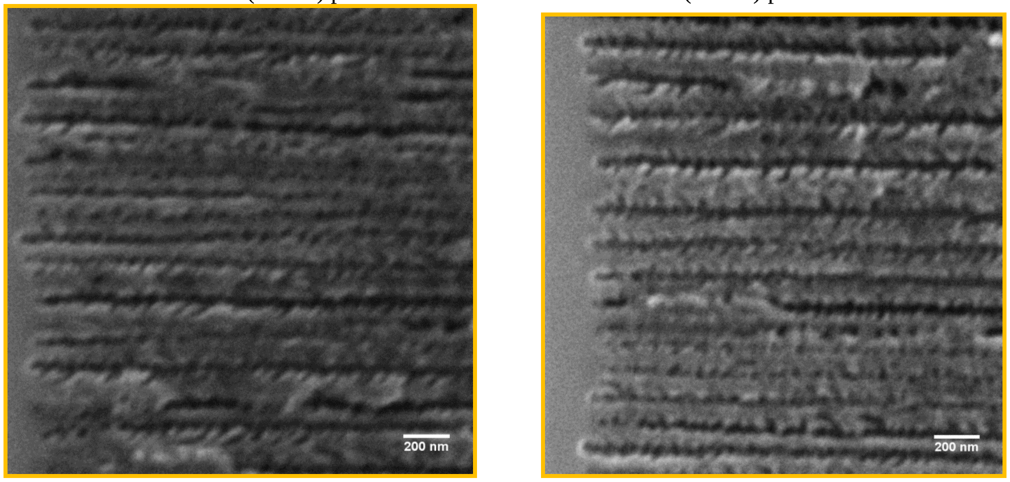

5minute TMAH (1.56%) post-treatment

10 minute TMAH (1.56%) post-treatment

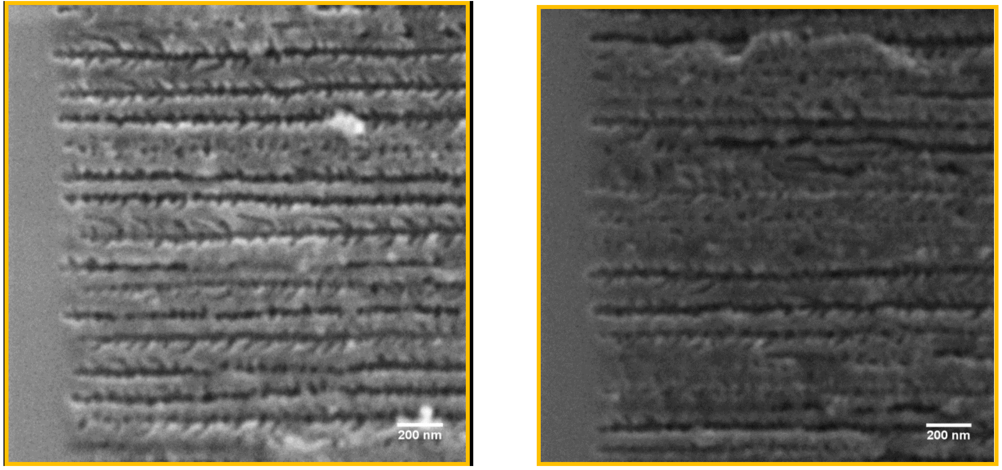

Figure 3.14. SEM images of sample after post etching with KOH and sample after TMAH based post etching. Scale bar: 200 nm.

Reference sample

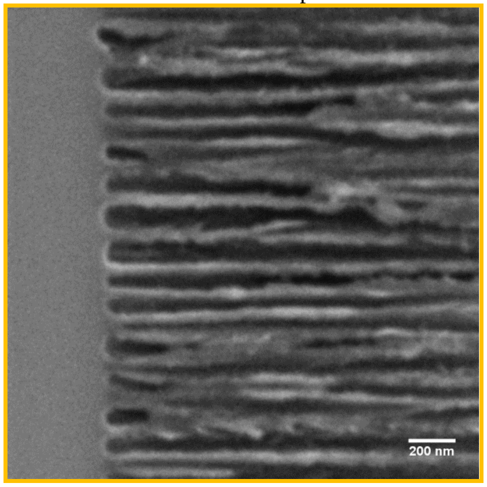

1minute KOH (1.73%) post-treatment

2minute KOH (1.73%) post-treatment

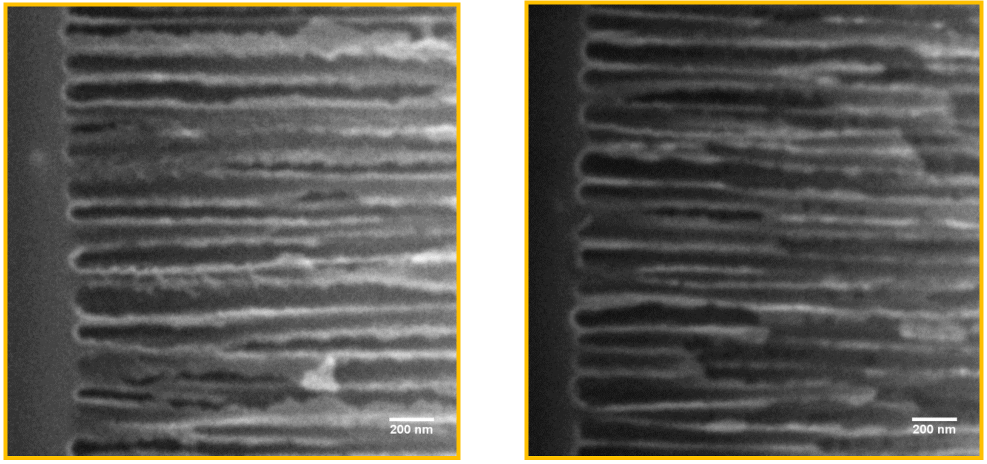

5minute TMAH (1.56%) post-treatment

10minute TMAH (1.56%) post-treatment

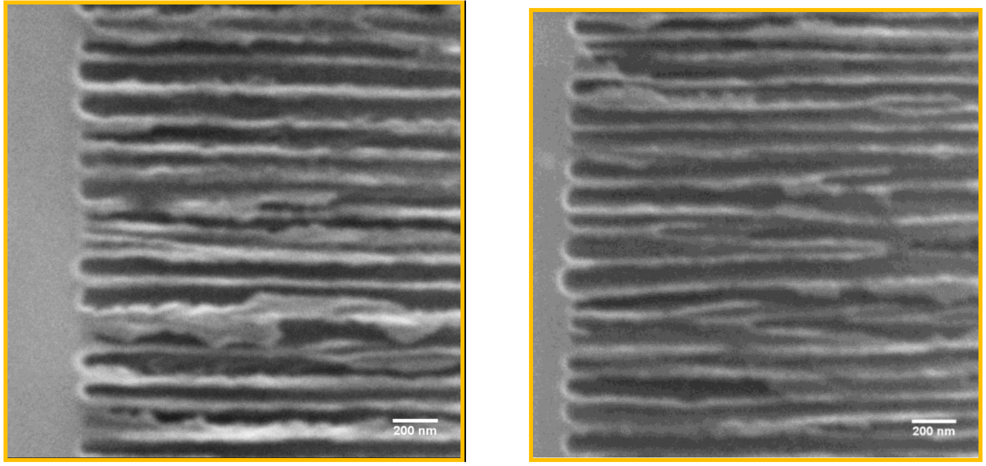

Figure 3.15. SEM images of sample after post etching with KOH and sample after TMAH based post etching. Scale bar: 200 nm.

Solution	**Oxidant**	**Treatment Time (minute)**	**Etch thickness**	**Pore size**
16.7%HF+32.05%Ethanol+32.05%H_2O +19.23%H_2O_2	*NO*	-	*15.43um*	*70-80nm*
	KOH	*1*	*6.95um*	*80-90nm*
	KOH	*2*	*3.69um*	*90-120nm*
	TMAH	*5*	*15.66um*	*75-85nm*
	TMAH	*10*	*15.52um*	*90-110nm*

Table.3.3 Effect of the post etching treatment on samples etched in water ethanolic solution

On the other hand post etching of samples that were fabricated using H_2O_2 containing solution shows a completely different behavior [15, 16, 31]. In this case we expect the pore surface to be much smoother and partially covered by silicon oxide, and thus to have a different surface polarity compared to samples etched without oxidizing agents. In fact the post etching treatments show a significant increase of pore sizes from initial 70 to 80 nm values, up to more than 100 nm in post etched samples. The main results obtained on PSi samples etched using H_2O_2 are reported in Table 3.3.

Thus the etching performed using hydrogen peroxide and the post etching treatment using KOH or TMAH is found to be a reliable method to both increase pore size and reduce their surface roughness by removing the branched structure of the pores, as can be seen in the SEM images of Figure 3.15. Despite the increase in the average pore size using these post etching methods, we cannot obtain pores larger than 100-110nm, because their initial density is mainly defined by the substrate resistivity and longer post etching treatments will produce a complete dissolution of the PSi layer (demonstrated by the PSi thickness reduction). In particular long post etching increased the sample porosity and rendered the membranes extremely fragile.

Another advantage of post etching treatment is that it allows the fabrication of thicker samples. In fact samples with 70 to 80nm pores cannot be etched for very long time, thus they have a limited maximum thickness. This is because direct chemical dissolution of the silicon in HF always produces a slow but continuous increase in pore size due to lateral etching (this is a severe and well known problem of p-type substrate but it is present in n-type as well). Post etching permits to etch long and smaller pores that are subsequently enlarged to the desired size.

3.4. Conclusions

In conclusion, to have better interface for sensing device and flow through sensing, thin self-supporting PSi membranes with pores from 40nm to 200nm are fabricated with optimized electrolyte solution on n-type silicon substrates. Experimental results suggest that water based solution produces larger pores, whereas ethanol based solution helps to detach thinner porous layers. A range of volumetric proportions of H_2O_2 and HF-acid are tested to achieve straight and smooth pores of about 100nm of diameter. Thin (~10µm) free standing membranes, with pores size around 70-80nm (porosity of 65%) are routinely fabricated using H_2O +ethanol+ H_2O_2+HF(16.67%) based solution with two step current density method. This method permits the fabrication of FSM as thin as 2 µm and of cm-sized diameter (the aspect ratio is of about 6000) with straight and smooth 100nm pores.

References

[1]Matthew A. Cooper "Optical biosensors in drug discovery" Nature Reviews Drug Discovery, 1, pp 515-528 (2002)

[2]Keiki-Pua S. Dancil, Douglas P. Greiner and Michael J. Sailor," A Porous Silicon Optical Biosensor: Detection of Reversible Binding of IgG to a Protein A-Modified Surface" J. Am. Chem. Soc., 121 (34), pp 7925–7930 (1999)

[3]Finny P. Mathew, Evangelyn C. Alocilja," Porous silicon-based biosensor for pathogen detection" Biosensors and Bioelectronics, 20(8),pp 1656–1661 (2005)

[4]Jarkko J. Saarinen, Sharon M. Weiss, Philippe M. Fauchet, and J. E. Sipe," Optical sensor based on resonant porous silicon structures" OPTICS EXPRESS, 13(10) pp 3754 (2005)

[5]Andrew Jane, Roman Dronov, Alastair Hodges, Nicolas H. Voelcker," Porous silicon biosensors on the advance" Trends in biotechnology, 27 (4), pp 230–239 (2009)

[6]C. S. Solanki, R. R. Bilalov, J. Poortmans, J. -P. Celis, J. Nijs and R. Mertens," Self-Standing Porous Silicon Films by One-Step Anodizing" J. Eletrohem. Soc. 151, pp C307 (2004)

[7]H. Ouyang, M. Christophersen, R. Viard, B. L. Miller and P. M. Faucher, Adv. Funct. Mater,. 15, pp 1851 (2005)

[8]V. Lehmann and H. Foll "Formation Mechanism and Properties of Electrochemically Etched Trenches in n-Type Silicon" J. Electrochem. Soc., 137(2), pp 653-659 (1990)

[9]P. C. Searson, J. M. Macaulay, F. M. Ross, "Pore morphology and the mechanism of pore formation in n-type silicon," Journal Applied Physics 72(1), pp 253-258 (1992).

[10]H. Foll, M. Christophersen, J. Carstensen, G. Hasse, "Formation and application of porous silicon" Materials Science and Engineering: R: Reports, 39 (4), pp 93–141 (2002)

[11]Alexandre Valance**,"** Theoretical model for early stages of porous silicon formation from n- and p-type silicon substrates", Phys. Rev. B 55, pp 9706–9715 (1997)

[12]S. Frey, M. Kemell, J. Carstensen, S. Langa, H. Föll," Fast pore etching", physica status solidi (a), 202 (8) pp 1369–1373 (2005)

[13]Huimin Ouyang, Marc Christophersen, Philippe M. Fauchet," Enhanced control of porous silicon morphology from macropore to mesopore formation", physica status solidi (a), 202 (8) pp 1396–1401 (2005)

[14] Harraz, F. A., El-Sheikh, S. M., Sakka, T., & Ogata, Y. H.," Cylindrical pore arrays in silicon with intermediate nano-sizes: A template for nanofabrication and multilayer applications", Electrochimica Acta, *53*(22), pp 6444-6451 (2008)

[15]D.H.Ge, J.W.Jiao, S.Zhang and Y.L.Wang," Fast speed nano-sized macropore formation on highly-doped n-type silicon via strong oxidizers" Electrochemistry Communications 12, pp 603 (2010)

[16]D.H. Ge, M.C. Wang, W.J. Liu, S. Qin, P.L. Yan, J.W. Jiao," Formation of macro–meso–microporous multilayer structures", Electrochimica Acta, 88, pp 141–146 (2013)

[17]Christopher C. Striemer, Thomas R. Gaborski, James L. McGrath and Philippe M. Fauche, "Charge- and size-based separation of macromolecules using ultrathin silicon membranes" Nature 445, pp 749-753 (2007)

[18]M. Hajj-Hassan, M.C. Cheung, V.P. Chodavarapu," Ultra-thin porous silicon membranes fabricated using dry etching", Micro & Nano Letters 6(4) pp226-228 (2011)

[19]D. Z. Fang, C. C. Striemer, T. R. Gaborski, J. L. McGrath and P. M. Fauchet," Methods for controlling the pore properties of ultra-thin nanocrystalline silicon membranes" J. Phy.:Condens. Matter, 22, pp 454134 (2010)

[20]A. J. Storm, J. H. Chen, X. S. Ling, H. W. Zandbergen and C. Dekker," Fabrication of solid-state nanopores with single-nanometre precision", Nature Materials, 2, pp 537 - 540 (2003)

[21]T E Bell, P T J Gennissen, D DeMunter and M Kuhl," Porous silicon as a sacrificial material", J. Micromech. Microeng., 6, pp 361 (1996)

[22]M. Ghulinyan, C. J. Oton, G. Bonetti, Z. Gaburro, L. Pavesi, "Free-standing porous silicon single and multiple optical cavities," Journal of Applied Physics 93(12), pp 9724-9729 (2003).

[23]Pushpendra Kumar and Patrick Huber," Effect of Etching Parameter on Pore Size and Porosity of Electrochemically Formed Nanoporous Silicon", Journal of Nanomaterials, 2007, Article ID 89718, (2007)

[24]J. Carstensen, M. Christophersen, H. Foll," Pore formation mechanisms for the Si-HF system", Materials Science and Engineering B, 69-70, pp 23–28 (2000).

[25]X.Q. Bao, J.W. Jiao, Y.L. Wang, K.W. Na, H. Choib," Macropore Formation Without Illumination on Low Doped n-Type Silicon", Journal of The Electrochemical Society 154 (3) D175-D181 (2007)

[26]Thonissen, M. Billat, S. ; Kruger, M. ; Luth, H. ; Berger, M.G. ; Frotscher, U. ; Rossow, U.," Depth inhomogeneity of porous silicon layers", J. Appl. Phys. 80, pp 2990 (1996)

[27]P. Allongue, C. Henry de Villeneuve, L. Pinsard and M. C. Bernard," Evidence for hydrogen incorporation during porous silicon formation" Appl. Phys. Lett. 67, pp 941 (1995)

[38]Yanjun Xiao, Xiaopeng Li, Han-Don Um, Xuejiao Gao, Zhongyi Guo and Jung-Ho-Lee," Controlled exfoliation of a heavily *n*-doped porous silicon double layer electrochemically etched for layer-transfer photovoltaics" Electrochimica Acta 74, pp 93 (2012)

[39]A.M. Tinsley-Bown, L.T. Canham, M. Hollings, M.H. Anderson, C.L. Reeves, T.I. Cox, S. Nicklin, D.J. Squirrell, E. Perkins, A. Hutchinson, M.J. Sailor, A. Wun," Tuning the Pore Size and Surface Chemistry of Porous Silicon for Immunoassays", physica status solidi (a), 182(1) pp 547–553 **(** 2000)

[30]Xiaopeng Li, Hong-Seok Seo, Han-Don Um, Sang-Won Jee, Yong Woo Cho, Bongyoung Yoo, Jung-Ho Lee," A periodic array of silicon pillars fabricated by photoelectrochemical etching", Electrochimica Acta, 54(27), pp 6978–6982 (2009)

[31]X. Li and P. W. Bohn," Metal-assisted chemical etching in HF/H_2O_2 produces porous silicon", Appl. Phys. Lett., 77, pp 2572 (2000)

Chapter 4

Investigation for surface stabilization of porous layers

4.1 Introduction

The large specific area of PSi allows the bonding of bio-molecules in a small volume and hence achievement of large sensitivity on very compact devices [1, 2, 3]. In particular PSi surface properties can be easily stabilized in order to get a reproducible optical response. The surface of freshly prepared PSi is strongly reactive due to presence of unstable silicon hydride “Si-H” species and easily oxidizes when exposed to air. In turn this results in a continuous change of the sensor optical properties [4]. In order to achieve stable sensor signal/performance, one needs to stabilize the PSi pore surface [5]. This can be achieved by using chemical treatment that substitutes the Si-H bond with a more robust ligand (e.g. by silanization methods), or with an oxidation step that induces a controlled growth of a thin oxide layer on the sample surface [6, 7, 8,]. This layer stabilizes the silicon surface against any other surface modification and allows the realization of a stable device with well controlled chemical and optical properties. To grow an oxide layer, two methods are commonly employed: the thermal and the electro-chemical ones [9, 10]. With the electrochemical method, the sample is immersed in a sulphuric acid solution and a current is applied to the cell [10]. Silicon oxidation occurs and a layer of oxide forms on the pore surface. However, electrochemically grown oxide has a limited reproducibility, in terms of both electrical and structural properties [311, 12]. To develop working devices, it is fundamental to have a very good control over the oxide properties because it has a strong impact on the final properties of the detection scheme.

Due to its simplicity and good control over oxide thickness, thermal oxidation method is used to stabilize PSi surface in this work [13]. Once samples are placed within an oven the water presents in the atmosphere reacts with PSi surface and produces a thin layer of SiO_2 [14]. In addition chemical modification method is also studied using both polar and non-polar molecules [15, 16, 17[. In this study, oxidation treatment is followed by a silanization step to introduce suitable functional groups i.e. CH_3, COOH or N-H on PSi surface.

The goal of this chapter is to describe PSi surface modification obtained by thermal oxidation and hydro-carbonization. Different chemical functionalization reactions are considered for covering the PSi surface with different organic molecular layers. These layers serve as an intermediate functional interface for attaching the target specific binding layer.

4.2 Synthesis and Experimental Details

Porous silicon layers and free standing membranes were prepared by electro chemical etching method as discussed in *Chapter 3*. After fabrication of porous samples, all samples were rinsed in ethanol and dried in N_2 flow. For structural morphology of PSi structure, high-resolution scanning electron microscopy (SEM, JEOL mod. JSM 7401F) studies were performed.

4.3 Results and discussions

4.3.1 Thermal oxidation

PSi oxidation was performed in ambient atmosphere and in dry environment. To optimize the oxide layer, we prepared multilayer samples [18]. Such structures are difficult to stabilize because of the presence of several thin low porosity layers that can act as an efficient diffusion barrier for oxidation allows us to find the thermal treatment that assures an efficient and complete oxidation of the surface. So, we maximized the refractive index differences between the low and high porosity layers, by using the larger current interval that the silicon substrate can sustain in order to obtain a high reflection stop band compatible with the fabrication of samples, robust enough to be further handle and functionalized.

The growth of an oxide layer produces an increased volume of the solid fraction and reduces the pore volume [19]. Moreover the oxide induces a compressive stress into the silicon phase that could bring about the sample’s collapse [19, 20]. For these reasons we found that the maximum temperature that PSi sample can sustain is around 500 °C (but this value depends on the sample’s structure). Furthermore in order to avoid sample damage, heating cannot be performed too fast, so slow heating rates 3 to 5°C/min have been used.

The extremely slow oxide growth rate that occurs at this low temperature allow us a fine tuning of the oxide thickness because we have to find the minimum oxide thickness that will assure a complete and stable passivation of the porous surface without degrading too much the optical contrast. In fact the presence of the oxide reduces the average refractive index of each layer and their refractive index contrast, in proportion to the oxide thickness [21]

Two types of samples were prepared as described in experimental *chapter 2*: a multilayer MC sample with a thin and low porosity defect layer and a Distributed Bragg Reflector (DBR) structure composed of 10 periods are shown in SEM images of the PSi sample below in Figure 4.1.

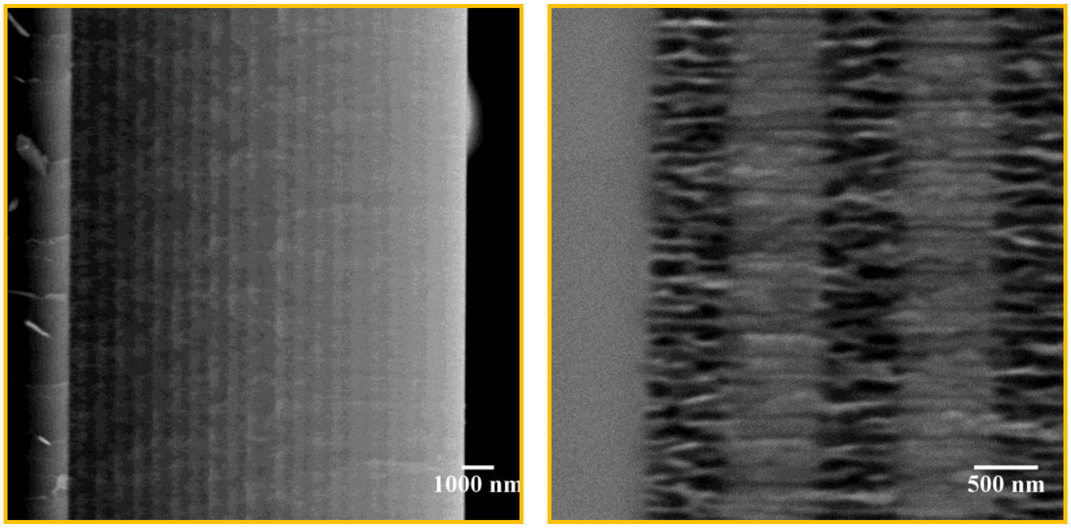

(a) **(b)**

Figure 4.1. The cross section of a 10 periods MC: (a) total cross section of the sample. The silicon substrate is visible in the left side. The cavity layer is centered within the multilayer (scale bar 1000nm). (b) A magnified view of the last periods. The gray are on the left side is the silicon substrate (scale bar = 500nm).

We prepared a set of four samples and oxidized them at 350 °C for different times (1, 2, 3 hours and multi-layer DBR was oxidized for 2 hour). The oxidation produces a definite blue shift of the spectral features due to the lower average effective index of the entire structure because of the oxide growth [21]. The amount of the shift depends strongly on the type of structure that is oxidized. In fact the dynamic of the oxidation process is strongly dependent on both pore sizes and layer porosity (because the rate of the process depends on gas diffusion coefficients [13, 19, 22]).

The shift of the spectral response is not rigid as should be expected from a theoretical point of view but is proportional to the energy range considered [23]. Such a small difference from the expected behavior could be due to an anisotropic oxidation rate that produces a more efficient oxide growth near the sample surface exposed upward in the oven and a thinner layer in the bottom part of the sample.

The wavelength shifts of the spectra ranges from 20 nm (at low energy side of the spectra) to 60 nm (high energy side) with comparable magnitude for all the analyzed samples are observed. The knowledge of these shift's magnitude enables the design of samples that will show the desired optical spectra after the oxidation treatment. The trend appears in shift magnitudes for each sample is shown in Figure. 4.2.

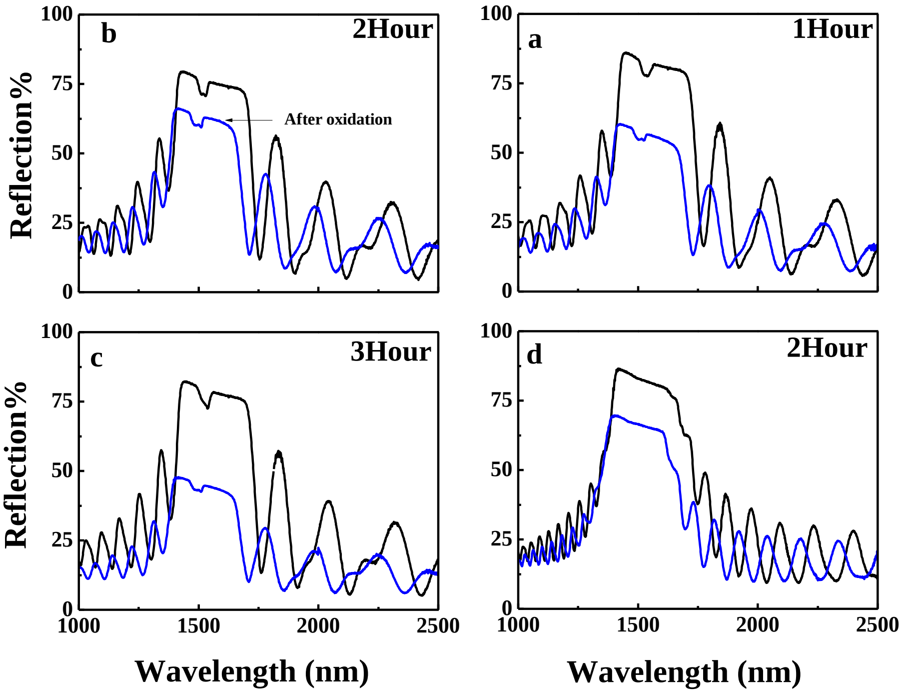

Figure 4.2. Effect of the thermal oxidation on sample with a MC-like structure annealed for different time (all sample were annealed at 350 °C) for 1 hour (a), 2 hour (b), 3 hours (c) and a DBR composed by 20 periods (d).

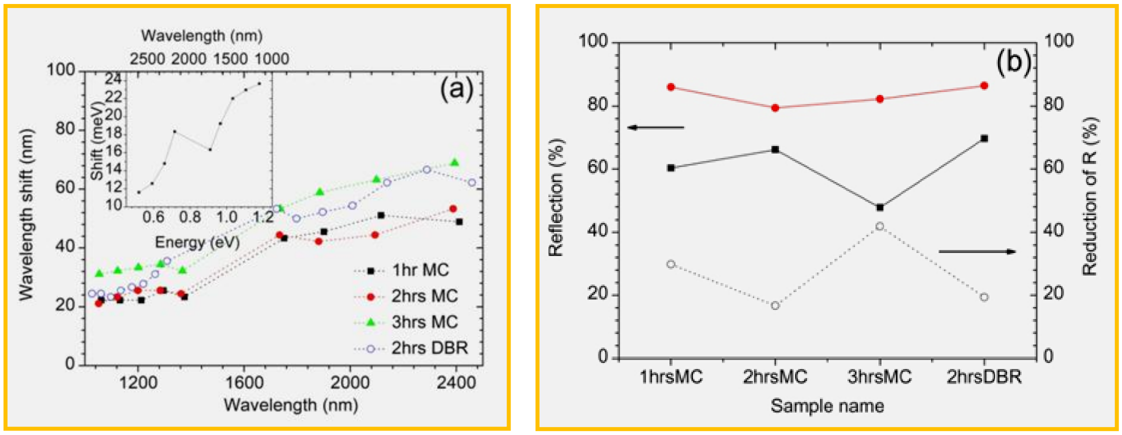

Figure 4.3 (a) Wavelength shift of the side lobe minima as a function of their wavelength. The different datasets refer to the different samples realized as indicates in the legend. The inset clarify that the shift is not rigid over the entire wavelength range but it's proportional to the energy. (b) Left axis - Values of the reflectance before (red data) and after oxidation (black data). The reflectance systematically decreases after the oxidation because of the reduced refractive index contrast. Right axis – This reduction can be quantified in 20 to 40%, with such oscillations dependent on the area of the sample.

Figure 4.3a shows that MC-like structures oxidized for 1, 2 and 3 hours at 350 °C show similar wavelength shift, while 3 hours thermal treatment create a systematically larger shift, probably due to a thicker oxide layer. The single DBR, oxidized for 2 hours, shift more than the corresponding MC-like sample, presumably because it lacks of the central defect layer. Furthermore it is found that shift of side lobe minima is proportional to energy as clearly shown in inset of Figure 4.3a. Figure 4.3b shows the reduction in the value of the reflectance induced by the oxidation. It is clear that the oxide thickness have to be minimized in order to maintain the highest reflectance value that in turn, determines the cavity Q-factor. The oscillation in the reflectance value is due to in-homogeneities in the sample surface and depends on the fraction of area investigated during the optical characterization [24].

4.3.1.1 Reproducibility of thermal oxidation data

During the measurements some discrepancies between spectra acquired on the same sample were noted. These arise from in-homogeneities on the surface of the porous samples. By measuring different points on same sample we get an estimation of the data dispersion.

Figure 4.4a shows a series of measurements taken along the 6 mm diameter of a sample and a zoom view around 1770nm is shown in Figure 4.4b. Because of the low quality of these first MC samples, we choose as a spectral reference the first minima on the right of the stop band (at 1770 nm). We have then monitored its position after each thermal treatment.

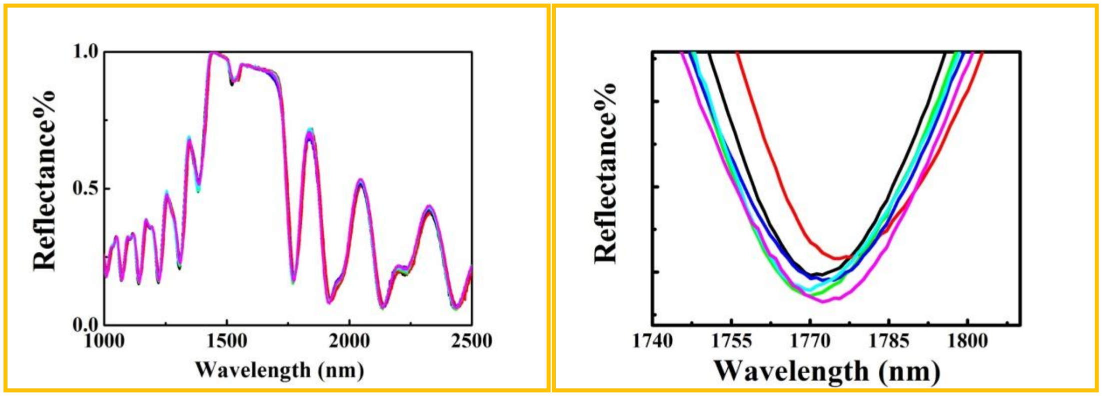

Figure 4.4 (a) Set of 6 measurements taken along the diameter of the same porous silicon sample. The minima at 1770nm indicate the area enlarged in the next panel. (b) Zoomed view of the first minima on the right of the fundamental stop band: all minima spread over a narrow range of 11 nm.

A set of six nominally identical samples was prepared and each of those was measured at 6 different positions randomly (an area of nearly 1 mm^2 is investigated during each measurement). The largest standard deviation (SD) found on a single sample was of about 12 nm. If the entire set of measurements is considered, the largest interval (LI) that contains all the reference points is of about 43 nm, while the standard deviation of the entire set is 13.5 nm. Of the 6 samples, three were oxidized at 300 °C for 1 hour, while the other three for 2 hours. After the oxidation the reference point shift of 34 nm for the samples treated for 1 hour (SD: 8.3 nm and LI: 25.6 nm) and of 57 nm for the samples treated for 2 hours (SD: 4.1 nm and LI: 14.5 nm).

In summary an oxidation step of at least two hours is required to efficiently stabilize the porous silicon samples

4.3.1.2 Simulated aging by immersion in water

To check the effectiveness of the surface passivation, we simulate samples ageing by immersing them in water and then monitoring their optical properties at different times. The results are shown in Figure 4.5. Spectra were normalized to make it easier the comparison among the samples. Reflectivity values within the complete set of samples varied up to 40% (as underlined previously). The optical shift of the reference point is within 20 nm and is thus compatible with the wavelength spreading induced by the surface sample in-homogeneities [24]. Moreover it is of interest to note that, for the set of measurements considered here, the comparison between the oxidized samples and those immersed for 15 hours in water always falls within only 12 nm of shift. This value is comparable with the data reproducibility and indicates a complete porous silicon oxidation.

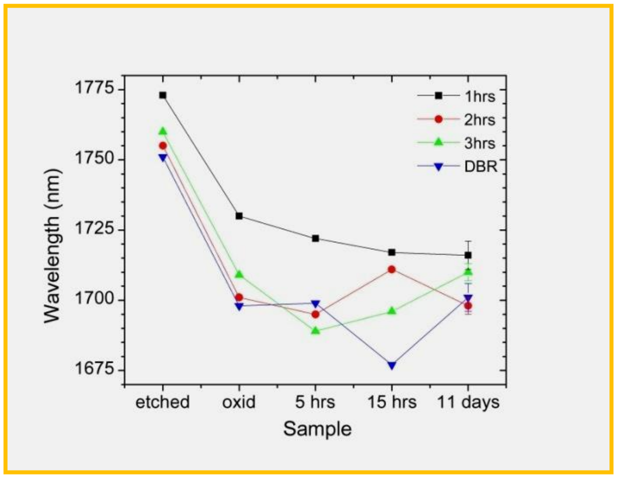

Figure 4.5 Shift of the reference point in the samples annealed at 350 °C for different times. Two hours of thermal treatment is the minimum duration to efficiently passivate the porous surface.

The analysis of the reference points shifts across the multilayer samples can be used to estimate the completeness of the oxidation process. The clear correlation between the duration of the thermal treatment and the shift of the spectra suggest that the oxidation process is nearly completed after just two hour of annealing, despite the low process temperature. The results found are compatible with already published data [4]. A second point to note is that the shift between the oxidized sample and those immersed in water for 5 or 15 hours is always within the uncertainties due to sample in-homogeneities. Also this fact indicates that despite the aging in an oxidizing agent, the optical properties of the samples do not change in time and that the porous surface can be considered stabilized.

4.3.1.3 Thermal oxidation of free-standing MC structure

It is important to note that so far all the oxidation process was performed on samples bound to the bulk silicon substrate and that the same process performed on free standing membranes should give a more homogeneous oxidation of the structure, due to its thin and open sided structure. However, the handling of such membranes is particularly difficult and so does not allow this kind of analysis. This problem was solved with a new set of multilayer samples, composed of free standing MC membranes which were fixed between two metal plates and exposed only a small area of about 1mm^2. In this way we obtained two results: we reduced the error homogeneity by measuring always the same sensor area and the small suspended area improves the mechanical strength of the samples. Figure 4.6 shows resonance shift observed due to thermal oxidation for different time duration.

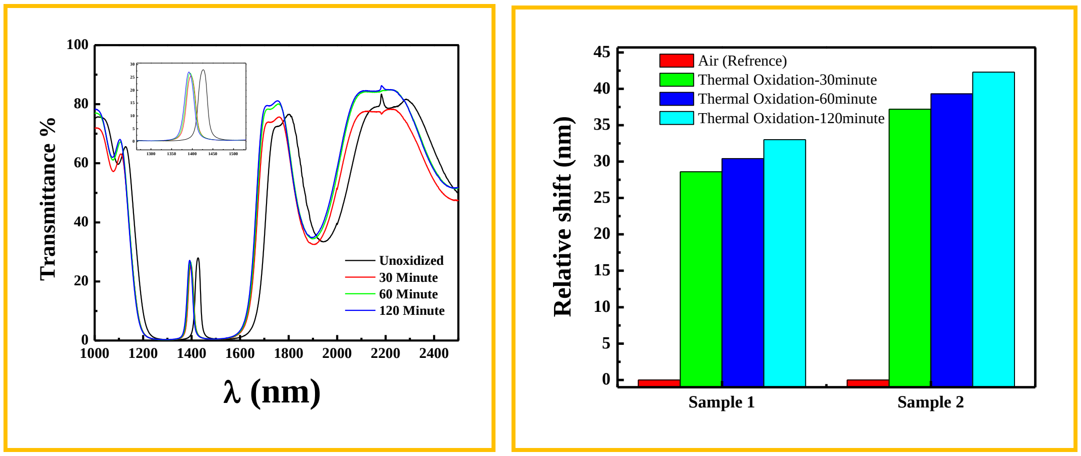

Figure 4.6. (a)Effect of the thermal oxidation on sample with a MC-like structure in freestanding nature annealed for different time (all sample were annealed at 350 °C) for 0.5 hour, 1 hour and 2 hours) composed by 10 periods. (b) Graphical representation for MC oxidation for different time for two studied samples

For an oxidation of 30 minute at 350^0C, the two samples shows a shift of about 28.6nm and 37.2nm respectively and could be due to different sensitivities of these MC samples or slightly different morphological (top and bottom) surfaces. However the shift in the resonance observed after this first oxidation is strongly correlated and additional ~2nm and 5nm of shift are observed in both samples after treating them for 60minute and 120 minute, respectively. We believe that during the first oxidation treatment the surface is somehow stabilized and treating them further, thermal process induces reproducible oxide growth. These results further confirm that a stable and adequate oxide layer is achieved in 2 hour at 350 °C during thermal oxidation as previous study suggest.

In conclusion, an oxidation step of at least two hours at 350 °C is required to efficiently stabilize the porous silicon samples.

4.3.2 Chemical surface modification

Thermal oxidation as described in previous section is usually done to stabilize the porous structure with good control over final samples properties. However under some conditions thermal oxidation may not work i.e. silicon oxide degrades the Q factor of MC structures to a much low value [25, 26]. In fact a thin layer of organic molecules (compatible with the PSi chemistry) allows the immobilization of different chemical and biological molecules onto its surface without affecting the quality of the photonic structure [7, 8]. Since the first report of chemical modification by Chidsey et al., large efforts have been made to find effective methods to replace the unstable Si-H species with an organic layer [27].

Hydro-silanization method and silanization methods provides an alternative to thermal process to stabilize PSi surface and to cover the pore surface with a proper functional layer [7, 8].

4.3.2.1 Sample fabrication for Chemical surface modification

MOLECULE	TYPE OF SAMPLE
Dodecene	Multilayer
10-undecenoic acid	Single layer
Heptenoic acid	Single layer
10-undecylenic acid	Multilayer
Amino-silane	Single layer, Multilayer (MC)

Table 4.1 Resume of the molecules used to infiltrate the fabricated samples.

Hydrosilyation. Hydrosilyation involves the substitution of a silicon-hydride bond with an unsaturated carbon-carbon bond [7]. Thus the reaction requires a silicon surface passivate with hydrogen that will react with organic molecules having double or triple carbon-carbon bond. Different molecules were considered as a surface modification reagents: Dodecene, 10-undecenoic acid, heptenoic acid and 10-undecynoic acid in toluene were used as surface modification reagents, with 0.1, 0.3, 0.3 and 0.3M (Aldrich chemicals, used without any further purification step). The molecules used and the type of samples are treated with are summarized in Table. 4.1

The hydrosilylation reactions we have considered are performed in liquid phase, thus the freshly prepared PSi samples were placed in the flask and the reagent dissolved in toluene was added. For 10-undecenoic acid and heptenoic acid all the reactions were allowed to proceed for 1 hour at boiling temperature (70°C) of toluene. After removing the solution, the samples were rinsed with high purity toluene, and then dried under a stream of high-purity N_2.

Silanization. An alternative well known reaction is the silanization [8, 27, 28]. Silane based coupling agent contains both organic and inorganic reactivity in the same molecule. Silane molecule has a hydrozable group such as methoxy and ethoxy that can form silioxane bonding (Si-O-Si) with other hydrozable grop. Evidently the substrate must have hydroxyl groups on its surface in order to achieve silanization [27, 28]. We used amino-silane (3-(diethoxymethyl-silyl) propylamine**)** as silane reagent. Amino-silane was dissolved in toluene with a volume concentration of 2%. The PSi terminated with OH (OH bonds were produced by putting porous silicon in water/Ethanol solution for three days or for 72 hours and sequent washed by water/Methanol, Methanol/toluene and finally in toluene) immersed in solution for one hour at 70°C . Finally the samples were rinsed with high purity toluene at the same temperature and allowed to cool to room temperature. Furthermore functionalized samples were subsequently washed in a solution of toluene/methanol and then pure methanol at room temperature. Then the sample was immersed for 2 hours in 5 ml fluorescein isothiocyanate (Fluorescent Dye) dissolved in 1 mM in carbonate buffer 0.1M, pH 9. After that it was rinsed first in a solution made by phosphate buffer 0.05M + NaCl 0.5M + TritonX-100 0.1%, then with water and finally dried with N_2.

Both single layer and multilayer porous silicon samples were fabricated for subsequent functionalization procedures. Figure 4.7 shows the structure of one of the multilayer samples used in the functionalization procedures. Low and high porosity layers are clearly visible as dark and bright layers, respectively. Pore sizes used during the functionalization processes were deliberately made smaller, to check PSi modification in extreme constrained conditions.

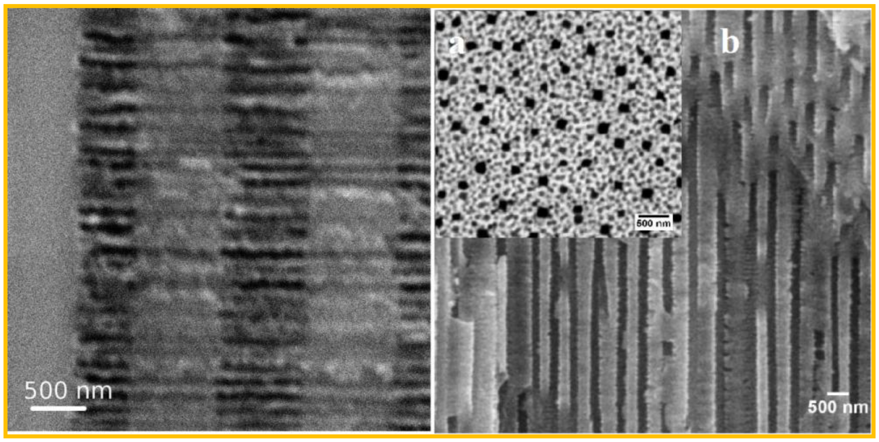

(a) (b)

Figure 4.7. SEM images of multilayer {a) and monolayer (b) PSi sample. (a) Current used to etch high porosity layers (darker layers~40ma/cm^2) is the double~80ma/cm^2 of that used for the low porosity ones (brighter layers). (b) On the right SEM image (top and cross-section) of PSi monolayer fabricated on 0.1Ωcm substrate.

4.3.2.2 <u>Optical characterization</u>

Infrared spectroscopic characterization: Samples were analyzed both with IR and micro-Raman spectroscopy. In particular IR spectroscopy was used to initially characterize the presence of the organic molecules on surface modified samples, while micro-Raman analysis was performed to investigate the homogeneity of the functionalization along the entire cross-section of porous structures.

Theoretical Approach.

Both Raman and infrared spectra of all the considered molecules were theoretically simulated using Gaussian 03 software with 6-31(d,p) basis set. DFT calculations were carried out using B3LYP [29, 30]. To reduce the computational problem complexities, we substitute the functional molecule group that react with silicon atom with a single Si atom, and do not consider the presence of the bulk silicon phase attached to the molecule. The optimized molecular structures (with substituted Si atom) are shown below in Figure 4.8 and 4.9.

(a) **(b)**

Figure 4.8. 10-undecenoic acid before (a) and after (b) the addition of a silicon atom to the double bond reactive site

(a) **(b)**

Figure 4.9. Dodecene before (a) and (b) after the addition of a silicon atom to the double bond reactive site

Experimental results

Figure 4.10 shows the theoretical infrared and Raman spectra for carboxylic acid. Black and red datasets indicate the pure gas phase and the carboxylic acid with a Si atom substituted to carboxyl group, respectively. Along with three main bands C=O vibration band at 1845cm^{-1} and asymmetric and symmetric stretching of CH_2 at 3031 and 3075cm^{-1} are observed respectively [31].

The experimental Attenuated Total Reflection infrared spectra obtained from the PSi samples surface functionalized with carboxylic acid is shown in Figure 4.11. The analysis performed clearly shows the presence of four main peaks that are visible only in functionalized samples and cannot be ascribed to the underlying PSi: at 1093 cm-1 the band can be ascribed to Si-O bonds, the resonance near 1695 cm-1 is the C=O vibration band [31]. The CH_2 stretching peaks are red shifted compared to the theoretical spectra and corresponds to experimental observed vibrations band at 2841 and 2920 cm^{-1}. The deep at 2351 cm^{-1} is due to CO_2 [31, 32]. The differences in vibration frequencies energies between theoretical and experimental data are most probably due to fact that theoretical analysis take into account molecules in gas phase, whereas the experimental measurements reflect the presence of the bulk silicon as a substrate. Nevertheless the observed and calculated data are quite in agreement with each other.

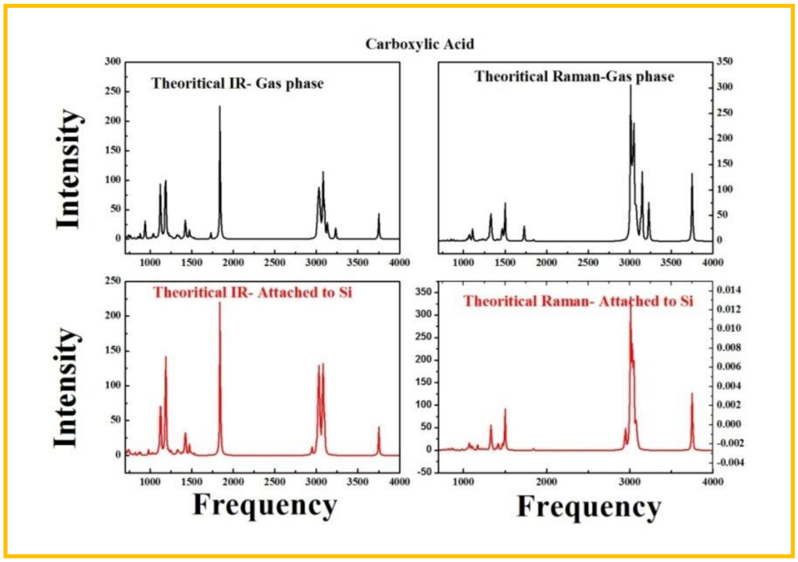

Figure 4.10. Simulated infrared and Raman spectra of carboxylic acid. Black dataset refer to pure gas phase, while red lines are for molecules with carboxy group substituted by a Si atom.

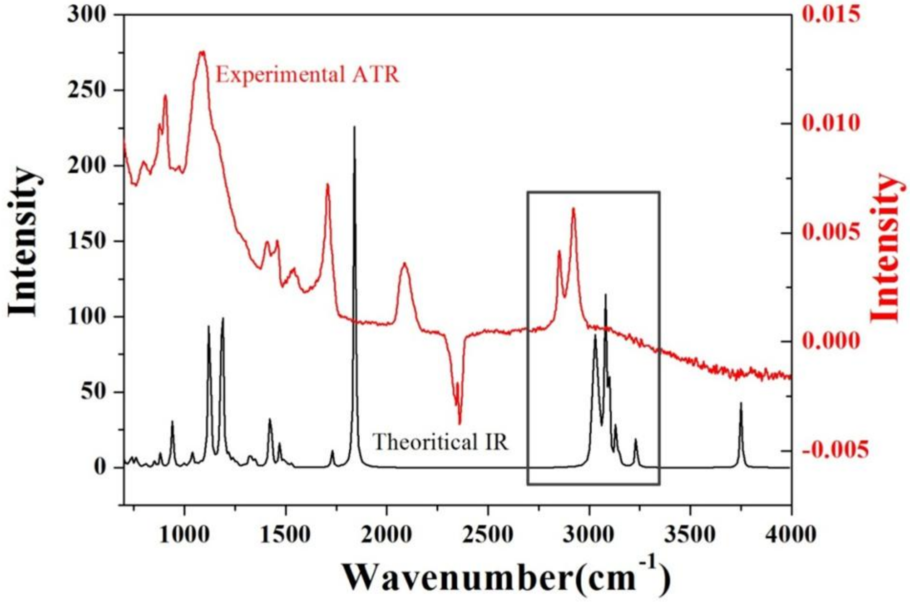

Figure 4.11 Theoretical and Experimental ATR spectra of a functionalized and reference PS samples. The intense band around 1093 cm^{-1} is due to Si-O bonds, while the deep around 2351 cm^{-1} is due to CO_2. In inset shows the shift in vibration bands may be attributed due to different phase: In theory calculation are made in gas phase and in experimental spectra is observed in solid phase.

Figure 4.12 shows the ATR of four PSi samples two of which were treated with both carboxylic acid and the other two functionalized with Dodecen. C-H and Si-H peaks are visible on both molecules. Asymmetric and symmetric stretching of CH_2 is clearly visible at 3031 and 3075 cm^{-1}, respectively. As expected C=O resonance are present only in carboxylic acid spectra at 1695 cm^{-1}. The similarity between the spectra confirms the good reproducibility of the functionalization technique. In both pristine porous silicon and functionalized porous silicon, the two intense peaks at 2099 cm^{-1} and 919 cm^{-1} correspond to Si-H vibration modes [33].

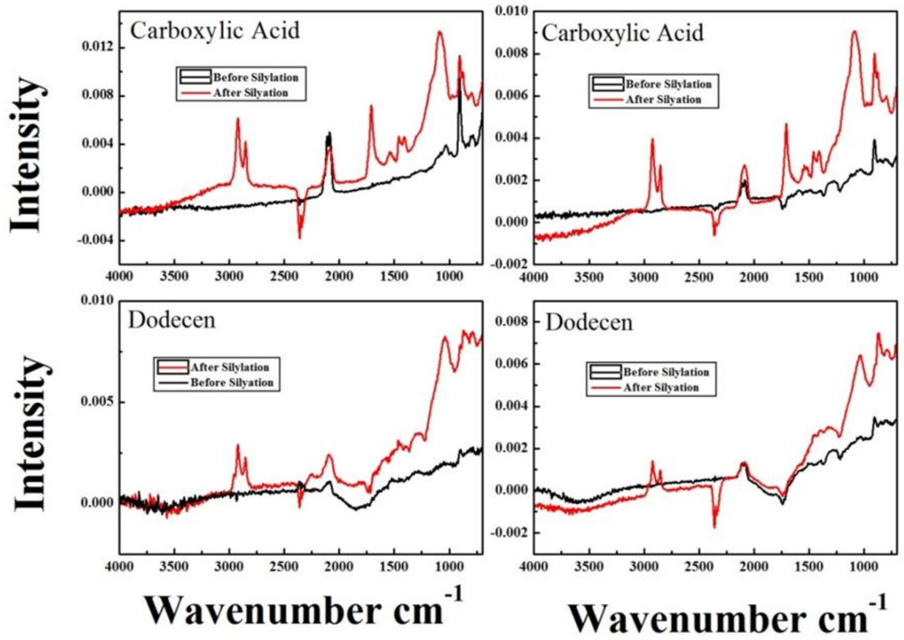

Figure 4.12 IR spectra of two samples functionalized with carboxylic acid and of two other samples treated with Dodecen

Micro-Raman cross sectional characterization:

A more detailed analysis of the silanized samples was performed using the micro-Raman technique. If compared with IR techniques, a Raman spectrometer coupled to an optical microscope permit to achieve a high spatial resolution (~1µm). Thus micro-Raman experiment enables a spatially resolved mapping analysis along sample cross section. Due to the roughness of the cleaved surface and of the underlying PSi sample, is extremely difficult to get quantitative measurements, because the collection efficiency of the optical system varies from point to point. Moreover some of the PSi investigated show an intrinsic photoluminescence (PL) [34]. This broad and intense background heavily influences the Raman spectra and hidden most of the Raman transition, so that only the most intense transitions can be seen. An He:Ne laser was used as excitation source to minimize the intensity of the PL band, nevertheless its intensity is at least of comparable magnitude to that of the Raman signal. For these reasons we cannot perform a quantitative analysis.

The functionalized samples were cleaved and the freshly exposed (100) surface was investigated. For each sample a certain number of profiles were realized on different positions along the cleaved surface, to check for the presence of the organic layer versus samples depth and the homogeneity of the functionalization reaction on samples area. Figure 4.13a, 4.13b and 4.13c show Raman depth profiles for a PSi samples treated with dodecene. Profiles were acquired along three different lines. Figure 4.13d shows the spectra of a silicon sample taken as reference. Each sample was analyzed by checking for the presence of the organic molecules at five different positions (corresponding to the five dataset of each graphics). A resonance located near 3000 cm^{-1} is present in all treated samples, whereas is absent in reference sample. Those features are reasonably due to CH_2 stretching modes [31].

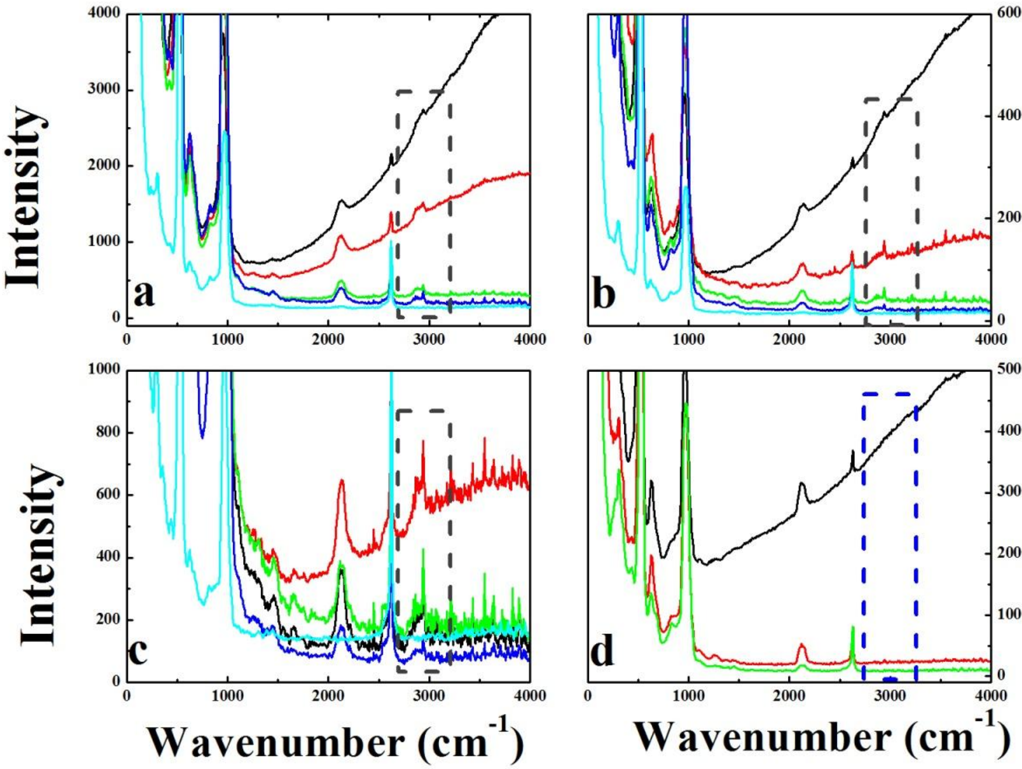

Figure 4.13 Raman spectra of PS samples treated with Dodecen. Panels (a), (b) and (c) are three depth profiles taken at different positions along the porous area. Dashed lines indicate the spectral position of the characteristic CH_2 vibronic transitions around 3000 cm^{-1} that is absent in reference sample (d).

Figure 4.14 shows the characterization of PSi samples treated with carboxylic acid. The main result with this molecule is the fact that micro-Raman technique does not have enough sensitivity to detect COOH group, even from the sample surface. As suggested above, the strong PL background could hide the peak. But another possible reason may be the following: carboxylic acid chain has a diameter of about 4.8 Å due to its COOH group, on the other hand Si-H (the binding site) is separated by 3.84 Å with each other, so that only half of available site could be functionalized by carboxylic groups [35]. As a result due to their low concentration of molecules could be possible reason for low intensity. Furthermore the absence of C=O mode may be due to its low intensity, as it strongly depends on reduced mass of functional group. Due to larger reduced mass, a small change in moment will be observed as a result low intensity will be observed. This fact could be supported as due to small reduced mass as in previous study (in case of dodecene) asymmetric and symmetric stretching of CH_2 bond can be easily observed that have strong Raman signal as shown in Figure 4.13.

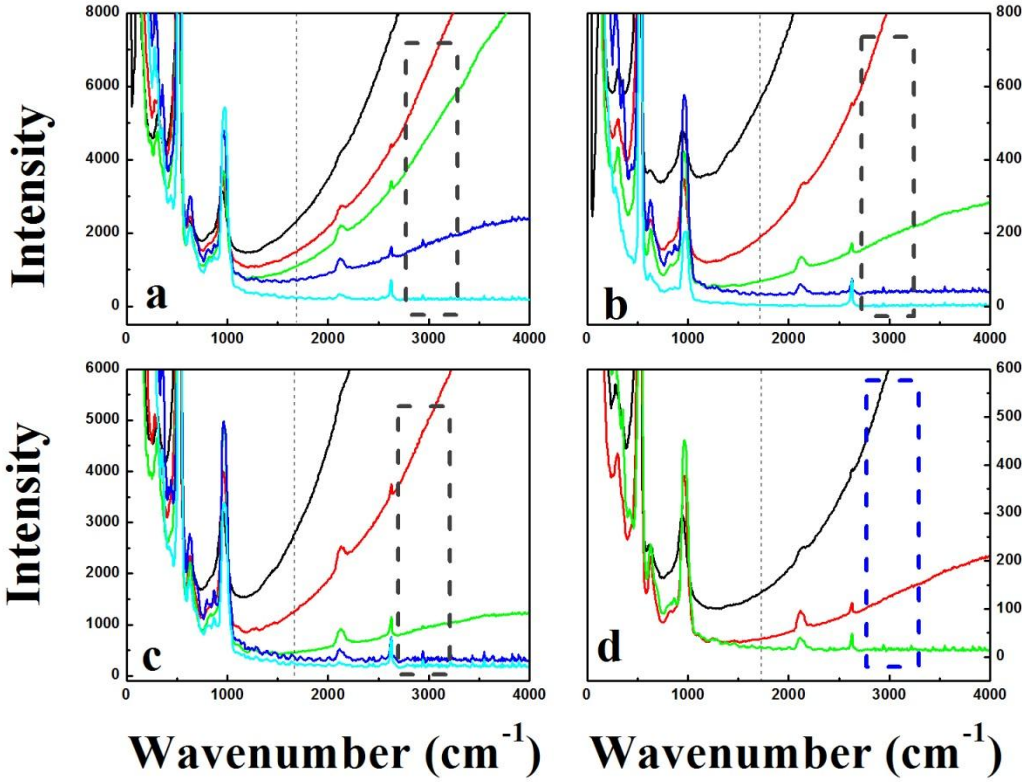

Figure 4.14 Raman spectra of PS samples treated with carboxylic acid. Panels (a), (b) and (c) are three depth profiles taken at different positions along the porous area. No peak is observed for C=O at 1695 cm^{-1}. Dashed lines indicate the spectral position of characteristic vibronic transitions around 3000 cm^{-1} for CH_2 stretching that is absent in all treated and in reference sample (d).

We perform similar functionalization treatments with two other types of acid molecules. Results are shown in Figures 4.15 and 4.16 for undecylenic and heptenoic acids, respectively.

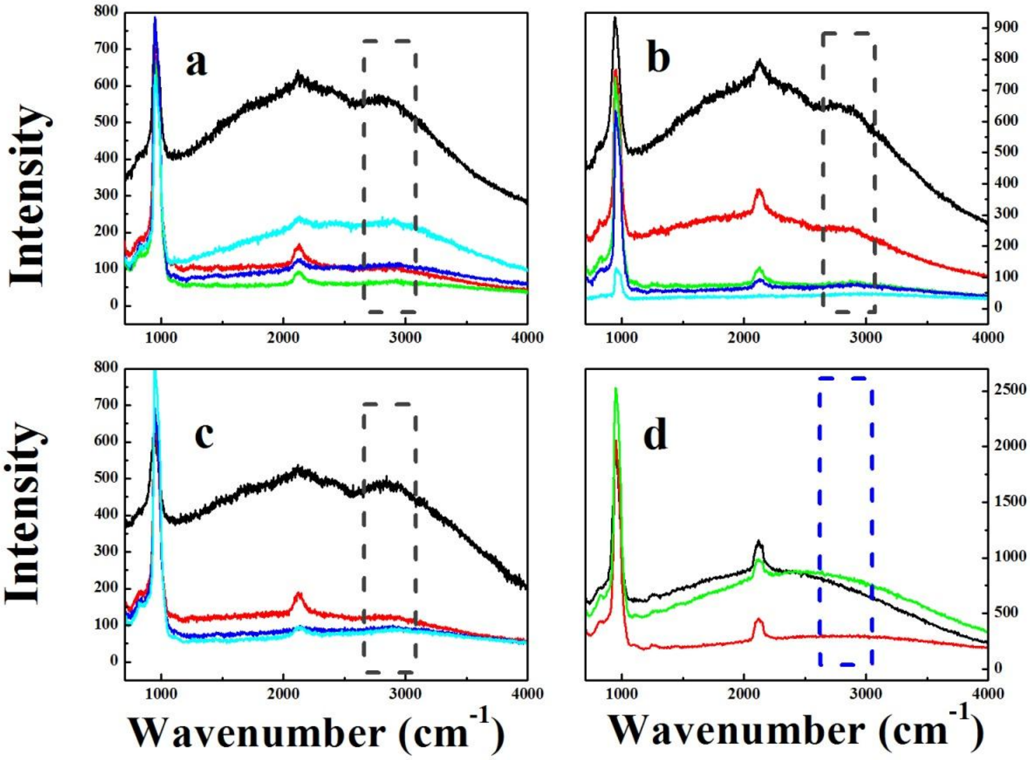

Figure 4.15 Raman spectra of PSi samples treated with 10-undecenoic acid. Panels (a), (b) and (c) are three depth profiles taken at different positions along the porous area. Dashed lines indicate the spectral position of characteristic vibronic transitions around 3000 cm^{-1}for CH$_2$ stretching that is absent in reference sample (d).

In both cases we are able to observe the broad peak that may refers to CH$_2$ bond vibration frequency [31]. For both molecules an evident shoulder appears near 3000 cm^{-1}. Reference PSi samples always show a broad PL band without any lateral shoulder. It is, thus, reasonable to assume that the broad shoulder around 3000 cm^{-1} is due to CH$_2$ vibration modes that is usually one of the most intense Raman mode in carboxylic acids.

For heptenoic acid the intensity of the Raman signal from the surface was order of magnitude stronger than that of the spectra acquired inside the porous layer. In Figure 4.16 the intensity of the spectra acquired near the surface were reduced by the factor shown in the graph. This fact could indicate a certain difficult of the heptenoic molecules to penetrate inside the pores. Nevertheless Raman analysis indicates that PSi surface is functionalized by organic molecules because of the presence of the CH_2 band.

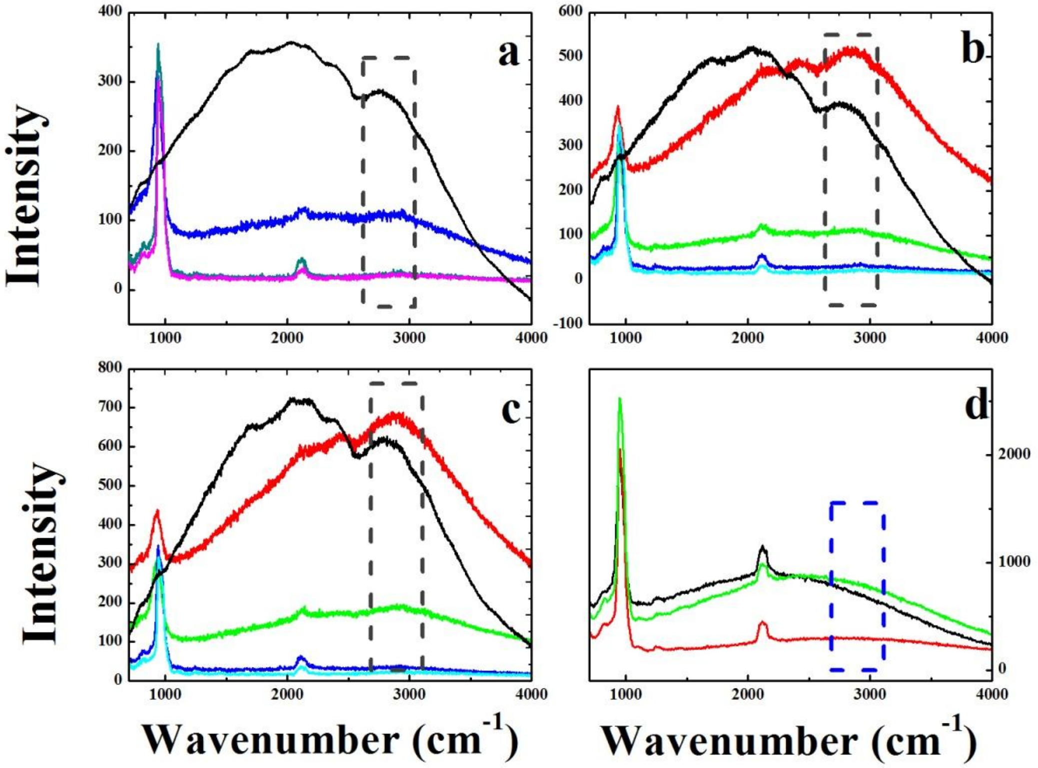

Figure 4.16 Raman spectra of PSi samples treated with heptenoic acid. Panels (a), (b) and (c) are three depth profiles taken at different positions along the porous area. As before, dashed lines indicate the spectral position of characteristic vibronic transitions around 3000 cm^{-1}. CH_2 stretching is absent in reference sample (d).

Lastly, we test silanization reactions to modify the PSi surface [8, 27, 28]. We investigate this type of reactions on several types of samples (both single layer and multi-layer either attached on silicon substrate or free-standing membranes). Single layer was chemically modified and characterize along the cross-section to check for the effectiveness of the reaction. The chemical modification was verified by micro-Raman along the cross-section as shown in Figure 4.17.

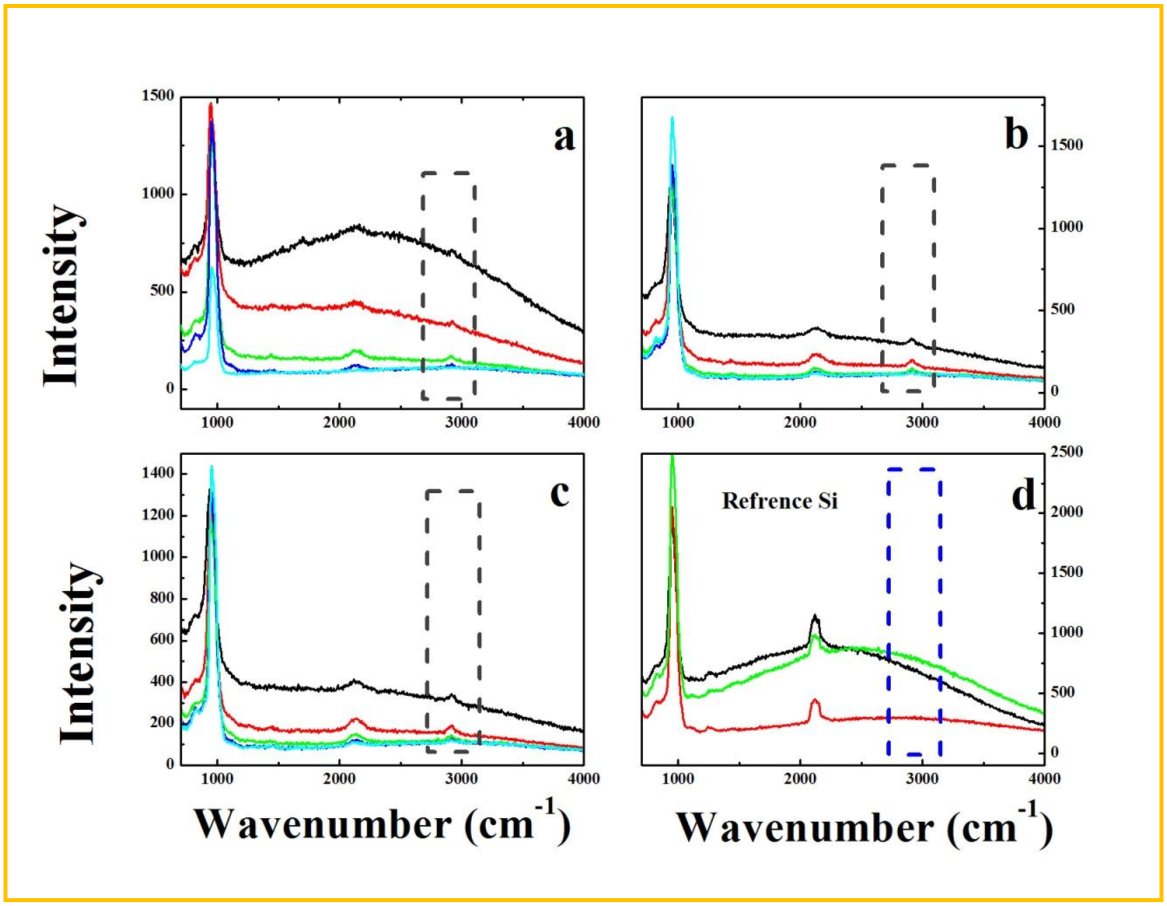

Figure 4.17 Raman spectra of PSi samples treated with amino-silane. Panels (a), (b) and (c) are three depth profiles taken at different positions along the porous area. As before, dashed lines indicate the spectral position of characteristic vibronic transitions around 3000 cm^{-1}. CH_2 stretching is absent in reference sample (d).

The CH_2 vibrational modes around ~3000cm^{-1} are visible in all the acquired spectra at different points. The un-reacted hydrated species Si-H at 2090cm^{-1} are also apparent in all [33]. However the presence of CH_2 mode clearly indicates the presence of organic molecules on the PSi surface along the pore length [31]. Fluorescein isothiocyanate is used to confirm silane modified surface [37]. The sample was immersed for 2 hours in Fluorescent Dye, and fluorescent molecules bind with the silane within porous structure. Cross-sectional florescence image are shown in Figure 4.18 below, acquired with Leica microscope mounting a filter.

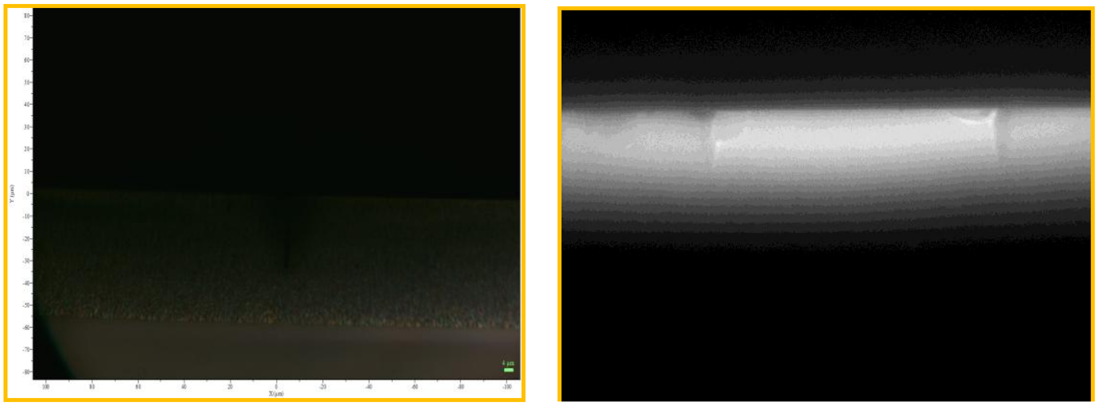

(a) (b)

Figure 4.18. Optical image of PSi surface (a) before and (b) after attaching the fluorescent dye to the amino-silane molecules (Scale bar is 1μm)

Florescence signal is clearly seen from the whole sample cross-section (Figure. 4.18b) and clearly indicates that silane successfully modified the entire porous layer.

The effectiveness of the silanization reaction was tested on MC samples. The shift in resonance position clearly and easily verifies the presence of silane molecules attached to the porous layer [38]. As a proof of functionalized process, MC structures (both free-standing and attached to the silicon substrate) were fabricated as discussed in section 4.3.1.4. We fabricate three MC samples: two were released from the substrate and one was left attached on the bulk SI. Figure 4.19 shows the transmission and reflectance spectra of MC structure for each step carried out for functionalization.

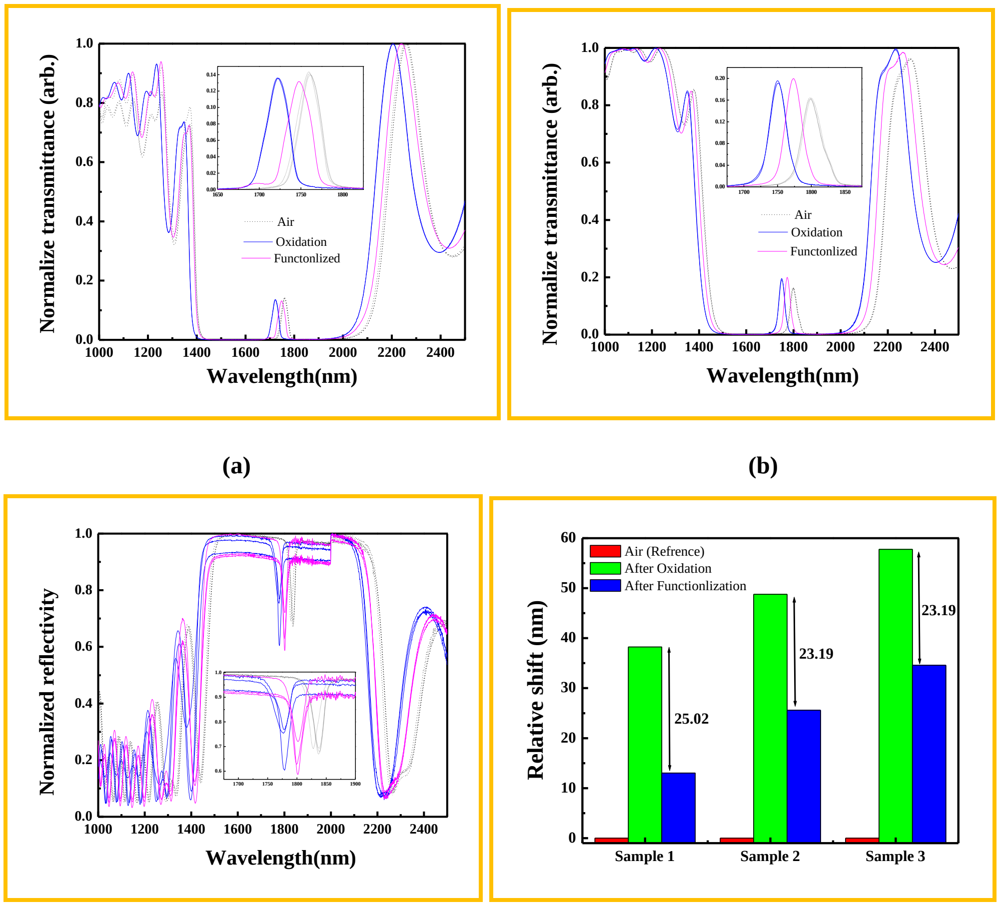

(a) (b)

(c) (d)

Figure 4.19. Effect of the surface modification at each step on sample with a MC-like structure in freestanding nature (a and b) and attached with the substrate shown in panel (c) (all sample were annealed at 350 °C for one hour before functionalization). Inset of Figure shows the zoom view around resonance peak. (d) Graphical representation for all samples for surface modification.

As already discussed in Section 4.3.1.4, oxidation introduces a blue shift of the spectra. Further adding silane layer to the porous MC structure produces a red shift of the resonance peak due to the added material within the pores. A monolayer of silane results in a red shift of about 25nm for both free-standing MC and for MC on silicon substrate. These observed results further confirm the successful activation of silane layer. Thus the reaction procedures considered here constitute an efficient and versatile method to modify the surface of the PSi and to serve as an intermediate layer to attach other functional groups or analyte.

4.4. Conclusions

In conclusion, the main results achieved in this chapter are the followings: we found thermal oxidation to be an effective method to passivate the PSi surface and to stabilize the optical properties of the sample against aging processes. The oxide grown on the sample surface is thin enough to maintain the sample optical quality and, at the same time, it avoids drift in the spectral response either after sample immersion in water for long time or storage in air for days. Moreover the functionalization procedures performed shown that PSi surface can be effectively functionalized using different organic molecules and with rather simple method. This chapter concludes that both polar and non-polar molecules can be used to modify porous silicon surface. The main difference being the state of the PSi surface prior to the functionalization process: fresh etched samples have to be used in the case non polar molecules, while aged or thermally oxidized PSi is required with polar molecules. The developed thermal stabilization and chemical stabilization process allows a safer storage conditions in the device context for the sensing devices.

References

[1]Keiki-Pua S. Dancil, Douglas P. Greiner and Michael J. Sailor," A Porous Silicon Optical Biosensor: Detection of Reversible Binding of IgG to a Protein A-Modified Surface" J. Am. Chem. Soc., 121 (34), pp 7925–7930 (1999)

[2]Finny P. Mathew, Evangelyn C. Alocilja," Porous silicon-based biosensor for pathogen detection" Biosensors and Bioelectronics, 20(8),pp 1656–1661 (2005)

[3]Rong-xia Liu, Liang-liang Chen, Hong-yan Zhang, "A label-free single photonic quantum well biosensor based on porous silicon for DNA detection" Optoelectronics Letters, 9(3) pp 225-228 (2013)

[4]Luca De Stefano, Paolo Arcari, Annalisa Lamberti, Carmen Sanges, Lucia Rotiroti, Ilaria Rea and Ivo Rendina," DNA Optical Detection Based on Porous Silicon Technology: from Biosensors to Biochips" Sensors, 7(2), pp 214-221 (2007)

[5]Mouna Hecini, Abdellah Khelifa, Bachir Bouzid, Nadjib Drouiche, Salaheddine Aoudj, Houria Hamitouche," Study of formation, stabilization and properties of porous silicon and porous silica" Journal of Physics and Chemistry of Solids, 74(9), pp 1227–1234 (2013)

[6]Rolfe C. Anderson, Richard S. Muller and Charles W. Tobias," Chemical Surface Modification of Porous Silicon" J. Electrochem. Soc., 140(5), pp 1393-1396 (1993)

[7]T. Jalkanen, E. Mäkilä, Y.-I. Suzuki, T. Urata, K. Fukami, T. Sakka, J. Salonen, Y. H. Ogata," Studies on Chemical Modification of Porous Silicon-Based Graded-Index Optical Microcavities for Improved Stability Under Alkaline Conditions" Advanced Functional Materials, 22(18), pp 3890–3898 (2012)

[8]Joakim Riikonen, Mikko Salomäki, Jessica van Wonderen, Marianna Kemell, Wujun Xu, Ossi Korhonen, Mikko Ritala, Fraser MacMillan, Jarno Salonen, and Vesa-Pekka Lehto," Surface Chemistry, Reactivity, and Pore Structure of Porous Silicon Oxidized by Various Methods", Langmuir, 28 (28), pp 10573–10583 (2012)

[9]A. E. Pap, K. Kordás, G. Tóth, J. Levoska, A. Uusimäki, J. Vähäkangas, S.Leppävuori and T. F. George," Thermal oxidation of porous silicon: Study on structure", Appl. Phys. Lett. 86, 041501 (2005)

[10]Rabah Boukherroub, Danial D. M. Wayner and David J. Lockwood," Photoluminescence stabilization of anodically-oxidized porous silicon layers by chemical functionalization", Appl. Phys. Lett. 81, 601 (2002)

[11]Gelloz B., Nakagawa T., Koshida N., "Enhancement of the quantum efficiency and stability of electroluminescence from porous silicon by anodic passivation", Appl. Phys. Lett., 73, 2021-2023 (1998).

[12]Bsiesy A., Gaspard F., Herino R., Ligeon M., Muller F., Oberlin J.C., “Anodic-oxidation of porous silicon layers formed on lightly p-doped substrates ”, J. Electrochem. Soc., 138, 3450-3456 (1991).

[13]B. E. Deal and A. S. Grove,” General Relationship for the Thermal Oxidation of Silicon” J. Appl. Phys. 36, 3770 (1965)

[14]Yukio Ogata, Hiroyuki Niki, Tetsuo Sakka and Matae Iwasaki,” Oxidation of Porous Silicon under Water Vapor Environment” J. Electrochem. Soc., 142(5). pp 1595-1601(1995)

[15]Karyn L. Jarvis, Timothy J. Barnes, Clive A. Prestidge,” Surface chemistry of porous silicon and implications for drug encapsulation and delivery applications”, Advances in Colloid and Interface Science,175, pp 25–38 (2012)

[16]Rabah Boukherroub, J. T. C. Wojtyk, Danial D. M. Wayner and David J. Lockwood,” Thermal Hydrosilylation of Undecylenic Acid with Porous Silicon”, J. Electrochem. Soc., 149(2) pp H59-H63 (2002)

[17]Wayne Yoshida, Robert P. Castro, Jeng-Dung Jou, and Yoram Cohen,” Multilayer Alkoxysilane Silylation of Oxide Surfaces”, Langmuir, *17* (19), pp 5882–5888 (2001)

[18]M. Ghulinyan, C. J. Oton, G. Bonetti, Z. Gaburro, L. Pavesi, “Free-standing porous silicon single and multiple optical cavities,” Journal of Applied Physics 93(12), 9724-9729 (2003).

[19]Hiroyuki Kageshima and Kenji Shiraishi,” First-Principles Study of Oxide Growth on Si(100) Surfaces and at SiO_2/Si(100) Interfaces”, Phys. Rev. Lett. 81, pp 5936–5939 (1998)

[20]J. T. Fitch, G. Lucovsky, E. Kobeda and E. A. Irene,” Effects of thermal history on stress-related properties of very thin films of thermally grown silicon dioxide” J. Vac. Sci. Technol. B, 7, pp 153 (1989)

[21]H. Zhang, Z. Jia, X. Lv, J. Zhou, L. Chen, R. Liu, J. Ma, “Porous silicon optical microcavity biosensor on silicon-on-insulator wafer for sensitive DNA detection,” Biosensors and Bioelectronics 44(1), 89-94 (2013).

[22] Ogata, Y. H., Tsuboi, T., Sakka, T., & Naito, S.,” Oxidation of porous silicon in dry and wet environments under mild temperature conditions”, Journal of Porous Materials, 7(1-3), 63-66. (2000)

[23]X. G. Zhang, “Electrochemistry of Silicon and Its Oxide”, Kluwer Academic Publishers, New York, 2001.

[24]A. Borghesi, A. Sassella, B. Pivac, L. Pavesi,” Characterization of porous silicon inhomogeneities by high spatial resolution infrared spectroscopy”, Solid State Communications, 87(1) pp 1–4 (1993)

[25] Mulloni, V., C. Mazzoleni, and L. Pavesi. "Elaboration, characterization and aging effects of porous silicon microcavities formed on lightly p-type doped substrates." Semiconductor science and technology 14(12), pp 1052 (1999)

[26] Palestino, G., Legros, R., Agarwal, V., Pérez, E., & Gergely, C.,”Functionalization of nanostructured porous silicon microcavities for glucose oxidase detection”. Sensors and Actuators B: Chemical, 135(1), pp 27-34 (2008)

[27]Christopher E. D. Chidsey, Dominic N. Loiacono,” Chemical functionality in self-assembled monolayers: structural and electrochemical properties,” Langmuir, *6* (3), pp 682–691 (1990)

[28]Nesrine Aissaoui, Latifa Bergaoui, Jessem Landoulsi, Jean-François Lambert, and Souhir Boujday,” Silane Layers on Silicon Surfaces: Mechanism of Interaction, Stability, and Influence on Protein Adsorption”, Langmuir, 28 (1), pp 656–665 (2012)

[29]Parr, Robert G. "Density functional theory." Annual Review of Physical Chemistry 34(1), pp 631-656 (1983)

[30]Orio, Maylis, Dimitrios A. Pantazis, and Frank Neese. "Density functional theory." Photosynthesis research, 102(2-3), pp 443-453 (2009)

[31]Raluca Voicu, Rabah Boukherroub, Vasiliki Bartzoka, Tim Ward, James T. C. Wojtyk, andDanial D. M. Wayner,” Formation, Characterization, and Chemistry of Undecanoic Acid-Terminated Silicon Surfaces: Patterning and Immobilization of DNA” Langmuir, 20 (26), pp 11713–11720 (2004)

[32]S. Sam, L. Touahir, J. Salvador Andresa, P. Allongue, J.-N. Chazalviel, A. C. Gouget-Laemmel, C. Henry de Villeneuve, A. Moraillon, F. Ozanam, N. Gabouze and S. Djebbar,” Semiquantitative Study of the EDC/NHS Activation of Acid Terminal Groups at Modified Porous Silicon Surfaces”, Langmuir, 26 (2), pp 809–814 (2010)

[33]Douglas B. Mawhinney, John A. Glass, Jr., and John T. Yates, Jr,” FTIR Study of the Oxidation of Porous Silicon”, J. Phys. Chem. B, 101 (7), pp 1202–1206 (1997)

[34]L. Pavesi, M. Ceschini, F. Rossi,” Photoluminescence of porous silicon”, Journal of Luminescence, 57(1-6), PP 131–135 (1993)

[35]Wayner, Danial DM, and Robert A. Wolkow. "Organic modification of hydrogen terminated silicon surfaces." Journal of the Chemical Society, Perkin Transactions *2*(1), pp 23-34 (2002)

[36]John Coates,” Interpretation of Infrared Spectra, A Practical Approach” Encyclopedia of Analytical Chemistry, DOI: 10.1002/9780470027318.a5606 (2006)

[37]Jilin Yan, M. Carmen Estévez, Joshua E. Smith, Kemin Wang, Xiaoxiao He, Lin Wang, Weihong Tan,”' Dye-doped nanoparticles for bioanalysis”’nano today, 2(3), pp 44–50 (2007)

[38]Gabriela Palestino, René Legros, Vivechana Agarwal, Elías Pérez, Csilla Gergely,” Functionalization of nanostructured porous silicon microcavities for glucose oxidase detection”, Sensors and Actuators B: Chemical, 135(1), pp 27–34 (2008)

Chapter 5

Sensing with porous silicon micro-cavity (MC) structure

5.1 Introduction

The complex functionalities foreseen in the future lab-on-chip (LoC) and point-of-care (PoC) devices require robust and reliable assay mechanisms. Sensors based on physical detection mechanisms (such as optical or electrical) have the advantage to be applicable to a widespread type of analysis [1-3] but show a poor chemical specificity. They require a proper functional interface to generate a signal proportional to the number of detection events. As in every type of sensors this functional layer should compete with the non-specific binding in order to generate reliable signals. However, this non-specific signal (NSS) is more pronounced in LoC and PoC devices because their rugged structure often renders them incompatible with reference channels and complex sample pretreatments. Different approaches have been explored so far to minimize the role of the NSS, like the use of antifouling materials [4], the development of specific assay procedures [5, 6] and the use of reference channels [7] or complex devices with sample pretreatment [8]. For sensing applications, porous materials have several advantages compared to flat surfaces based sensors. The tailoring of their nanostructure allows a fine tuning in the interaction strength between the analyte and the matrix and their large specific area can be exploited to maximize the sensor response. Both these factors increase the sensor detection limit compared to flat surface devices [9-14]. Furthermore porous materials can be used as filter to remove part of the contaminants and to reduce the net effect of the NSS on the signal generated by the sensor [15].

Porous materials can be used in either flow-over (FO) or flow-through (FT) geometry. FO technique allows clear and easy measurements but suffers from severe limitations in real devices. The weaknesses are mainly due to a poor homogenous binding of the molecular species to the active area, and to the dependence of both response and detection limit on the dynamic of the measurement [16] and on the geometry of the reaction chamber [17]. On the other hand, FT approach can be used on sensors based on free standing membrane and composed by open-ended pores. This geometry maximizes the efficiency of the binding reactions because of a forced diffusion of the analyte over the entire porous material surface. Furthermore the sample can be thoroughly rinsed after the assay to quantitatively remove the not bound material from the porous host.

Several materials were proposed so far as host matrices to fabricate nanoporous sensors [18-20]. Among all, Porous Silicon (PSi) is an ideal candidate for the fabrication of sensors because of the large tunability of its porous structure, its high optical quality and the multi-parametric sensor development opportunity and because of its well versatile surface chemistry [21-29]. In this chapter, we fabricate and investigate good quality factor (Q-factor) n-type PSi microcavity (MC) either bound to Si substrate (FO approach) or in FSM configuration (FT approach).

Recently, even if size exclusion based separation was demonstrated in [30] for p-type freestanding single layer porous silicon membrane, the study of FT based FSM sensors has not been exposed convincingly [31]. Furthermore, using an innovative fabrication protocol as discussed in *chapter 3*, we obtain large membranes of PSi of high optical quality and pore size compatible with liquid mass transport. These membranes behave as excellent reflectance cavities. Moreover they can be detached from the silicon substrate and their mechanical strength permits the operation under FT conditions, even by applying a pressure gradient. In this way, we investigated the performances of the FO versus the FT approach using PSi as analytical sensing substrate. In the first part, we optimize the fabrication of freestanding MCs with large pores. Free-standing MCs were fabricated with the configuration, consist of two Bragg mirrors (three different sample composed by five, seven and ten periods) surrounding a defect layer with pore size of about 40 and 110nm in the low and high porosity layers respectively. In this way we facilitate the penetration of molecules and we were able to quantify a detection limit of $1.5*10^{-4}$RIU (RIU stands for Refractive Index Unit) using methanol/ethanol solution in FO condition (and considering an instrumental resolution of 0.1nm). Furthermore we obtained quantitative data demonstrating that NSS is strongly reduced under FT conditions. Conversely, FO conditions lead to a systematic overestimation of the device sensitivity. These results support the superiority of the FT sensing scheme while raise some questions about the reliability of FO analyses performed on porous substrates.

5.2 Synthesis and Experimental Details

N-type silicon wafer (0.01-0.02 Ω-cm) was used as the initial study material and MCs were fabricated with water based solution contains 12.5% HF as discussed in *Chapter 3*. To detach thin MC from silicon substrate 12%HF + ethanol + 30%H_2O_2 solution was used. After fabrication of PSi, all samples were rinsed in ethanol and dried in N_2 flow. For structural morphology of PSi structure high-resolution Scanning Electron Microscopy (SEM, JEOL mod. JSM 7401F) studies were also performed. Optical characterization was carried out with Varian Cray-5000 UV-VIS-NIR Spectrophotometer with halogen VIS-NIR lamp source.

5.3 Results and Discussions

5.3.1 Organic Vapor Sensing with PSi MC Structure

5.3.1.1 Fabrication of n-type freestanding multi-layer micro-cavity (MC) structures

λ/4 MC structures consists of two Bragg mirrors, which are periodic stacks of quarter wavelength optical thickness layers of two different porosity layers (according to Bruggeman approximation [32]). The cavity is formed by adding a defect layer sandwiched in between the two Bragg mirrors. MC structure acts as highly selective wavelength filter, defined by its resonance in its stop band. MC PSi sample was fabricated using 40mA/cm^2 and 80mA/cm^2 current density for higher refractive index/lower porosity (2.2/30%) and low refractive index/higher porosity (1.7/45%) porous layers respectively. Etching time for these current densities were 9.26 seconds and 8.14 seconds. Cross-sectional SEM image of MC is shown in Figure 5.1. Pore diameter measured from SEM image for these MCs was 40nm and 100nm for two layers that is sufficient for any analyte infiltration within this diameter.

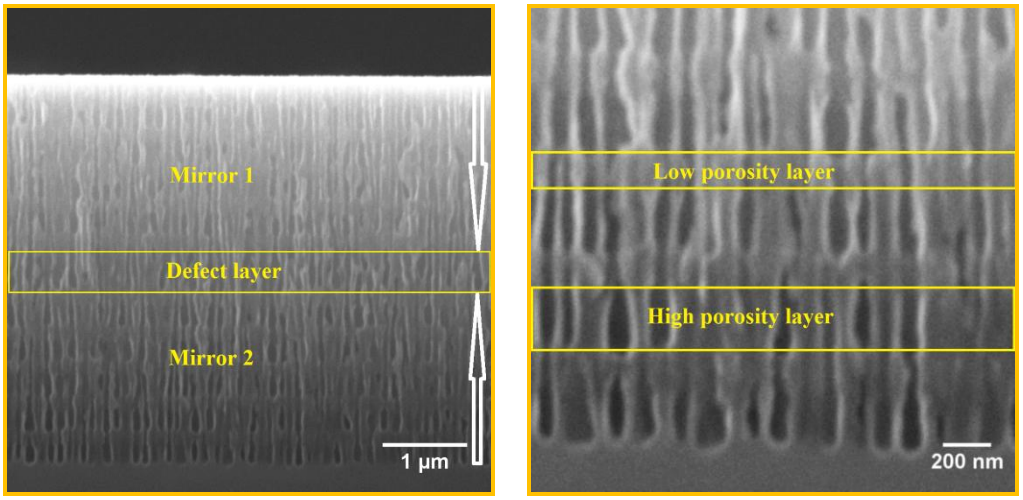

(a) (b)

Figure 5.1. (a) SEM images of porous silicon (PSi) multi-layer fabricated on N-type high resistive wafer (0.02Ωcm) with water based solution (Right) (b) zoom image of multi-layer structure

MCs of different quality factor (Q=30, 50 and 70) were fabricated depending on the number of pair of alternating layers i.e. 10 layer, 14 layer and 20 layer. Transmittance spectrum of these MC (Q=30, 50 and 70) are shown in Figure 5.3, Figure 5.4 and Figure 5.5. The resonance for the three samples is observed at ~1488, ~1448 and ~1515nm, respectively. Ideally the quality of the MC can be further improved by introducing higher refractive index contrast between the two alternating layers or by increasing number of alternating. However a larger refractive index contrast limits the size of the analyte that could be infiltrated. Moreover the maximum number of layers is also limited, in fact we were not able to etch MC with more than 20 layer because of an (increasing number of alternating layer, it destroys spectral quality of MC structure). To detach the MC structures from the silicon substrate, we use another solution having 12% HF acid with a strong oxidizer H_2O_2 with an applied current density of 60mA/cm^2. With this current density porous layer detaches from the substrate in 25sec. However by increasing applied current density separation time can be reduced (100mA/cm^2 separation time reduces to ~8sec). More detail study with this etching solution was already discussed in *Chapter 3*. Photograph of free-standing MC structure and glued on a metallic holder are shown in Figure 5.2.

Figure 5.2 Photograph of free-standing PSi MC Structure glued on a metallic holder

5.3.1.2 Organic sensing with freestanding multi-layer micro-cavity (MC) structure

It is known that electrochemical etching produces in-homogeneities on the silicon substrate, so to get an idea about the homogeneity of the optical response; we optically characterized the MCs at different points on their surface. We found an irregular optical response both in intensity and resonance position. Moving from the center of the porous area to the edges, reflectance decreases and an average shift of up to 36nm is observed. Figure 5.3 shows the observed reflectance spectra of MC (Q=50) synthesized with water based electrolyte solution. This optical in-homogeneity should be taken into account and always keep in mind, if we are moving our samples during the analysis. However by fixing the exposed area, we can overcome these limitations.

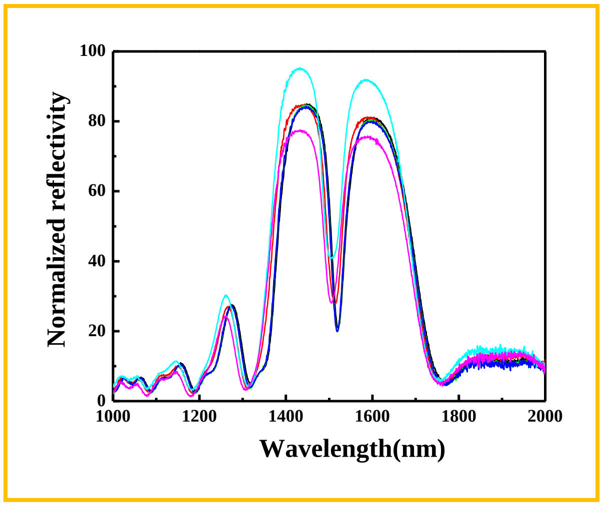

Figure 5.3. Reflectance spectra of MC sample fabricated on 0.01-0.02Ωcm resistive silicon wafer. A resonance at 1518nm in the middle of the stop band is observed. Reflectance spectra of MC sample at different points chosen randomly.

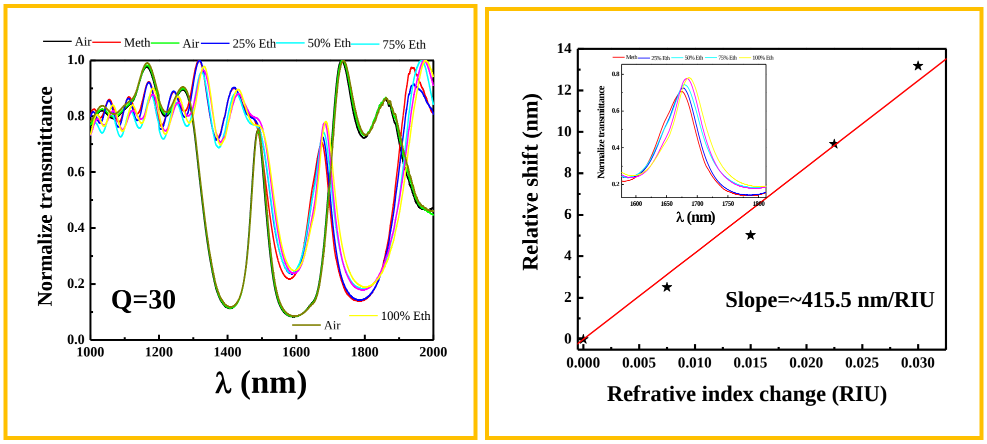

Figure 5.4. Transmittance spectra of MC Q=30 and resonance red shift due to methanol and methanol-ethanol solutions. Resonance shift of MC after expose to various concentrations of ethanol (in Inset) and linear fit represents the sensitivity of this structure.

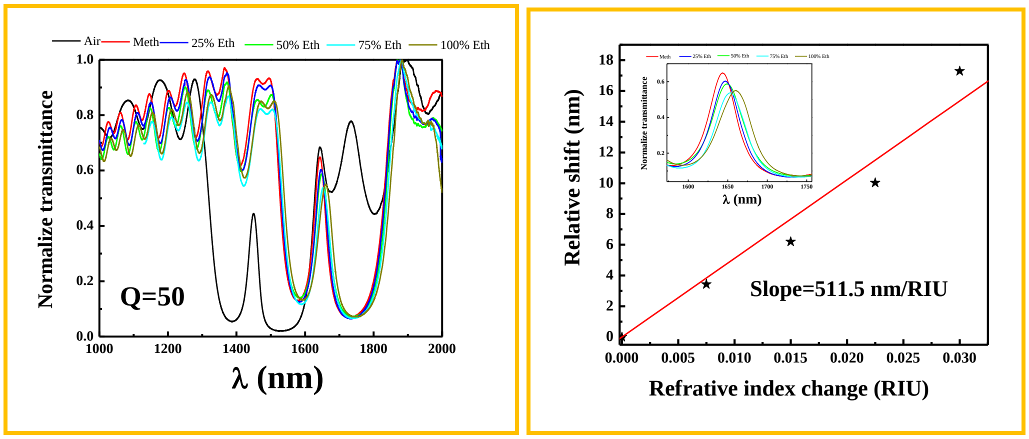

Figure 5.5. Transmittance spectra of MC Q=50 and resonance red shift due to methanol and methanol-ethanol solutions. Resonance shift of MC after expose to various concentrations of ethanol (in Inset) and liner fit represents the sensitivity of this structure.

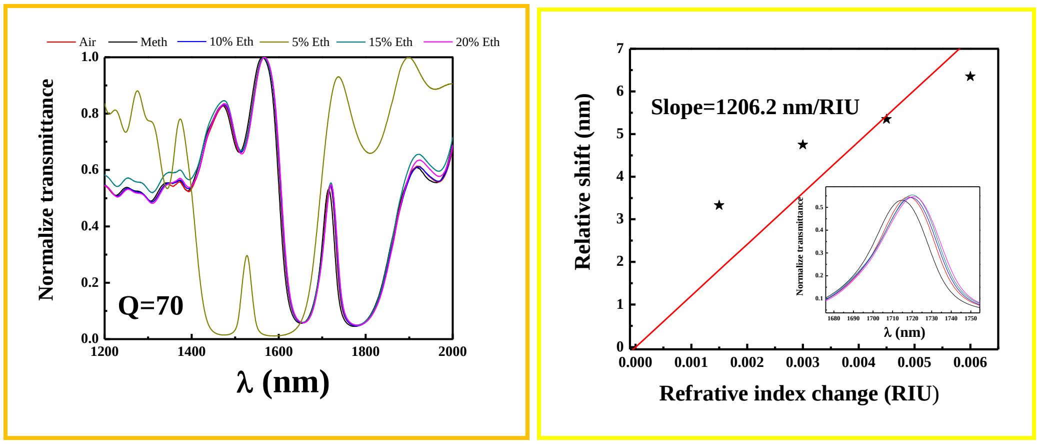

Figure 5.6. Transmittance spectra of MC Q=70 and resonance red shift due to methanol and methanol-ethanol solutions. Resonance shift of MC after expose to various concentrations of ethanol (in Inset) and liner fit represents the sensitivity of this structure.

Figure 5.4, Figure 5.5 and Figure 5.6 show the shift of the MC resonance position when MCs with Q=30, Q=50 and Q=70 are exposed to methanol and methanol-ethanol mixed solutions in FO condition. A red shift is observed due to the change in refractive index within the porous structure as liquid fills the pores and results in an increase of the effective material refractive index. A shift of ~186.3nm, 194.7nm and 200nm is observed when MCs Q=30, 50 and 70 are filled with methanol. Furthermore MC with 5 layer and 10 layer shows a resonance shift of 13.18nm and 17.29nm respectively due to change in refractive index (0.03 RIU), when exposed to ethanol. In addition on exposing to organic liquids, MCs quality also degrades to Q=24 for 5 layer and to Q=47 from Q=50 for 10 layer. To check further the sensitivity of the devices against organic liquids, we tested these MCs to methanol-ethanol mix solution. The refractive index of the solutions was calculated according to their volume fraction and assuming a linear relation. An increase of ethanol volume proportion in methanol (from 0% to 100%) shows a red shift with respect to increase in refractive index. Figure 5.4, Figure 5.5 and Figure 5.6 shows a red shift exposing to methanol-ethanol solution with an increase in ethanol concentration. To quantify these results, we calculate relative wavelength-shift refractive index sensitivity by plotting the magnitude of optical shift Vs the refractive index of methanol-ethanol solution. We notice a linear relation between the parameters and the slope of the straight line quantifies the sensitivity of the photonic structure due to change in refractive index. Sensitivity of ~$2.4*10^{-4}$, $1.9*10^{-4}$ and $8.3*10^{-5}$ is calculated from the observed slope of 415.5, 511.5 and 1206.5nm/RIU for three fabricated MC samples respectively (resolution limit of instrument ~0.1nm). To compare sensitivity of these MCs with available structure in literature, $\Delta\lambda$ (resonance shift due to change in refractive index within pores) is calculated and is found that the observed shift of ~186.3nm, 194.7nm and 200nm for respective MCs are well comparable to ~180nm with p-type MC structures as reported by Luigi et al. [33, 34].

Furthermore the reversibility of sensor is also tested by let it drying and monitoring the optical response should be return of to its original state after evaporation of the liquid. As shown in Figure 5.4 and 5.7, the observed resonance initially before exposing to organic liquid was at 1487.30nm and shifts to higher wavelength to 1673.6nm after exposing it. Then sample is allowed to dry and the resonance of MC returns back to nearly initial position at 1489.58nm after drying.

In summary because of pore sizes compatible with many biological samples and having good sensitivity, these n-type MC structures could be of great interest for bio-sensing applications.

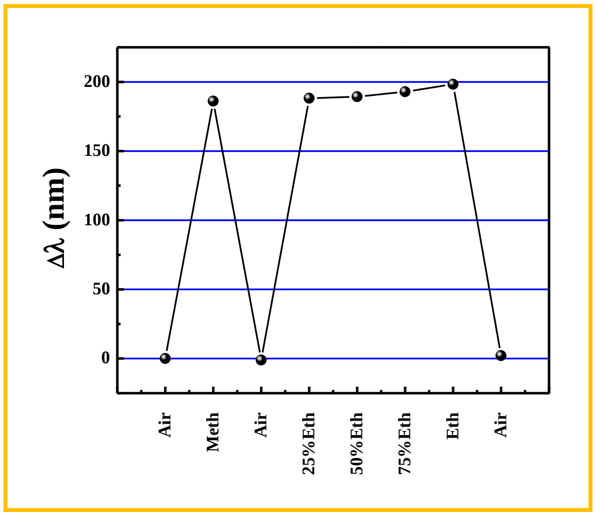

Figure 5.7. Reversibility of MC, Resonance shift of MC Q=30 to higher wavelength due to increase refractive index corresponding to methanol and methanol-ethanol solutions. As MC pores dry again, resonance returns back to its zero position. (Meth - Methanol. Eth - Ethanol)

5.3.2 Bio-sensing with MC structure

5.3.2.1 Fabrication of n-type multilayer MC structure for BSA sensing

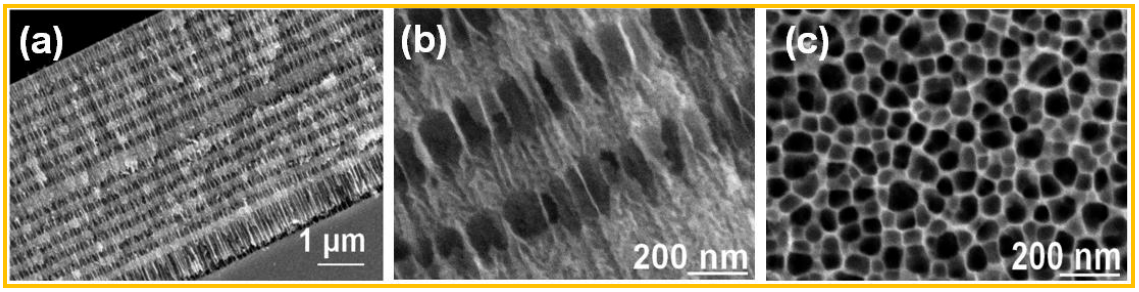

Figure 5.8(a) SEM image of a multilayer PSi MC consisting of 7 period Bragg mirrors. The bottom layer clearly has a larger porosity (darker color) and is the layer used to detach the FSM from the substrate. (b) Zoom of the alternating low and high porosity layers. (c) SEM image of top surface after the detachment of MC. Each pore is clearly visible and perfectly opened up to the surface of the sample.

As discussed in *Chapter 2-3,* by introducing changes in the applied etching current, we can create multiple porous silicon layers with different refractive index *n*, leading to the fabrication of MCs. Our PSi MCs, as shown in Figure 5.8a, consist of two Bragg mirrors (each one composed by seven periods) surrounding a defect layer with a total device thickness of only 5.5 µm. The fabrication of samples with high optical quality compatible with FT operations requires etching of high porosity layers (50 and 70% for the high and low refractive index layer, respectively). Thus the Bragg mirrors consist of alternating layers of low porosity (pore diameter of about 30nm, 20mA/cm^2 for 12 s, *n*=2.2) with a thickness of 150 nm and high porosity (pore diameter of about 80nm, 80mA/cm^2 for 9.5 s, *n*=1.7) with a thickness of 200 nm. A zoomed SEM image of the alternating layers is presented in Fig. 5.8b. The central defect layer has a thickness of around 300 nm and the same porosity as the low porous ones (20mA/cm^2 for 24s). The top surface of the MC is shown in Fig. 5.8c.

5.3.2.2 Surface modification and sensing

Amino terminations were introduces on the PSi surface using a slightly modified silanization procedure reported by Howarter et al. [35]. Briefly, the samples (which are FSM in case of the FT configuration and MCs bound to Si substrate for the FO method) were dipped in toluene containing 2%v/v 3-aminopropyltrietoxysilane (APTES) for 1 hour at 70°C. After rinsing in deionized water, the samples were immersed in PBS (pH 7.4) containing 2.5% glutraldehyde (GA). The reaction was left to proceed for 2 hours at room temperature, then the samples were thoroughly rinsed three times with PBS and water, respectively and dipped in PBS containing Bovine Serum Albumin (BSA, Sigma)at various concentrations. After 2 hours, the samples were thoroughly rinsed with water and gently dried under nitrogen flow.

Optical characterization measurements were performed using a bench top Varian Cary-5000 UV-VIS-NIR Spectrophotometer (spectral bandwidth of 0.5 nm) with the FSMs suspended over a 1 mm large pinhole in order to have a large S/N ratio. Because of the intrinsic fragility of the membranes, we dipped the MCs sequentially in protein solutions with different concentration and measured the shift of the resonance after each dip. Even if this is a nonstandard assay, the samples were exposed to the same amount of analyte and their comparison can be used to extract reliable information about the effect due to NSS [36].

5.3.2.3 Optical characterization of PSi MCs in FT and FO configurations

It is well known that the electrochemical etching produces a certain degree of in-homogeneities on the sample surface so that the optical response depends on the sampled area. To overcome this problem, we fixed the sample between two metal plates with a 1 mm hole in the center. In this way we measured always the same area and avoid uncertainties due to surface in-homogeneities, which results in good response linearity for all samples fabricated. In the case of the FO configuration, reflectance spectra were obtained on MCs bound to Si substrate in a wavelength range from 1000 to 2000 nm, with a cavity Q-factor of about 60 centered at around 1560 nm (Figure 5.9(a), red squares). For the FT experiments, transmittance spectra were performed in the same wavelength range on MCs free standing membranes and a similar cavity Q-factor was observed (Figure 5.9b, red squares). The resonance peak is centered at around 1480 nm. It is important to note that the Q-factor of fabricated n-type MC is well comparable to the ones reported earlier and is enough high to sense a shift down to 1 nm [36]

As both BSA and GA molecules are small enough to easily penetrate inside the pores [37], we used them as model system. Figures 5.9(a) and 5.9(b) show the reflectance and transmittance MC resonance in FO and FT configuration respectively, after functionalization, GA activation and two hour incubation in a BSA solution. The spectra showed a remarkable red shift of the resonance peak of the functionalized and GA activated MCs exposed to BSA which increases at increasing BSA concentration (i.e. 20 µM, 230 µM and 460 µM). Transmittance and reflectance measurements were repeated on three different samples (with the same cavity Q-factor) and the average shift was calculated for each BSA concentration. Figure 5.9(c) shows that a linear relationship between the relative resonance shift and the BSA concentration holds for both FO and FT configurations. From the slope, we estimated the sensitivity of our sensor to be 57pm/µM for FO configuration and 23pm/µM for the FT configuration. This difference in sensitivity is unexpected for FO and FT cavities with very similar Q-factors. This effect was noticed also by De Louise et al. [38] for p-type MC structure; however, the authors did not justify this large difference. We assumed the FO approach to be more sensitive mainly because of a greater contribution of the NSS, due to a non effective rinsing of the closed-ended pores.

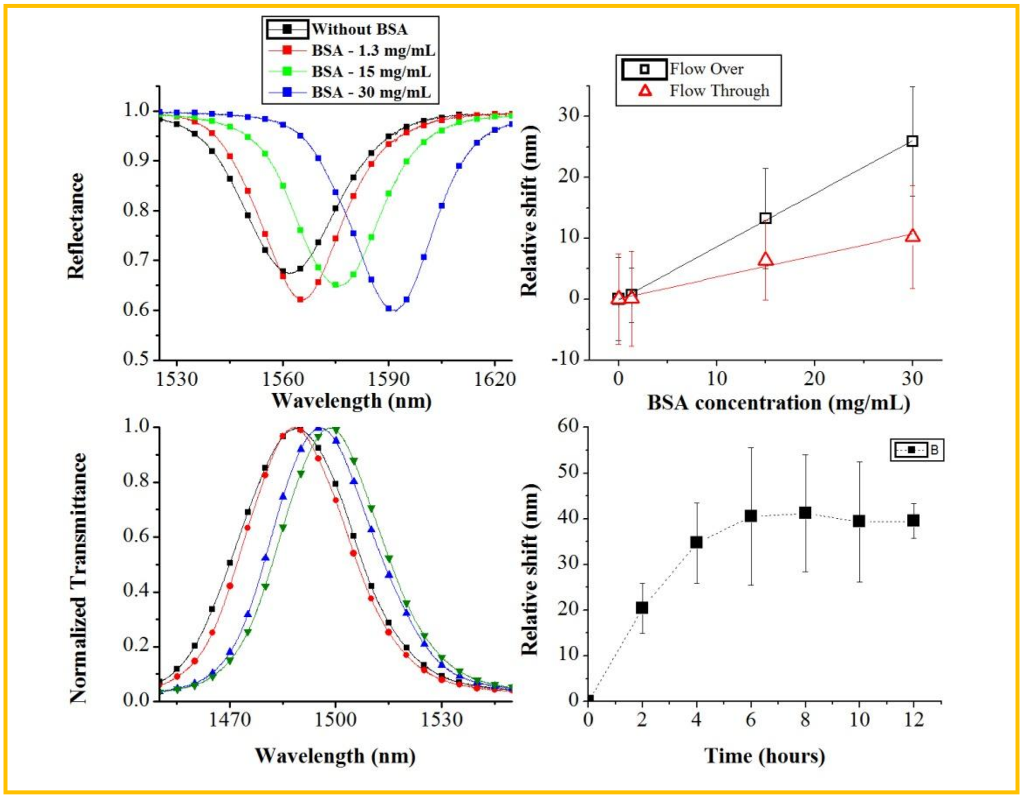

Figure 5.9(a) Reflectivity spectra versus wavelength for MCs bound to silicon substrate after two hours incubation in solutions of variable BSA concentration. The inset shows a scheme of the FO experiment (b) Transmission spectra versus wavelength for MCs free standing membranes after two hours dipping in solutions of variable BSA concentration. The inset shows a scheme of the FT experiment (c) Relative resonance shift as a function of the BSA concentration for both FO and FT configurations (d) Relative resonance shift as a function of the dipping time of MCs bound to silicon substrate in a solution containing 460 µM BSA .

To prove our hypothesis, first we demonstrated that the linear relationship between the sensor response and the BSA concentration could be due to the non-saturation regime under which we are working, so that the entrapment of molecular species by the porous sponge is proportional to the assay time as predicted by a simple diffusion model. To demonstrate that all these measurements were done in the non-saturation regime, we performed time-varying experiments. Functionalized MCs bound to Si substrate have been incubated in the 460 µM BSA solution for different intervals of time and the shifts in the reflectance spectrum after each dipping process are reported in Figure 5.9(d). The relative shift saturates after 6 hours dipping, which is far beyond the dipping time used in the experiments previously described (2 hours) confirming that they have been performed under diffusion-controlled regime. Under these conditions, physisorption of the un-reacted BSA molecules can occur, thus contributing to the apparent sensor sensitivity. We also noticed that the large errors bars near the saturation regime are due to the different dynamics of the binding for the different samples. In fact the actual structure of the porous surface varies from sample to sample because of the aforementioned difficulties in the fabrication of the FSM. Errors bar decrease significantly with the saturation of the samples and are greatly reduced at the end of the assay when most of the active sites have reacted (the total shift being dependent on the specific surface area and on the density of the binding sites).

Finally, we checked the amount of NSS in the case of saturated sensors in both FO and FT configurations. We blocked first all the available reactive sites of the functionalized FO and FT sensors by dipping them in a solution containing glycine (35mM) and BSA (1%) for a whole night. Then the sensors were washed in order to remove all the unbound particles and exposed again to a highly concentrated solution of BSA (460 µM). After this second dipping the FO sensor showed a further positive shift of 2 nm which can’t be due to BSA covalently bound (since no reactive sites are still available) but surface physisorbed. It is important to notice that such a positive shift did not occur in the previous experiment (Figure 5.9(d) as a result of the complete filling of all MC pores. Conversely, the FT sensors showed a small negative shift of 0.5 nm, probably due to sample oxidation during the second immersion in BSA solution [39] or the removal of a small amount of bounded-BSA molecules during the rinsing. This experiment confirms the influence of NSS in the sensitivity of FO systems unlike in FT configuration.

5.3.2.4 Forced flow-through sensing with n-type freestanding MC structure

Having demonstrated previously that free-standing membranes sensor with high aspect ratio pores are easily fabricated with low cost electrochemical etching method on n-type Si substrate, we now established for the first time the realization of n-type freestanding FT MC based sensor. This further test allows us to check the validity of our previous assumption by comparing two type of assay realized in FT membranes.

The features of the free standing membranes we were able to obtain on n-type Si substrate (i.e. high aspect ratio and open-ended pores, efficient rinse, low NSS of proteins together with easy fabrication and low cost) suggest their successful use in FT sensor devices. We explored if the superior characteristics of these membranes are maintained under forced FT operation. Two free standing MCs were prepared as explained in section 5.3.2.1. Samples were placed in a sample holder chamber filled with a BSA solution; a pressure was applied to achieve forced FT operation. Optical characterization measurements were performed for each BSA concentration.

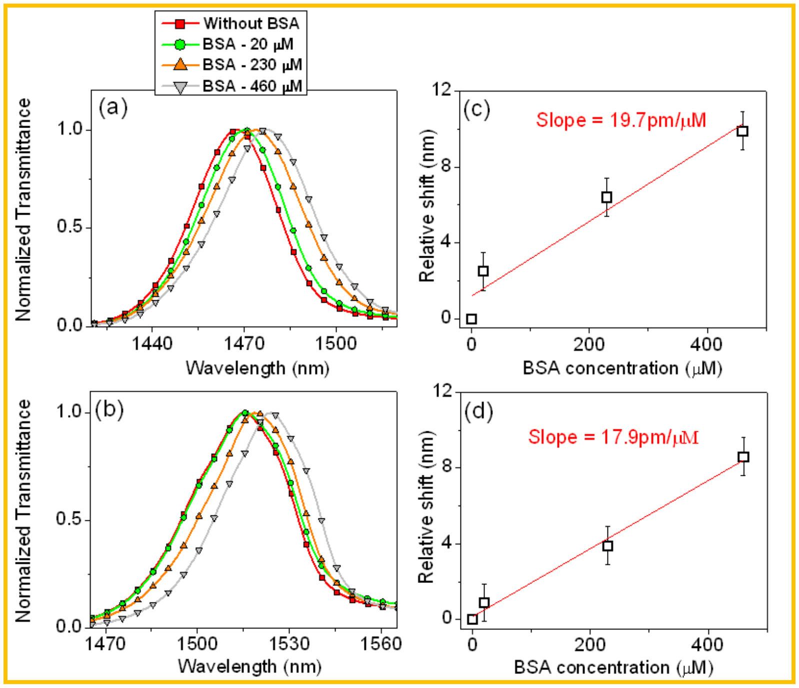

Figure 5.10(a, b) Transmission spectra versus wavelength for MCs free standing membranes after two hours fluxing in various BSA concentrations with applied pressure (forced FT) (c, d) Relative resonance shift in function of the BSA concentration for forced FT configuration.

The results of these measurements are shown in Figure 5.10a and 5.10b and were compared with those of the previous FT configurations used above. We noticed that when the freestanding MC sensors were exposed to different BSA concentration in the forced FT configuration, as expected, MC resonance shifted to longer wavelength proportionally to the concentration of the BSA. Figure 5.10c and d shows the sensitivity of these samples exposed to different BSA concentrations. These resonance shifts are very similar to those obtained with FT approach (Figure. 5.10c) and described in the previous section. From the linear fit of the experimental points two slopes of 19.7pm/µM, 17.9pm/µM for forced FT sensors are observed. Again, these data are very similar to those obtained by simply diffusion of molecules within the porous structures of the FT membranes. The fact that the FT sensitivity does not varies significantly between the "forced" and the "diffusive" test is probably due to the limited thickness of the samples (around 5 μm).

5.4. Conclusions

In conclusion, the main results achieved in this chapter are: Compared to various MC Photonics structure on n-type silicon substrate with among the highest quality factor (Q=70) and sensitivity of 606nm RIU^{-1} has been observed. The quality and sensitivity of MCs Q=30, 50 and 70 are quantified with methanol-ethanol solution and change of ~$2.4*10^{-4}$, $1.9*10^{-4}$ and $8.9*10^{-5}$ RIU can be sensed in refractive index. Furthermore the role of NSS is investigated and quantified in nanoporous silicon by comparing FO and FT geometries. By performing three different types of measurements (FO, FT and forced FT), we demonstrate that the FO approach in porous material systematically overestimates the real sensor sensitivity because of a poor removal of non-specifically bound molecules. We notice that, despite its complete different origin, the magnitude of the NSS is linearly proportional to the assay time and it is easily confused with specific signal. Moreover, we demonstrated that FT approach - either performed by pumping the liquid through the sensor or by simply dipping the MC- produces a linear response of the sensor with similar sensitivity, which is probably due to the limited thickness of the sample.

This preliminary investigation provides the first study of NSS effect in porous based sensors and is the basis for further investigation of more sophisticated and adequate free-standing nanoporous structures.

References

[1]P. Xie, Q. Xiong, Y. Fang, Q. Qing & Charles M. Lieber, “Local electrical potential detection of DNA by nanowire–nanopore sensors,” Nature Nanotechnology 7, pp 119–125 (2012).

[2]T. Someya, A. Dodabalapur, J. Huang, K. C. See, H. E. Katz, “Chemical and Physical Sensing by Organic Field-Effect Transistors and Related Devices,” Advanced materials 22(34), pp 3799-3811 (2010).

[3]T. Kang, S. M. Yoo, I. Yoon, S. Y. Lee, B. Kim, “Patterned Multiplex Pathogen DNA Detection by Au Particle-on-Wire SERS Sensor,” Nano Letters 10 (4), pp 1189–1193 (2010).

[4]J. Piehler, A. Brecht, R. Valiokas, B. Liedberg,G. Gauglitz, “A high-density poly(ethylene glycol) polymer brush for immobilization on glass-type surfaces” Biosensors & bioelectronics 15 (9-10), pp 473-481 (2000).

[5]H. Dai, M. Meyer, S. Stepaniants, M. Ziman, R. Stoughtona, “Use of hybridization kinetics for differentiating specific from non-specific binding to oligonucleotide microarrays,” Nucleic Acids Research 30(16), pp e86 (2002).

[6]F. Lasne, “Double-blotting: a solution to the problem of nonspecific binding of secondary antibodies in immunoblotting procedures,” Journal of immunological methods 253 (1-2), pp 125-131 (2001).

[7]B. H. Schneider, E. L. Dickinson, M. D. Vach, J. V. Hoijer, L.V. Howard, “Highly sensitive optical chip immunoassays in human serum,” Biosensors & Bioelectronics 15(1-2), pp 13-22 (2000).

[8]E. Stern, A. Vacic, N. K. Rajan, J. M. Criscione, J. Park, B. R. Ilic, D. J. Mooney, M. A. Reed, T. M. Fahmy, “Label-free biomarker detection from whole blood,” Nature nanotechnology 5(2), pp 138-142 (2010).

[9]C. Pacholski, “Photonic Crystal Sensors Based on Porous Silicon,” Sensors 13(4), pp 4694-4713 (2013).

[10]L. Jia, W. Cai, “Micro/Nanostructured Ordered Porous Films and Their Structurally Induced Control of the Gas Sensing Performances,” Advanced Functional Materials 20 (21), pp 3765-3773 (2010).

[11]C. Sanchez, C. Boissiere, D. Grosso, C. Laberty, L. Nicole, “Design, synthesis, and properties of inorganic and hybrid thin films having periodically organized nanoporosity,” Chemistry of materials 20 (3), pp 682-737 (2008).

[12]B. J. Melde, B. J. Johnson, P. T. Charles, "Mesoporous silicate materials in sensing" Sensors 8 (8), pp 5202-5228 (2008).

[13]F. Jia, C. Yu, Z. Ai, L. Zhang, "Fabrication of nanoporous gold film electrodes with ultrahigh surface area and electrochemical activity," Chemistry of materials, 19(15), pp 3648-3653 (2007).

[14]A. Palaniappan, X. Li, F. E. H. Tay, J. Li, X. Su, "Cyclodextrin functionalized mesoporous silica films on quartz crystal microbalance for enhanced gas sensing," Sensors and actuators B-chemical 119 (1), pp 220-226 (2006).

[15]K. Bonroy, J. M. Friedt, F. Frederix, W. Laureyn, S. Langerock, A. Campitelli, M. Sára, G. Borghs, B. Goddeeris, P. Declerck, "Realization and characterization of porous gold for increased protein coverage on acoustic sensors," Analytical chemistry, 76(15), pp 4299-4306 (2004).

[16]M. Zhao, X. Wang, D. Nolte, "Mass transport limitations in spot-based microarrays," Biomedical Optics Express 1(3), pp 983-997 (2010).

[17]N. S. Lynn, H. Šípová, P. Adam, J. Homola, "Enhancement of affinity-based biosensor: effects of sensing chamber geometry on sensitity," Lab on a Chip 13, pp 1413-1421 (2013).

[18]E.D. Gaspera, D. Buso, M. Guglielmi, A. Martucci, V. Bello, G. Mattei, M.L. Post, C. Cantalini, S. Agnoli, G. Granozzi, A.Z. Sadek, K. Kalantar-zadeh, W. Wlodarski, "Comparison study of conductometric, optical and SAW gas sensors based on porous sol–gel silica films doped with NiO and Au nanocrystals," Sensors and Actuators B: Chemical 143(2), pp 567-573 (2010).

[19]T. N. Huan, T. Ganesh, K. S. Kim, S. Kim, S. H. Han, H. Chung, "A three-dimensional gold nanodendrite network porous structure and its application for an electrochemical sensing," Biosensors & Bioelectronics 27(1), pp 183-186 (2011).

[20]M. Scampicchio, A. Arecchi, A. Bianco, A. Bulbarello, C. Bertarelli, S. Mannino, "Nylon nanofibrous biosensors for glucose determination," Electroanalysis 22(10), pp 1056-1060 (2010).

[21]J. Alvarez, P. Bettotti, I. Suarez, N. Kumar, D. Hill, V. Chirvony, L. Pavesi, J. Martinez Pastor, "Birefringent porous silicon membranes for optical sensing," Optics Express 19(27), pp 26106-26116 (2011).

[22]M. Lee, P.M. Fauchet, "Two-dimensional silicon photonic crystal based biosensing platform for protein detection," 15(8), pp 4530-4535 (2007).

[23]J. Alvarez, N.Kumar, P. Bettotti, D. Hill, J. Martinez-Pastor, "Phase-Sensitive Detection for Optical Sensing With Porous Silicon," IEEE Photonics Journal 4(3), pp 986-995.

[24]X. Lv, L. Chen, H. Zhang, J. Mo, F. Zhong, C. Lv, J. Ma, Z. Jia, "Hybridization assay of insect antifreezing protein gene by novel multilayered porous silicon nucleic acid biosensor," Biosensors and Bioelectronics 39(1), pp 329-333 (2013).

[25]H. Zhang, Z. Jia, X. Lv, J. Zhou, L. Chen, R. Liu, J. Ma, "Porous silicon optical microcavity biosensor on silicon-on-insulator wafer for sensitive DNA detection," Biosensors and Bioelectronics 44(1), pp 89-94 (2013).

[26]T. Jalkanen, E. Makila, Y. I. Suzuki, T. Urata, K. Fukami, T.Sakka, J. Salonen and Y. H. Ogata, "Studies on Chemical Modification of Porous Silicon-Based Graded-Index Optical Microcavities for Improved Stability Under Alkaline Conditions," Advanced Functional Materials 22(18), pp 3890-3898 (2012).

[27]M. Ghulinyan, C. J. Oton, G. Bonetti, Z. Gaburro, L. Pavesi, "Free-standing porous silicon single and multiple optical cavities," Journal of Applied Physics 93(12), pp 9724-9729 (2003).

[28]P. C. Searson, J. M. Macaulay, F. M. Ross, "Pore morphology and the mechanism of pore formation in n-type silicon," Journal Applied Physics 72(1), pp 253-258 (1992).

[29]H. J. Kim, Y. Y. Kim, K. W. Lee, S. H. Park, "A distributed Bragg reflector porous silicon layer for optical interferometric sensing of organic vapor," Sensors and Actuators B, 155(2), pp 673-678 (2011).

[30]L. Velleman, C. J. Shearer, A. V. Ellis, D. Losic, N. H. Voelcker, J. G. Shapter, "Fabrication of self-supporting porous silicon membranes and tuning transport properties by surface functionalization," Nanoscale 2(9), pp 1756-1761 (2010).

[31]J. De Jong, R. G. H. Lammertink, M. Wessling, "Membranes and microfluidics: a review," Lab on a Chip 6(9), pp 1125-1139 (2006).

[32]M. J. Sailor, "Properties of porous silicon, INSPEC, London, 1997, pp. 364-370

[34]Luigi Moretti, Llaria Rea, Luca De Stefano and Lvo Rendina, "Periodic versusaperiodic:Enhancing the sensitivity of porous silicon based optical sensors" Appl. Phys. Lett. 90, pp 191112 (2007)

[35]John A. Howarter and Jeffery P. Youngblood, "Optimization of Silica Silanization by 3-Aminopropyltriethoxysilane," Langmuir 22(26), pp 11142-11147 (2006).

[36]H. Ouyang, M. Christophersen, R. Viard, B. L. Miller, P. M. Faucher, "Macroporous Silicon Microcavities for Macromolecule Detection," Advanced Functional Materials 15(11), pp 1851-1859 (2005).

[37]M. Hiraoui, M. Guendouz, N. Lorrain, A. Moadhen, L. Haji, M. Oueslati, “Spectroscopy studies of functionalized oxidized porous silicon surface for biosensing applications,” Materials Chemistry and Physics 128(1-2), pp 151-156 (2011).

[38]L. A. De Louise, P. M. Fauchet, B. L. Miller, A. A. Pentland, “Hydrogel-Supported Optical-Microcavity Sensors,” Advanced Materials 17(18), pp 2199-2203 (2005).

[39]L.Tay, N. L. Rowell, D. J. Lockwood, R. Boukherroub, “Bovine serum albumin adsorption on functionalized porous silicon surfaces,” Proceeding SPIE 5578, pp 99-184 (2004).

Chapter 6

Polarimetry sensing with porous silicon/alumina membranes

6.1 Introduction

Porous membranes based photonic devices have recently attracted significant attention due to its large surface to volume ratio that permits higher sensitivity of device [1]. Porous silicon (PSi) and porous alumina are important materials in this category. Since the discovery these materials, this material have been focused for many lab on chip devices [2, 3]. Besides their electrical properties by measuring change in capacitance or change in electrical conductivity, special attention on these materials is due to their high sensitivity towards refractive index changes due to species confined within their porous structure [4, 5]. Numerous articles have been published on bio-sensing, gas/vapor sensing and other sensing applications using these materials [6, 7, 8].These porous materials can be used in either flow-over (FO) or flow-through (FT) geometry. In FO sensing applications, spectroscopic ellipsometry technique is mainly used to sense change in refractive index induced by analyte [9]. The weakness of this technique is mainly due to a poor homogenous binding of the analyte species throughout the active sites within the pores [10]. However FT approach provides an alternative for more accurate and fast sensing over FO approach [11]. Furthermore open-ended pores on both sides in FT approach based on free standing membrane (FSM), maximizes the efficiency of the binding reactions over the entire porous material surface that enhances their sensitivity and reduces the response time.

Both PSi and porous alumina materials are optically birefringent. This optical property is well studied and explained by well ordered skeleton of their porous structure [12]. Several articles are published on the presence of birefringence in these porous materials [13, 14]. Among these, most of study is focused on p-type <110> silicon substrates, which is not compatible to flow-through application because of their small pore size. Only few are on n-type silicon self-supporting membranes [15]. Using FT geometry with PSi and porous alumina membranes along with polarimetric approach to sense the presence of analyte, fast and highly sensitive sensor can be assembled [16]. A major difficulty encountered with medium and highly doped n-type silicon substrates lies in the fact that free-standing membranes fabrication requires a more careful tuning of the experimental conditions compared to p-type PSi [17]. Furthermore due to complexities in flow through for PSi and measurement, only few groups are so far able to demonstrate real time sensing applications. Recently we have reported PSi membranes with sensitivity as high as 1245nm/RIU at 1500nm wavelength using various organic solutions [18]. However porous structure was quite rough and an improvement in pore roughness along with pore size was needed. In the same line very recently Alvarez et al. demonstrated flow through real time sensing with free standing porous alumina membrane (of 200nm pore diameter) and a sensitivity of ~10^{-6} RIU [16].

In this chapter, we compare PSi and porous alumina (Whatman-anodisc membranes of thickness 60µm and pore diameter of 200nm) freestanding membranes in flow through configuration for real time sensing applications. Both "in-plane and out-plane birefringence" is studied for both type of FSM. NaCl solution with constant flow rate was allowed to flow through PSi FSMs (15.54µm thick) and porous alumina FSM (60µm thick). A sensitivity of 0.25°/%NaCl and 0.30°/ % NaCl was achieved for the two sensing platforms. Lastly flow through BSA sensor as model system for LOC devices is demonstrated in PSi and porous alumina FSM. Concluding the results observed supports the higher sensitivity achieved in PSi FSM compared to the porous alumina membranes.

6.2 Synthesis and Experimental Details

N-type silicon wafer (0.01-0.02 Ω-cm) was used as the initial study material and porous layers were fabricated with water based solution contains 25ml HF acid (48.99%), 200ml de-ionized water and 1ml "Triton" as a surfactant as discussed in *Chapter 3*. After fabrication of PSi, all samples were rinsed in ethanol and dried in N_2 flow. For BSA sensing all samples (PSi and porous alumina membranes) were functionalized as discussed in *Chapter 5*. Optical characterization/Phase shift is measured using PAX570-T Free space polarimeter with an accuracy of 0.02° at 1525nm and at 1350nm wavelength.

6.3 Results and Discussions

6.3.1 In-plane and Out-plane birefringence of PSi and porous Alumina FSM

The setup for the measurement of phase shift of PSi and porous alumina FSM is shown in *Chapter 2*. Linearly polarized light of wavelength 1525nm is incident on the sample in a direction perpendicular to its surface. Because of the form birefringence induced by the porosity, light that travel across the membrane may show phase delay between the two orthogonal polarization states, depending on their orientation to respect the refractive index ellipsoid [19]. In a (100) oriented PSi sample the optical axis is demonstrated to be perpendicularly oriented to respect the surface [20]. Thus PSi sample should not shows any birefringence if illuminated perpendicularly and mapped azimuthally.

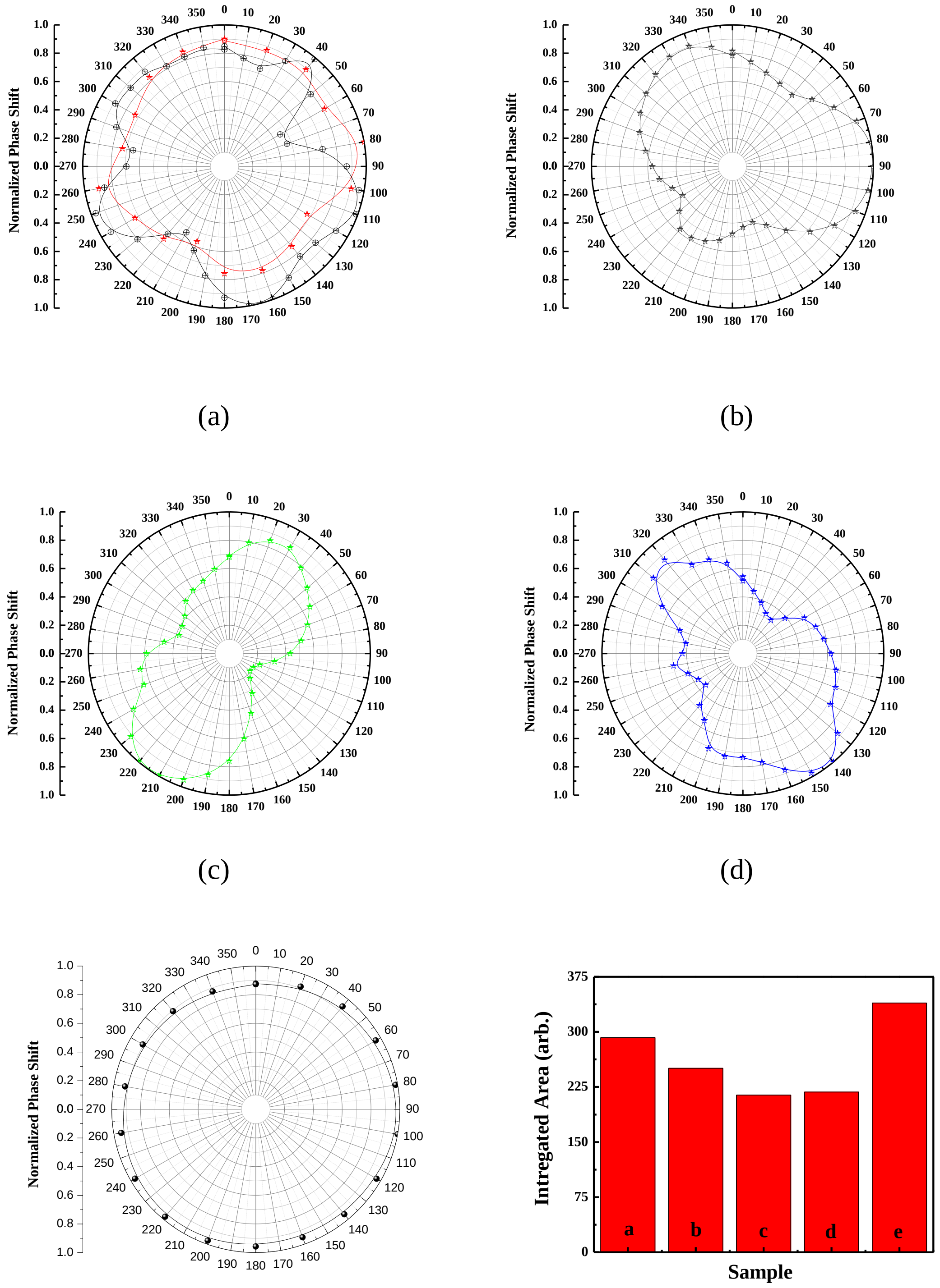

(a)

(b)

(c)

(d)

(e)

(f)

Figure 6.1 Normalized Phase shift as a function of sample rotation relative to its surface (a) PSi sample with 60mA/cm^2 (b) PSi sample with 40mA/cm^2 (c) PSi sample with 20mA/cm^2 (d) Porous alumina sample and (e) glass substrate. For the analysis, area composed by the curve is calculated (f)

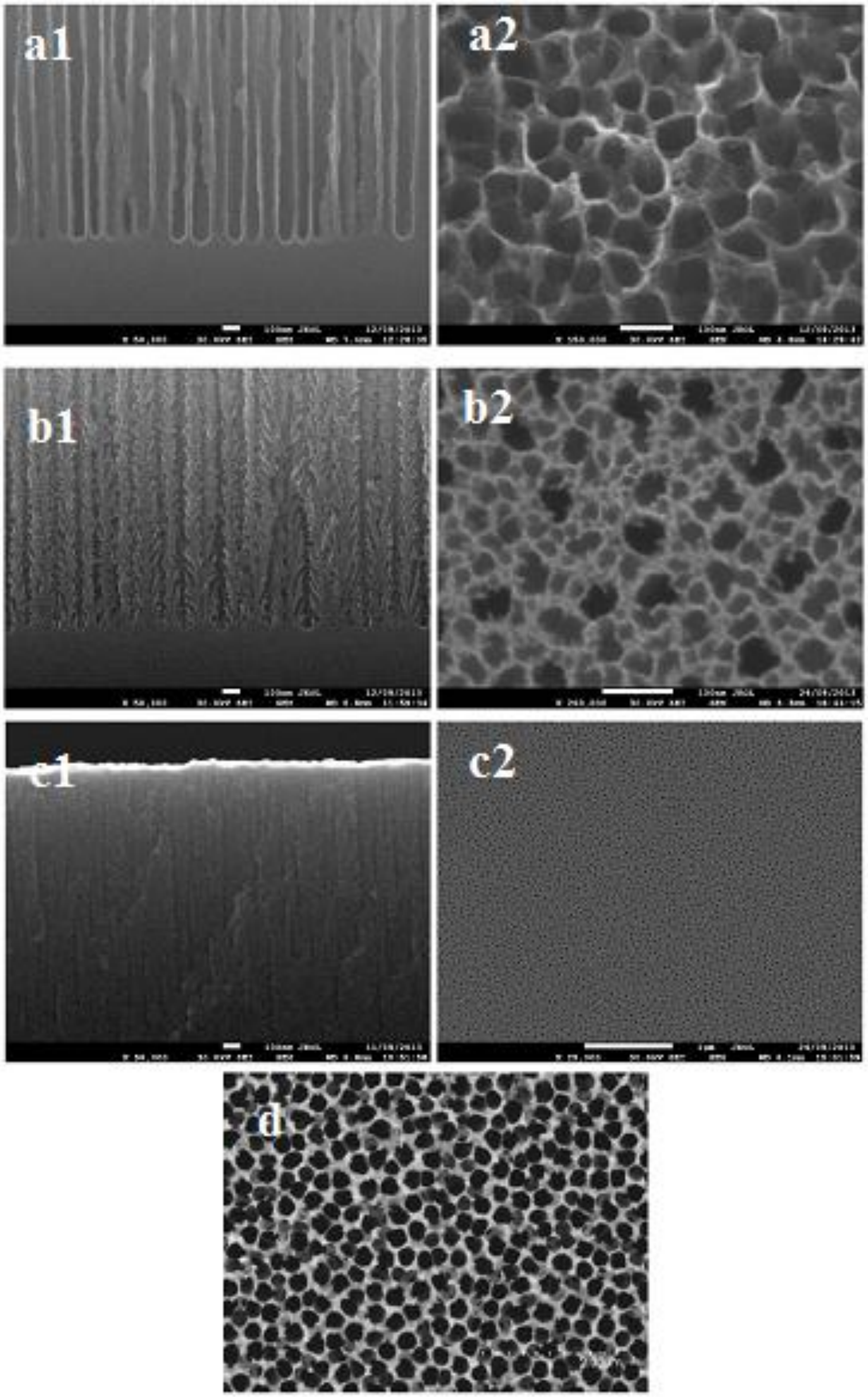

Figure 6.2. SEM images of cross-section (left) and (Right) top surface of (a) PSi sample with 60mA/cm^2 (b) PSi sample with 40mA/cm^2 (c) PSi sample with 20mA/cm^2 (d) Porous alumina sample

Phase shift is measured as a function of in-plane rotation angle shown in Figure 6.1 a, b, c for three different type of PSi sample etch with different current density i.e. 60mA/cm^2, 40mA/cm^2 and 20mA/cm^2, hence different pore morphology i.e. a straight 100nm pore (a) and dendrite structures with 60nm (b) and 20nm (c). Figure 6.1d show the results for a porous alumina FSM with straight pores of 200 nm of diameter. Figure 6.1e reports the data for a homogeneous glass slide. For the analysis, area composed by the curve of each sample is calculated (f). Area integrated within the curve increases as spatial isotropy for in-plane increases, further more calculated area composed by porous alumina FSM and PSi FSM fabricated with 20mA/cm^2 is nearly equal. For all the studied samples an azimuthal rotation of the FSM does not give a homogeneous response as it should be expected. Initially we supposed that the crystalline structure of the Si could induce a square like shape to the pores (as in the extreme case of the star-like pores). In this case we do expect to see the same symmetry in the optical response of the material, too. But experimental does not show any periodicity in the birefringence (i.e. a $\pi/4$ periodic relation is never observed) [21].

In-homogeneous birefringence is observed for all studied FSM sample for in-plane rotation. Furthermore it is well known that electrochemical etching have different etching rates along different crystalline plane (i.e. 100:16:1=(100):(110):(111)) thus this fact may be related with observed phase anisotropy [22]. Figure 6.2 shows the SEM images of cross-section of PSi samples fabricated with different current density. It is clearly observed that PSi fabricated at lower current density have more rough pores with dendrite like structure whereas, samples etched at higher current density have smooth and straight pores (as already discussed about pore growth in *Chapter 3*). Thus a possible reason for the anisotropy could be due to their inner pore morphology. Because the inner porous structure is not perfectly smooth the scattering generated by the small pore branching may induces an inhomogeneous phase shift versus in-plane rotation. Recently Shichi et al reported a correlation between the porous structure and the in-plane birefringence for p-type <110> PSi samples and demonstrated that inner pore morphology strongly affects the shape of index ellipsoid [23].

At a first sight a direct relation between pore roughness and in plane anisotropy can be observed. For rough pores observed for 20mA/cm^2, 40mA/cm^2, several maxima and minima are observed for azimuthal mapping of the birefringence, possibly induced by dendrite structure. However more straight and smooth pore reduces the in-plane anisotropy of the phase shifts (i.e. PSi fabricated with 60mA/cm^2 with ~100nm pore as shown in Figure 6.1a supports this view). The two samples produces similar behavior indicates that observed optical property is independent of PSi sample and related with their structural morphology.

Furthermore anisotropic nature of the porous alumina in plane birefringence is also studied. Circular pores observed from SEM image shown in Figure 6.2e. As pore seems nearly circular, we expect a nearly constant phase change. Contradictory Porous alumina FSM shows asymmetric nature for in-plane rotation and an elongated pattern is observed. Such results not fully understood and could be either due to top surface or pore growth that is not perfectly along the incident direction of light.

The reliability of the experimental setup is demonstrated by looking at the in-plane pattern obtained from a glass slide. In this case the birefringence is nearly homogeneous and only small deviations can be seen from the ideality. For any sensing purpose this limitation should be taken into account for more accurate sensing, if sample is not fixed and may have in-plane rotation.

In order to exploit its maximum birefringence, a (100) aligned PSi sample have to be tilted to respect the incident light. The maximum birefringence is achieved at 45° of tilt. The general relation that describes the phase delay accumulated by light beams that travel across the sample is given by:

$$\Delta\phi(\lambda) = \frac{2\pi}{\lambda} \cdot d \cdot \Delta n(\lambda) \qquad (1)$$

λ is the incident wavelength of light, d is the PSi membrane thickness and $\Delta n(\lambda)$ is its birefringence. Given a certain PSi refractive index, phase shift can be calculated for a known incident angle. Among various available methods i.e. Maxwell-Garnett theory, Looyenga method and the Bruggman model can be used to calculate theoretically birefringence for porous materials [18]. Figure 6.3 shows the observed phase shift (normalized for the sample thickness) for both PSi and porous alumina FSM as a function of incident angle. For all studied samples phase shift increases as incident angle increase as expected. Effect of pore morphology can be deducted by comparing the normalized birefringence: straight and smooth pores are more sensitive because of smaller depolarization factors due to less rough pores. Furthermore porosity of sample also has strong effect on phase sensitivity of FSM and has maxima for 50% porosity [18, 16]. Different porosity of PSi samples also have contribution in observed phase change as 20mA/cm^2, 40mA/cm^2 and 60mA/cm^2 have 30%, 36% and 48% porosity respectively calculated by reflectance Interferometric spectroscopy (RIFS) [24]. However PSi FSM fabricated with 60mA/cm^2 and porous alumina has nearly same porosity, but PSi sample shows higher sensitivity/degree than porous alumina membrane that could be understand in terms of larger refractive index difference between birefringent material and air as porous alumina FSM have refractive index of about ~1.6 than PSi (refractive index~1.7) FSM and due to its smaller pore size. From these observed results PSi FSM with 100nm pores seems more suitable for bio-sensing than porous alumina FSM.

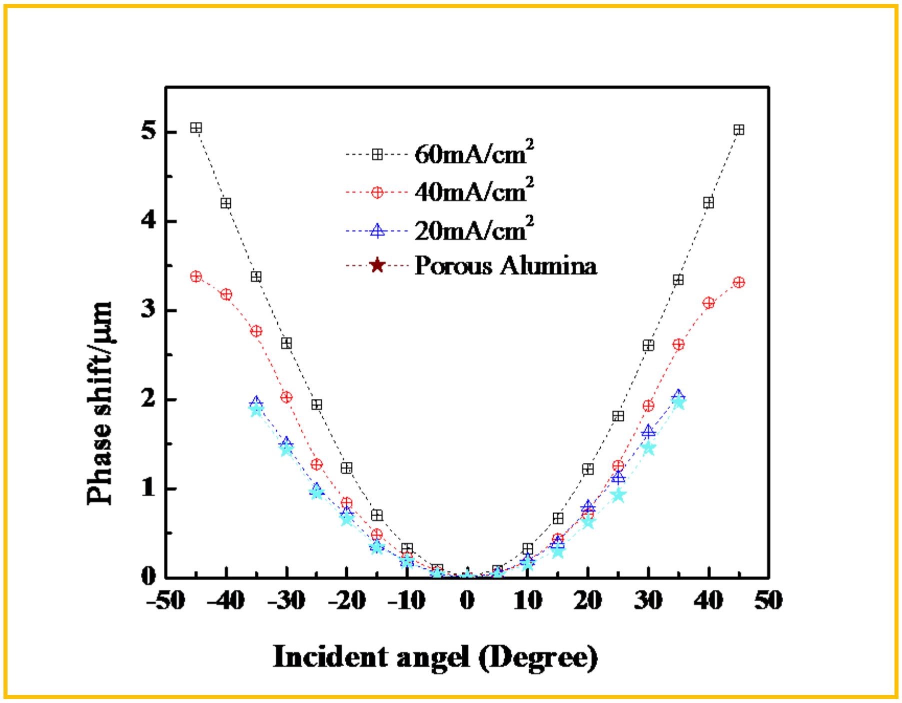

Figure 6.3 Phase shift as a function of sample rotation relative to incident light for PSi sample with 60mA/cm^2, PSi sample with 40mA/cm^2, PSi sample with 20mA/cm^2 and Porous alumina FSM at 1525nm

6.3.2 Sensing with PSi and porous Alumina FSM

To our best knowledge there are only few reports of liquid flux through a PSi FSM of submicron pore size. The difficult is due to both its hydrophobic nature and to the narrow pore size [16, 25, 26]. Taking the advantage of the straight and smooth pores PSi membranes were first characterize for flow of water as shown in Figure 6.4. It is important to note that freshly prepared FSM does not allow for flow through, a thermal oxidation is required to change its wet-ability. Three different samples were characterized for liquid flow: two rough and narrow pores with ~30nm (thickness of FSM~5.5µm) and 50nm size (thickness of FSM~6.1µm), and a sample with smooth and straight pore of ~100nm (thickness of FSM~8.7µm) in size. Flow up to 1µl/minute can easily be obtained on these PSi FSMs. As expected smooth pores required lower differential pressure than rough and narrow pores and encourages further to the use for flow-through sensing application.

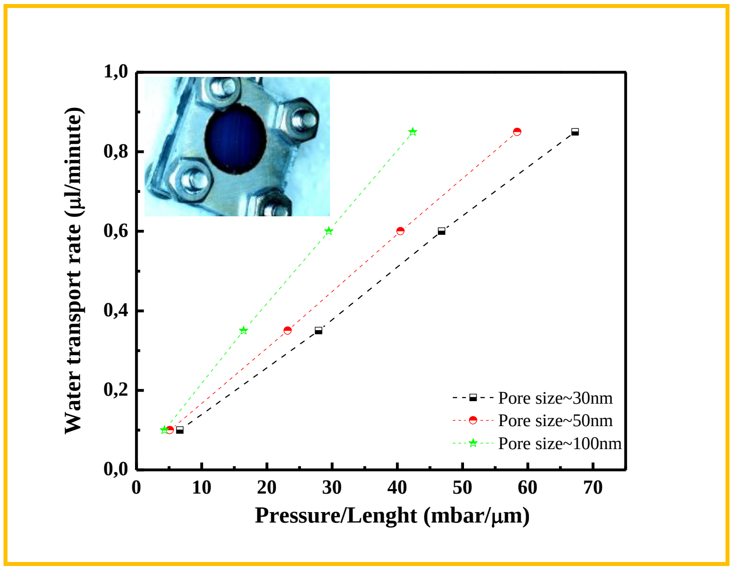

Figure 6.4 Water transport as a function of pressure applied for PSi sample fabricated with 60mA/cm^2, PSi sample fabricated with 40mA/cm^2, PSi sample fabricated with 20mA/cm^2 and Porous alumina FSM

W tested the sensitivity of both PSi and porous alumina membranes by flowing through them liquid of different refractive index. Optical photograph of complete experimental setup is shown in Figure 6.5. PSi FSM of 15.54µm thick with ~100nm pore and porous alumina FSM of 60µm thickness with 200nm pore was mounted on a perforated aluminum plate with PMMA resist. The mounted FSM were then placed in a glass flow cell at an angle of 40° (As shown in previous section 6.3.1 that maxima is obtained at 45°, but at this angle, transparency the alignment of the setup becomes very difficult . So we use 40° for sensing experiment), in which liquid flows with a constant flow rate of either 0.5µl/minute or 1.5µl/minute for PSi and porous alumina samples, respectively. All these measurement were carried out at a wavelength of 1350nm to reduce the absorption of light by water. As water fills the pore of PSi and porous alumina FSM, phase shift of ~40.50° and ~108.25° is observed for respective membrane, as shown in Figure 6.6a and 6.7a. As the liquid flowing through the membrane is exchanged with solutions of different NaCl concentration (we tested 5, 10 and 15% of NaCl), a proportional phase shift is recorded.

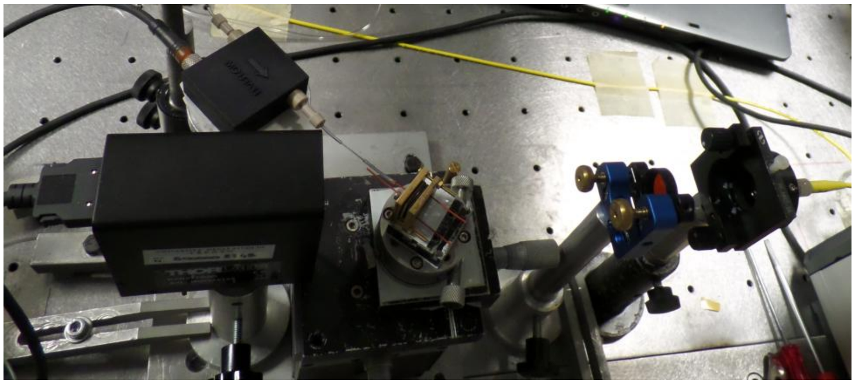

Figure 6.5 Optical photograph of measurement setup for polarimetric experiment with fluidic setup (For more detail see chapter 2)

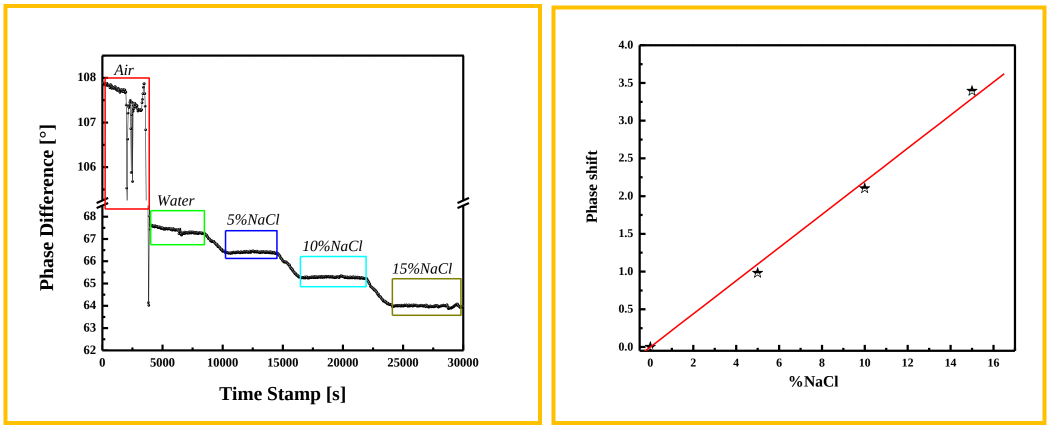

(a) **(b)**

Figure 6.6a Real time sensing with PSi FSM fabricated with 60mA/cm^2 at a wavelength of 1350nm, Phase shift increases as NaCl concentration in water increases due to increase in refractive index within porous structure. (b) Phase change as a function of NaCl concentration in water. Linear fit (R^2=0.9944) shows a sensitivity of 0.226°/%NaCl

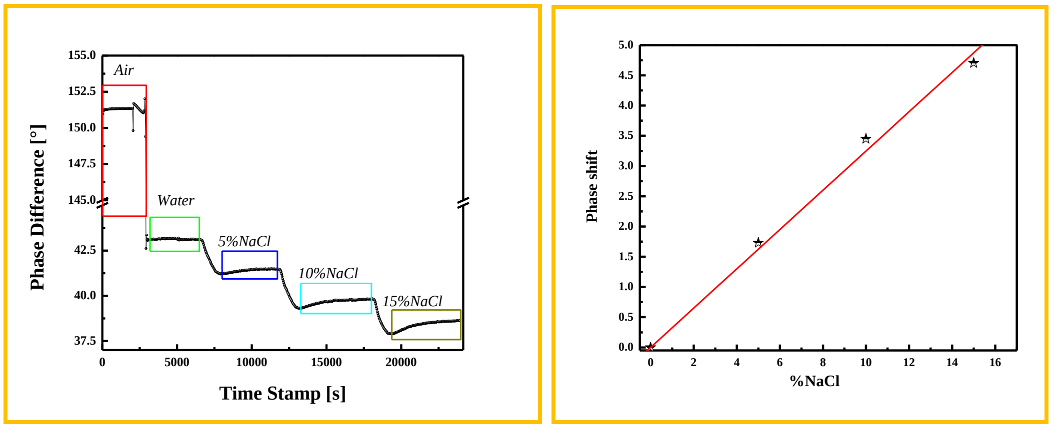

(a) **(b)**

6.7a Real time sensing with Porous alumina FSM at a wavelength of 1350nm, Phase shift increases as NaCl concentration in water increases due to increase in refractive index within porous structure.(b) Phase change as a function of NaCl concentration. Linear fit (R^2=0.9920) shows a sensitivity of 0.316°/%NaCl.

For PSi FSM a negative phase shift of 0.98°, 2.10° and 3.39° is observed for 5%, 10% and 15% NaCl, respectively, whereas porous alumina shows shifts of 1.73°, 3.45° and 4.70° for the three solutions (the uncertainty in these measurements is of ±0.02° detection limit as calculated for the instrument without an sample). Sensitivity of these FSM can be obtained from the slope of phase shift versus NaCl concentration. From linear fit of curves in Figure 6.6b and Figure 6.7b a sensitivity of 0.23°/NaCl% and 0.32°/NaCl% is observed for PSi and porous alumina membrane respectively. The refractive index change of NaCl solution is 0.001747RIU/%NaCl at 632nm [16]. We assume that the value measured in the visible is also valid at the wavelength of 1350nm. In terms of RIU the observed sensitivity is 129.36°/RIU and 180.88°/RIU for PSi and porous alumina FSM, respectively. LOD for refractive index change observed for PSi membranes is ~$3.8*10^{-4}$, where as for porous alumina membrane LOD is $2.7*10^{-4}$. Although observed bulk sensitivity is higher for porous alumina FSM, considering the thickness of these two studied sample PSi FSM is ~3 times more sensitive. In fact if we normalize the sensitivity for the thickness of the FSM we obtain: 1.48E-2 °/NaCl%/µm (correspondent to an LOD of about $6.0*10^{-3}$) for PSi and 0.53E-2 °/NaCl%/µm (LOD~$1.7*10^{-2}$) for porous alumina. Finally we made some preliminary tests using BSA molecules. Both PSi and porous alumina membrane were functionalized with 2%v/v 3-aminopropyltrietoxysilane (APTES) for 1 hour at 70°C as discussed in *Chapter 5*. After rinsing in de-ionized water, the samples were immersed in PBS (pH 7.4) containing 2.5% glutraldehyde (GA). The reaction was left to proceed for 2 hours at room temperature, and then the samples were thoroughly rinsed with PBS and finally washed with water before BSA binding in FT geometry. 10µl of each BSA concentration were fluxed through PSi and 40µl for porous alumina membrane. The membranes were rinsed in FT with water. Figure 6.8a and 6.8b shows the variation of phase shift of FSM as BSA molecules are added into the pores. Phase shift increases as BSA concentration increases (i.e. BSA concentration is increased from 0.075mg/ml to 2.5mg/ml for PSi and from 10mg/ml to 30mg/ml for porous alumina FSM) and nearly saturate for higher BSA concentration i.e. 2.5mg/ml and 30mg/ml. We checked the reproducibility of BSA sensing on another set of FSMs. In both cases we measure a response which is proportional to the BSA concentration. Unfortunately reproducibility is not very good and it requires more precise and careful study. The results observed for this second set of FSM is shown in Figure 6.9a and 6.9b for PSi and porous alumina FSM sample respectively.

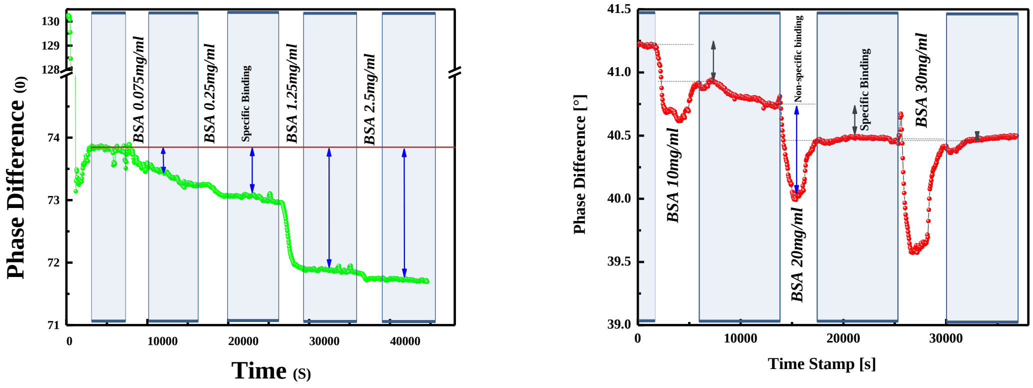

(a) (b)

6.8 (a) Real time sensing with PSi FSM, and (b) sensing with Porous alumina FSM at a wavelength of 1350nm, Phase shift increases as BSA molecules are attached within pores due to increase in refractive index within porous structure.

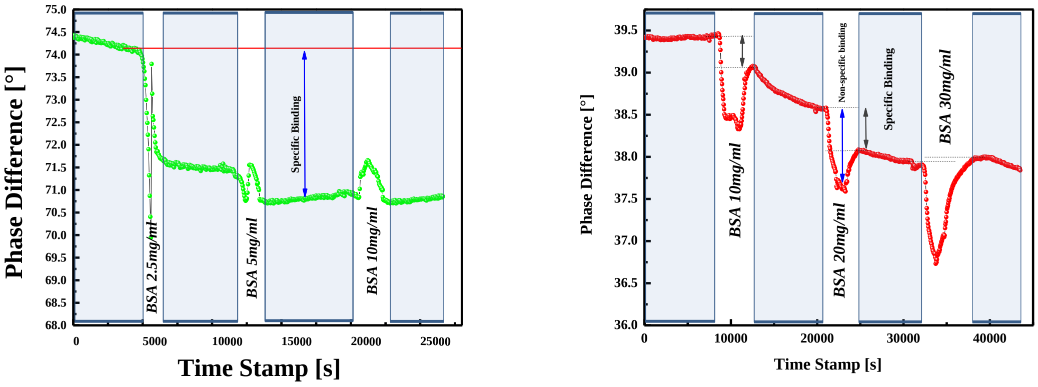

(a) (b)

6.9 (a) Real time sensing with another PSi and porous alumina FSM sample (b), Phase shift increases as BSA molecules are attached within porous structure. For porous alumina FSM a continuous change in phase is observed, that could be due to fluidic behavior.

6.4. Conclusions

A highly sensitive device for refractive index sensing is demonstrated. PSi freestanding membranes with different pore morphology and porous alumina membrane are characterized for both in-plane and out-plane optical anisotropy. A qualitatively description of the in-plane anisotropy is described in terms of pore morphological effects and pore alignment with respect to incident beam. PSi with straight and smooth pore shows a better isotropic azimuthal behavior. Similarly out-plane anisotropy increases as pores become smoother. Real time sensing experiment carried out with PSi FSM and with porous alumina membranes using NaCl solution shows that PSi FSM shows higher sensitivity compared to porous alumina membrane because of their larger specific area and due to large contrast between refractive index on birefringent material (PSi~1.7 and porous alumina~1.6) and NaCl solution. Sensitivity of 8.32°/RIU-µm and 3.01°/RIU-µm is observed for respective FSM. Refractive index change of ~10^{-4} is experimentally sensed with our system resolution. Furthermore experimentally, we demonstrated a label-free sensor. Because of the ease of the proposed FT geometry; sensor requires small volume of analyte solution, and has a reasonable fast detection time. Furthermore it may significantly reduce NSS compared to FO geometry. These experimental demonstrations opens new possibilities for the development of PSi based LOC devices with fast and low detection/highly sensitive sensing as well.

References

[1]Reimhult, Erik, and Karthik Kumar. "Membrane biosensor platforms using nano-and microporous supports." Trends in biotechnology 26(2), pp 82-89 (2008)

[2]Kasianowicz, John J., et al. "Nanoscopic porous sensors." Annu. Rev. Anal. Chem. 1, pp 737-766 (2008)

[3]Reimhult, Erik, and Karthik Kumar. "Membrane biosensor platforms using nano-and microporous supports." Trends in biotechnology 26(2) pp 82-89 (2008)

[4]C Baratto, E Comini, G Faglia, G Sberveglier, G Di Francia, F De Filippo, V La Ferrara, L Quercia, L Lancellotti, "Gas detection with a porous silicon based sensor" Sensors and Actuators B: Chemical, 65 (1-3), pp 257–259 (2000)

[5]Keiki-Pua S. Dancil, Douglas P. Greiner and Michael J. Sailor," A Porous Silicon Optical Biosensor: Detection of Reversible Binding of IgG to a Protein A-Modified Surface" J. Am. Chem. Soc., 121 (34), pp 7925–7930 (1999)

[6]C. Pacholski, "Photonic Crystal Sensors Based on Porous Silicon," Sensors 13(4), 4694-4713 (2013)

[7]Optical DNA sensing based on resonant porous silicon structures", Proc. SPIE 6477, Silicon Photonics II, 647717 (February 09, 2007)

[8]Finny P. Mathew, Evangelyn C. Alocilja," Porous silicon-based biosensor for pathogen detection" Biosensors and Bioelectronics, 20(8), pp 1656–1661 (2005)

[9]Lin, Victor S-Y., et al. "A porous silicon-based optical Interferometric biosensor." Science 278(5339), pp 840-843 (1997)

[10]Mulloni, V., and L. Pavesi. "Porous silicon microcavities as optical chemical sensors." Applied Physics Letters 76(18), pp 2523-2525 (2000)

[11]Eftekhari, Fatemeh, et al. "Nanoholes as nanochannels: flow-through plasmonic sensing." Analytical Chemistry 81(11), pp 4308-4311 (2009)

[12]Timoshenko, V. Yu, et al. "Anisotropy of optical absorption in birefringent porous silicon." *Physical Review B* 67(11), pp 113405 (2003)

[13]Liu, Rong, T. A., Li, Y. Y., Sailor, M. J., & Fainman,"Novel porous silicon vapor sensor based on polarization interferometry." Sensors and Actuators B: Chemical, 87(1), pp 58-62 (2002)

[14]Kompan, M. E., J. Salonen, and I. Yu Shabanov. "Anomalous birefringence of light in free-standing samples of porous silicon." Journal of Experimental and Theoretical Physics 90(2) pp 324-329 (2000)

[15]Yanjun Xiao, Xiaopeng Li, Han-Don Um, Xuejiao Gao, Zhongyi Guo and Jung-Ho-Lee," Controlled exfoliation of a heavily *n*-doped porous silicon double layer electrochemically etched for layer-transfer photovoltaics" Electrochimica Acta, 74, pp 93 (2012)

[16]Álvarez, J., Serrano, C., Hill, D., & Martínez-Pastor, J.," Real-time polarimetric optical sensor using macroporous alumina membranes" Optics letters, *38*(7), pp 1058-1060 (2013)

[17]C. S. Solanki, R. R. Bilalov, J. Poortmans, J. -P. Celis, J. Nijs and R. Mertens," Self-Standing Porous Silicon Films by One-Step Anodizing" J. Eletrohem. Soc., 151, pp C307 (2004)

[18]Jesús Álvarez, Paolo Bettotti, Isaac Suárez, Neeraj Kumar, Daniel Hill, Vladimir Chirvony, Lorenzo Pavesi, and Juan Martínez-Pastor," Birefringent porous silicon membranes for optical sensing", Optics Express, 19(27), pp. 26106-26116 (2011)

[19]Sarbey, O. G., Frolova, E. K., Fedorovich, R. D., & Dan'ko, D. B.,"Birefringence of porous silicon". Physics of the Solid State, *42*(7), pp 1240-1241 (2000)

[20]Oton, C. J., Ghulinyan, M., Gaburro, Z., Bettotti, P., Pavesi, L., Pancheri, L.,& Capuj, N. E. (2003). Scattering rings as a tool for birefringence measurements in porous silicon. Journal of applied physics, 94(10), 6334-6340

[21]P. C. Searson, J. M. Macaulay, F. M. Ross, "Pore morphology and the mechanism of pore formation in n-type silicon," Journal Applied Physics 72(1), 253-258 (1992)

[22]X.Q. Bao, J.W. Jiao, Y.L. Wang, K.W. Na, H. Choib," Macropore Formation Without Illumination on Low Doped n-Type Silicon", Journal of The Electrochemical Society 154 (3) D175-D181 (2007)

[23]Shichi, S., Fujii, M., Nishida, T., Yasuda, H., Imakita, K., & Hayashi, S.," Three-dimensional structure of (110) porous silicon with in-plane optical birefringence" Journal of Applied Physics, 111(8), pp 084303-084303 (2012)

[24]Herino, R., Bomchil, G., Barla, K., Bertrand, C., & Ginoux, J. L.," Porosity and pore size distributions of porous silicon layers" Journal of the electrochemical society, 134(8), pp 1994-2000 (1987)

[25]van den Berg, Albert, and Matthias Wessling. "Nanofluidics: silicon for the perfect membrane." Nature 445(7129), pp 726-726 (2007)

[26]Striemer, C. C., Gaborski, T. R., McGrath, J. L., & Fauchet, P. M.,”Charge-and size-based separation of macromolecules using ultrathin silicon membranes”, Nature, *445*(7129), pp 749-753. (2007)

Conclusions

Conclusions

Here I summarize the main results about fabrication and sensing with n-type porous silicon freestanding membranes.

First, we described an improved etching method to fabricate porous silicon freestanding sample with highly controlled morphology in moderately doped n-type silicon substrates (0.01-0.02 Ω-cm). Our protocol enables the realization of porous film that combine micro-meso and macro pores to be etched within the same structure, so that pore size can be tuned from few tens up to around 100 nm in diameter. Of particular interest thin as 2µm and thick porous membranes up to 60µm with straight and smooth 100nm pores is fabricated with two solution method. A notable difference compared to p-type substrates is that the porous layer lift-off does not require any high burst of current but is a self limited process, mainly dependent from the solution composition.

The fabricated PSi structures were stabilized by both thermal oxidation and chemical surface modification. This study is needed to develop a stable sensing platform. Furthermore the chemically modified PSi layer acts as intermediate layer for further binding of other bio-molecule i.e. BSA.

Finally sensing capabilities of PSi porous layers are demonstrated with multilayer micro-cavity structure and with single porous layer via polarimetric approach. The quality and sensitivity of PSi MCs with different quality factor=30, 50 and 70 are quantified with methanol-ethanol solution and a sensitivity of about 10^{-4} RIU is demonstrated. Furthermore the role of non-specific signal (NSS) is investigated in nanoporous silicon by comparing flow-over (FO) and flow-through (FT) geometries. For the first time we demonstrate that in FO geometry, NSS strongly contributes in the final output sensing signal and this preliminary investigation provides the first study of NSS effect in nanopores-based sensors.

At last, we were able to design and characterize a FT optical polarimetry sensor based on PSi FSM and results are compared with porous alumina FT sensor. We have quantified the birefringence of PSi and porous alumina FSM with aqueous NaCl solutions. Sensitivity of 8.32°/RIUμm and 3.01°/RIUμm is achieved for PSi and porous alumina FSM, respectively. BSA sensing is also demonstrated as a model system for future lab on chip (LOC) devices.

As a final outcome, the length scale of the porous structure investigated here is of interest in many application fields: from biosensor able to detect large molecules, to filtering device and self cleaning surfaces. Furthermore in this thesis experimental demonstration of flow-through sensing opens new possibilities for the development of PSi based LOC devices with fast and low detection/highly sensitive sensing as well.

Publication on Thesis

1. "**Birefringent Porous Silicon membranes for Optical Sensing**"
Jesús Álvarez, Isaac Suárez, Paolo Bettotti, ***Neeraj Kumar****, Daniel Hill, Lorenzo Pavesi, and Juan Martínez-Pastor* (Optics express, 19(2011)26106)

2. "**Phase sensitive detection for optical sensing with porous silicon**"
Jesús Álvarez, , ***Neeraj Kumar,*** *Paolo Bettotti, Daniel Hill and Juan Martínez-Pastor*
(IEEE Photonics, 4(2012)986)

3. **"Dry adhesive bonding of nano-porous inorganic membranes to micro-fluidic devices using the OSTE(+) dual-cure polymer"** *F Saharil, F Forsberg, Y Liu, P Bettotti,* ***N Kumar****, F Niklaus, T Haraldsson, W van der Wijngaart and K B Gylfason* (Journal of Micromechanics and Microengineering 23 (2013) 025201)

4. **"Self detachment of free-standing porous silicon membranes in moderately doped n-type silicon"** ***Neeraj Kumar,*** *Paolo Bettotti Salvatore Gennaro,Pradeep Vallachira Warriam Sasikumar, Gian Domenico Sorarù* (Journal of Applied Physics A, (2013) 10.1007/s00339-013-8104-6)

5. **"Flow through versus flow over approach in nano-porous silicon sensors Flow through approach reduces non-specific binding in nano-porous sensors"**
Neeraj Kumar, Elena Froner, Romain Guider, Marina Scarpa, Paolo Bettotti (Analyst, (2013) 10.1007/s00339-013-8104-6)

Conferences

1. “**Optimization and synthesis of thin transparent free standing n-type porous silicon membranes”**
   Neeraj Kumar*, *Paolo Bettotti and Lorenzo Pavesi*
   Accepted for oral presentation at “8thPorous semiconductors science and technology Conference ", Marchr 25, 2012

2. **“Optimization and synthesis fo n-type microcavity (MC)**
   Neeraj Kumar*, *Paolo Bettotti and, Lorenzo Pavesi,*
   Accepted for oral presentation at “conference on photonics” B2.5, 15 May 2013
   http://www.fotonica2013.it/documenti/Fotonica2013_Programma_Tecnico.pdf

3. **“Dry transfer bondig of porous silicon membranes to OSTE(+) polymer microfludic devices”***Farizah Saharil, Kristinn B. Gylfason, Yitong Liu, Tommy Haraldsson, Paolo Bettotti,* ***Neeraj Kumar****, and Wouter van der Wijngaart “*Micro Electro Mechanical System (2012) Conference ", http://dx.doi.org/10.1109/MEMSYS.2012.6170133

4. **“Highly-Sensitive Anisotropic Porous Silicon based Optical Sensors”**
   Jesús Álvarez[*] *Paolo Bettotti*, ***Neeraj Kumar,*** *Isaac Suárez, Daniel Hill, Lorenzo Pavesi, and Juan Martínez-Pastor* “SPIE photonics west (2012) Doi:10.1117/12.908214

5. **“A Polarimetric sensor based on nanoporous free standing membranes”**
   Paolo Bettotti, ***Neeraj Kumar,*** *Lorenzo Pavesi, Jesús Álvarez and Daniel Hill* “SENSOR (2012) IEEE Doi:10.1109/ICSENS.2012.6411315**",**

Other Publication

1. “Experimental investigation by UV-VIS and IR Spectroscopy to reveal electronic and vibrational properties of pyrrole 2- carboxyldehyde: A Theoretical Approach
Neeraj kumar* *Sankar chakravorti and Papia Chowdhury,* Journal of Molecular Structure, 891 (2008) 351-356

***2,* “Effect of Pr Doping in La-Sn-Mn-O System”**
Neeraj Kumar, Rahul Tripathi, Anjana Dogra, V.P.S. Awana, and H. Kishan* Letter-Journal of Alloys and Compounds, 492 (2010) L28-L32

***3.* “Structural, electrical & magnetic studies of Cr doped $La_{0.7}Ca_{0.3}Mn_{1-x}Cr_xO_3$ ($0 \leq x \leq 1$)”**
Neeraj Kumar, H. Kishan, A. Rao and V.P.S. Awana (* Journal of Applied Physics, 107 (2010) 083905

***4* “Structural, magnetic, and dielectric studies of Pr doped $Bi_{1-x}Pr_xFeO_3$ multiferroics”**
Neeraj Kumar, Neeraj Panwar, G. Bhasker, Neelam Singh, V.P.S. Awana, and H. Kishan (*Letter- Journal of Alloys and Compounds-2010- doi:10.1016/j.jallcom.2010.04.095

5* “Fe ion doping effect on electrical & magnetic properties of $La_{0.7}Ca_{0.3}Mn_{1-x}Fe_xO_3$ ($0 \leq x \leq 1$)”** ***Neeraj Kumar*, *H. Kishan, A. Rao and V.P.S. Awana (*Journal of Alloys and Compounds-2010- doi:10.1016/j.jallcom.2010.04.187

***6.*“Structural, electrical & thermal studies of Nb doped $Pr_{0.7}Sr_{0.3}Mn_{1-x}Nb_xO_3$ ($0 \leq x \leq 0.07$)”** *S.K. Agarwal, **Neeraj Kumar**, Neeraj Panwar, Bhasker Gahtori, Ashok Rao, P. C. Chang, and Y. -K. Kuo* Solid State Communications (150 (2010) 684 doi:10.1016/j.ssc.2009.11.041

7. “Impact of particle size on room temperature ferro-magnetism of $SrFe_{12}O_{19}$”
Neeraj Kumar, Anuj Kumar, R. Jha, Anjana Dogra, Renu Pasricha, R.K. Kotnala, Hari Kishan and V.P.S. Awana (*Letter- Journal of Superconductivity and Novel Magnetism- 23 (2010) 423

8.”Magneto-Transport of $La_{0.70}Ca_{0.3-x}Sr_xMnO_3$ (Ag): A Potential room temperature bolometer and magnetic sensor” *V.P.S. Awana[1,*], Rahul Tripathi, **Neeraj Kumar** H. Kishan, G. L. Bhalla, R. Zeng, L. S. Sharth Chandra, V. Ganesan and H. U.Habermeier* (Journal of Applied Physics 107(2010) 09D723

9.“Nano-vanadium doping driven low temperature structural phase transformation in Titania” *Anuj Kumar, Bhasker Gahtori, **Neeraj Kumar**, V.P.S. Awana, A.K. Shrivastava, Neeraj Panwar, Hari Kishan and I.Flener* Modern physics letters B 23 (2009) 3543-3549

10. “Doped $Pr_{0.7-x}Bi_x Sr_{0.3}MnO_3$ manganite: A structural, electrical and magnetic effect”
***Neeraj Kumar**, Hari Kishan, A. Rao and V.P.S. Awana (*Letter-Journal of Alloys and Compounds-504 (2010) L39*)*

11. **“A neutron diffraction and magnetization study of $La_{0.7}Ca_{0.3}FeO_3$”** *Anjana Dogra, **Neeraj Kumar***, V.P.S. Awana , S. Rayaprol, S. D. Kaushik, V. Siruguri and H. Kishan* (Journal of Applied Physics-109(2011) 07E132)

12. **“Comparative study of Bi Doped $Pr_{0.7}Sr_{0.3}MnO_3$ & $Pr_{0.6}Sr_{0.4}MnO_3$ manganite”**
Neeraj Kumar*, A.Rao, V.P.S. Awana* (AIP Conference Proceedings, Volume 1349, pp. 993-994 (2011))

13. **“Mixed-exchange: Cr & Fe Doped $La_{0.7}Ca_{0.3}MnO_3$”**
Neeraj Kumar*, A.Rao, V.P.S. Awana* (AIP Conference Proceedings, Volume 1349, pp. 989-990 (2011)

14. **”*Electrical* conduction and Thermal properties of Bi Doped $Pr_{0.7}Sr_{0.3}MnO_3$ manganite”**
Neeraj Kumar*, Mamatha Reddy, Ashok Rao, Y.K. Kuo, H. Kishan and V.P.S. Awana* (Accepted in Journal of Material Bulletin

15 **“Electrical and magnetic properties of $Pr_{0.6-x}Bi_xSr_{0.4}MnO_3$ manganites”**
*Mamatha D Daivajna, **Neeraj Kumar**, V.P.S. Awana, Bhasker Gahtori, Benedict Christopher J Manjunath S.O., K. Z. Syu, Y.K.Kuo and Ashok Rao* (Accepted in Journal of Alloys and Compounds http://dx.doi.org/10.1016/j.jallcom.2013.11.033)